# Energy Efficient Thermal Management for Natural Gas Engine Aftertreatment via Active Flow Control

## Annual Technical Progress Report

**October 1, 2003 to September 30, 2004**

**David K. Irick**
**Ke Nguyen**
**Vitacheslav Naoumov**
**Doug Ferguson**

**April 2005**

**DE-FC26-02NT41609**

**The University of Tennessee**
**404 Andy Holt Tower**
**1331 Circle Park**
**Knoxville, TN 37996-0140**

## Disclaimer

## Abstract

The project is focused on the development of an energy efficient aftertreatment system capable of reducing NOx and methane by 90% from lean-burn natural gas engines by applying active exhaust flow control. Compared to conventional passive flow-through reactors, the proposed scheme cuts supplemental energy by 50%-70%. The system consists of a Lean NOx Trap (LNT) system and an oxidation catalyst. Through alternating flow control, a major amount of engine exhaust flows through a large portion of the LNT system in the absorption mode, while a small amount of exhaust goes through a small portion of the LNT system in the regeneration or desulfurization mode. By periodically reversing the exhaust gas flow through the oxidation catalyst, a higher temperature profile is maintained in the catalyst bed resulting in greater efficiency of the oxidation catalyst at lower exhaust temperatures. The project involves conceptual design, theoretical analysis, computer simulation, prototype fabrication, and empirical studies.

This report details the progress during the first twelve months of the project. The primary activities have been to develop the bench flow reactor system, develop the computer simulation and modeling of the reverse-flow oxidation catalyst, install the engine into the test cell, and begin design of the LNT system.

# Table of Contents

## Table of Figures

# Table of Tables

## Introduction

Lean burn natural gas engines have high thermal efficiency and durability. However, lean burn engine exhaust has a wide temperature span and is rich in oxygen, which makes aftertreatment difficult. Lean burn $NO_x$ levels can be much lower than stoichiometric burn levels, but are still too high to meet the 0.1 g/hp-hr target and a de- NOx scheme has to be applied. The leading de-NOx contenders for lean burn engines are Lean NOx Catalyst (LNC), Selective Catalytic Reduction (SCR), and Lean $NO_x$ Trap (LNT) [1].

A Lean $NO_x$ Trap, or $NO_x$ adsorber, is a flow-through catalyst-bed that temporarily stores exhaust $NO_x$ during typical lean burn operations. Before the $NO_x$ adsorbent becomes fully saturated, the exhaust gas composition must be adjusted to produce a fuel-rich exhaust. This adjustment may be accomplished by either by modifying engine fueling strategy or by introducing fuel into the exhaust stream. Under fuel rich conditions, the stored $NO_x$ is released from the adsorbent and subsequently reduced to $N_2$ over precious metal sites. A desulfurization process must be conducted at high temperature and fuel rich conditions [3-8]. Such Lean $NO_x$ Traps have demonstrated high $NO_x$ conversion efficiencies; approaching 95%, for lean burn gasoline engines and diesel engines [4-8].

The LNT is the focus of this research. It should be pointed out that the LNT approach has to overcome the dilemma that while the oxidation of methane requires high temperatures, the $NO_x$ absorption requires much lower temperatures. Significantly, de-$NO_x$ systems normally involve hydrocarbon slip. In the case of compressed natural gas (CNG) fuel, the predominant hydrocarbon is methane, which is difficult to destroy in downstream catalytic treatment of the exhaust. Presently, LNT research has not been as successful for CNG applications as when applied to lean burn gasoline engines or diesel engines [4-11]. Energy efficient breakthroughs are needed for LNT regeneration, desulfurization, and methane oxidation. The objective of this project is to develop a system capable of improving the effectiveness of LNTs applied to CNG-fueled lean-burn engines.

This project is focused on the development of an energy efficient aftertreatment system capable of reducing $NO_x$ and methane by 90% from lean-burn natural gas engines by applying active exhaust flow control. The system consists of a Lean $NO_x$ Trap (LNT) system and an oxidation catalyst. Through alternating flow control, a major amount of engine exhaust flows through a large portion of the LNT system in the absorption mode, while a small amount of exhaust goes through a small portion of the LNT system in the regeneration or desulfurization mode. The restricted partial flow has a very low space velocity that reduces the requirement for secondary fuel. By periodically reversing the exhaust gas flow through the oxidation catalyst, a higher temperature profile is maintained in the catalyst bed resulting in greater efficiency of the oxidation catalyst at lower exhaust temperatures. The project involves conceptual design, theoretical analysis, computer simulation, prototype fabrication, and empirical studies.

An integrated LNT -oxidation embedment is being developed which will have no negative impacts on engine operation in terms of output, efficiency, durability, and maintenance. The flow reversal system is being designed with zero slip during switching. The results of this research will help to attain the long-term $NO_x$ emission target of 0.1 g/hp-hr, energy efficiency of 50%, and cost reduction of 10%.

## Overview

The goals of the project will be achieved through a union of modeling, bench testing, conceptual design, fabrication, and experimental testing. To reach these goals, the following tasks were outlined and presented in the Annual Technical Progress Report dated April 2004.

I. Bench Flow Reactor Design and Modeling

II. Conceptual Design of a Partial Flow LNT Regeneration and Gas Divider System

III. Lean Burn Natural Gas Engine Testing and $NO_x$ Reduction Strategy Development

Each of these tasks be reviewed briefly, updated with the most recent progress and any new tasks will be presented.

## Bench Flow Reactor Design and Modeling Review

Bench-Flow Reactor System

The bench-flow reactor (BFR) was built to supply necessary kinetic data and system optimization information for the ARES natural gas (NG) stationary power-generating engine. The data collected provided the ARES program with vital information pertaining to nitric oxides (NOx) and total hydrocarbon (THC) conversion efficiency. Both NOx and THC conversion are functions of the catalyst type and loading, space velocity, temperature, and exhaust gas mixture. Each of these parameters were controlled and examined to obtain the needed data in a laboratory setting. A full design of the reactor can be reviewed in the Annual Report from April of 2004.

Reverse-Flow Oxidation Catalyst Reactor

At elevated temperatures, the total hydrocarbon (THC) catalytic chemical reaction is exothermic and the reverse-flow configuration of the reactor has the capacity to take advantage of this increased temperature event. The switching of the inlet and outlet exhaust direction "traps" the temperature inside the reactor, thus increasing the overall temperature of the exhaust gas through the catalyst. THC reduction was investigated as a function of the direction and duration of the exhaust gases through the catalyst, space velocity, exhaust gas mixture concentration, and temperature. The catalyst used in the reactor was a palladium oxidation catalyst provided by EmeraChem.

Lean $NO_x$ Trap Catalyst Reactor

The objective of the lean $NO_x$ trap catalyst reactor (LNT) was to study the reduction of NOx in the simulated natural gas exhaust flow. At varying temperatures and space velocities, the following parameters were investigated; $NO_x$ breakthrough time, NOx capacity storage, catalyst saturation, maximizing the storage by shifting between the lean phase mode and the rich phase mode, maximizing the storage by direct fuel injection, and identifying the best reductant (CO or $H_2$) in the rich phase.

Data Acquisition System

The data acquisition system (DAC) consists of hardware and software components purchased commercially from National Instruments. The purpose of the DAC, besides simply data logging, is to be a flexible system that can adapt with the BFR system as the experiments change. The system was designed with the capability for multiple component interfaces to be logged at a user defined sampling rate.

Mathematical Modeling of Reverse Flow Oxidation Catalyst

The most important objective of modeling the BFR was to simulate the forward-flow and reverse-flow of the exhaust gas through the RFOCR. With the help of a one-dimensional model, a mathematical code was developed in FORTRAN. To keep the modeling code compact and uncomplicated, the complex energy and mass balance equations, which are non-linear partial differential equations, were simplified into algebraic equations by using the backward difference method.

The main objective of the RFOCR is to increase the temperature profile over the catalyst surface and hence to increase the THC conversion efficiency. To gain an understanding how this was optimized, it was important to predict the effect of the following parameters on the temperature profile and methane ($CH_4$) conversion:

1. exhaust gas flow rate
2. exhaust gas temperature
3. switching time

The model required the kinetics of the global reaction over palladium. By operating the BFR in a differential mode with a ½" palladium based catalyst, the kinetics of the global reaction can be extracted.

## Bench Flow Reactor Design and Modeling Progress

Bench-Flow Reactor System Modifications

A number of revisions have been made to the BFR systems instrument cabinet in order to accomplish goals set for the system. In order to have the capability to switch from lean and rich banks, described in the LNT reactor section of 2004 Annual report, additional mass flow controllers (MFC), solenoids, and a solid-state relay were added to the instrument cabinet. Modifications of the previous and present set-up of the cabinet can be compared in Figure 1 below and Figure 10 of the 2004 Annual Report.

The importance of water to the BFR system was discussed in the 2004 report and to properly simulate an actual engine exhaust mixture it is necessary for water vapor to be incorporated into the feed stream. A syringe pump, made by Harvard, was initially utilized for water injection into the system. Due to the relatively small reservoir of the syringe pump, it proved impractical to use for experimental runs with longer durations. Subsequently, the syringe pump was replaced by a peristaltic pump manufactured by Masterflex and was incorporated for use on the longer duration runs. The peristaltic pump, shown in Figure 2, allows for continuous water injection due to the pump's inlet being placed into a large water reservoir

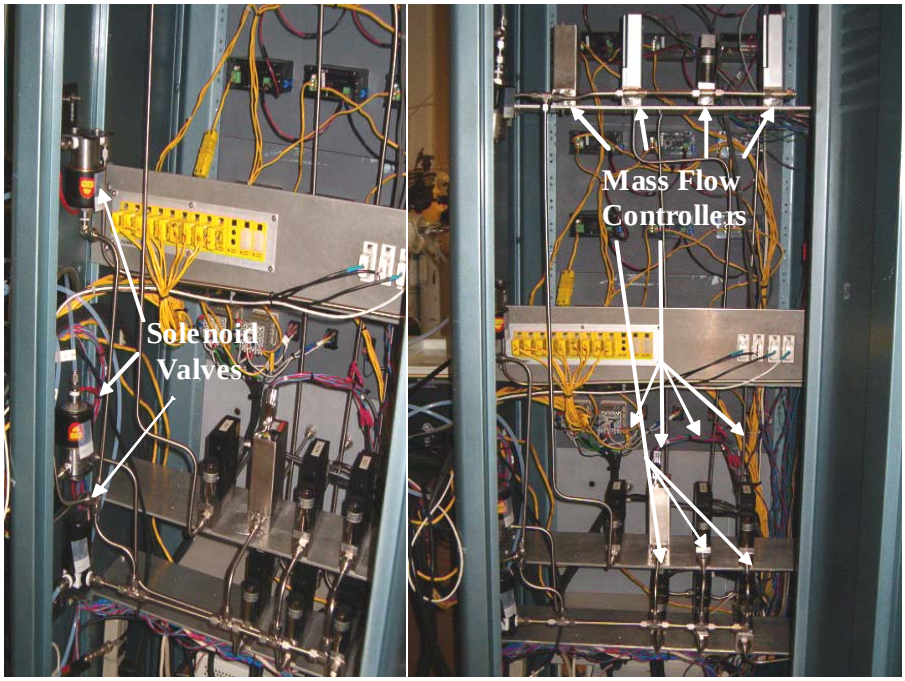


**Figure 1 Instrument Cabinet Modifications**

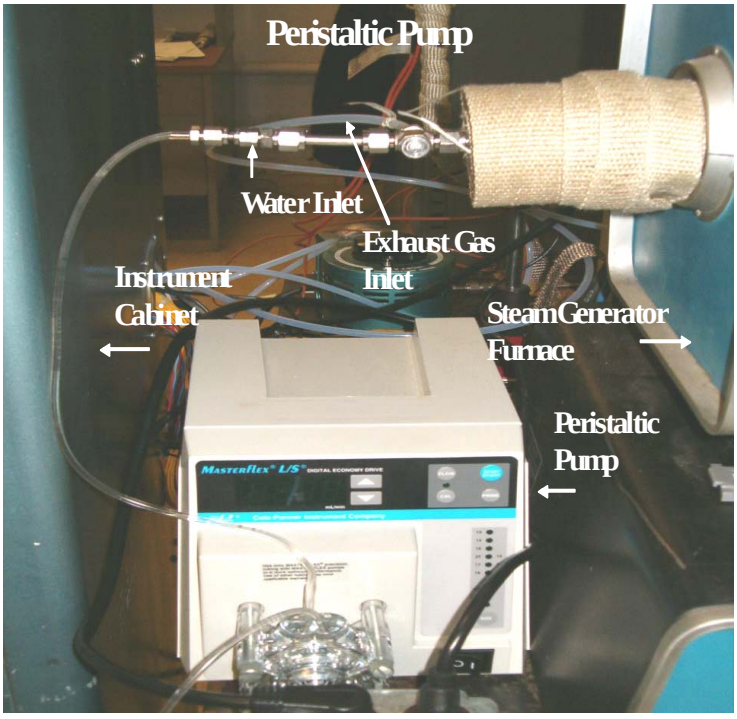


**Figure 2 Peristaltic Pump**

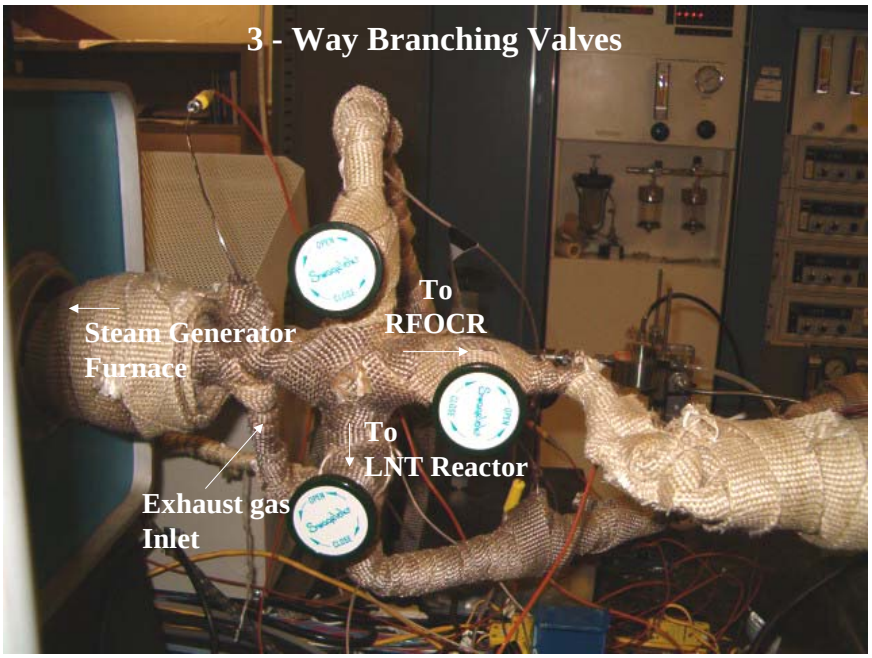


**Figure 3 Three-Way Branching Valves**

The BFR consists of two reactors, the RFOCR and the LNT reactor. Both reactors use the same components upstream of the reactor branching valves, shown in Figure 3. The major upstream components consist of the instrument cabinet, peristaltic pump, and steam-generating furnace. Because each particular reactor experiment must be run independently, a valve system was devised to stop the gas flow to the reactor that is not being utilized. This system of valves replaces the pneumatic valve that directed the exhaust mixture to the RFOCR or the LNT reactor.

Data Acquisition Modifications

Although no major hardware changes or additions have been made to the data acquisition system since last year's report, a modest amount of modifications have been made to incorporate the BFR system modifications with additions in the LabVIEW controlling program. Switching between the rich and lean bank and fuel injection pulsing were implemented into LabVIEW program giving the BFR system greater capability and flexibility when compared with the previous version.

In the new LabVIEW program, the BFR operator is now able to switch between a fuel-rich or fuel-lean mixture. The program allows for variable switching times between one bank to the other during the experiment, which is similar to the program designed for varying the forward- and reverse-flow durations in the RFOCR. Additionally, this particular program function is used in regenerating the LNT catalyst. In this part of the program, the operator can open or close the valve for fuel injection into the LNT reactor, the duration of the pulse, and the number of cycles during the experiment. One cycle consists of the fuel injection valve opening, closing, and opening again.

Reverse-Flow Oxidation Reactor Modifications

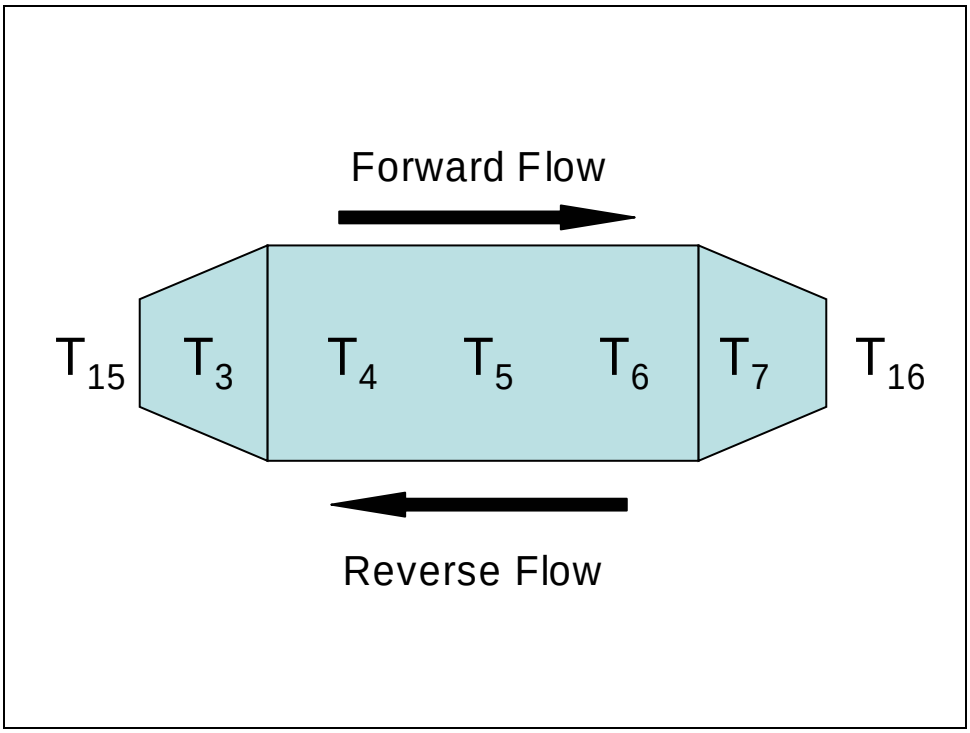


**Figure 4 Catalyst Thermocouple Orientations**

A number of revisions to the RFOCR have been made to improve the data collected for the ARES program. These modifications to this reactor include temperature stabilization of the system, oxidation catalyst replacement, and the modification of the reactor end fittings. Furthermore, two additional thermocouples were added to the RFOCR and placed to record the inlet and outlet temperature of the reactor furnace. Figure 4 shows the thermocouple orientation in relation to the catalyst sample inside the RFOCR.

The earlier version of the RFOCR obtained adiabatic conditions by an insulating jacket and a heating tape assembly. The heating tape was coiled around the reactor for temperature regulation while the insulating jacket was used to prevent heat loss. As seen in Figure 5, this temperature-regulating set-up resulted with the reactor temperature being unable to reach a steady-state temperature. As discussed in the 2004 annual report, the heating tape is controlled via LabVIEW, in conjunction with a steady-state relay and a thermocouple. The LabVIEW temperature-control program works similar to a home thermostat. A temperature set point is set and if the actual reactor temperature is greater than the set point, the voltage to the heat tape is shut off. Likewise if the temperature inside the reactor is less than the set point, a voltage is applied to the heat tape controller to raise the temperature. Because the heating time response of the heating tape was slow, oscillations occurred in the experiment. This resulted in severe temperature over and undershoots from the temperature set point. Moreover, due to the method of coiling the heat tape around the reactor, non-uniform temperature heating resulted in RFOCR. This produced a non-

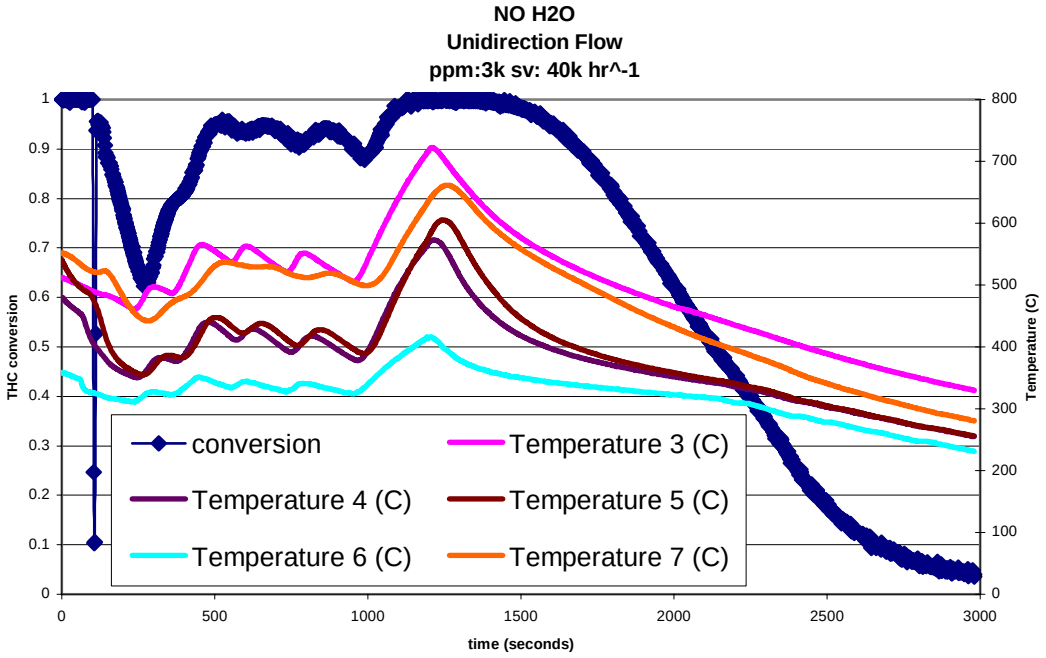


**Figure 5 No Water Addition, Unidirectional Flow, Methane 3000ppm Space Velocity - 40,000hr-1**

uniform temperature distribution throughout the reactor during experimental runs. The inability for accurate and uniform temperature control resulted in data that does not appear useful for real-world engine applications and were thought to have consequences to Total Hydrocarbon (THC) conversion

To alleviate the problem of temperature oscillations, a new approach was developed to control the RFOCR temperature. The early version was replaced with a tubular furnace, similar the set-up for the LNT reactor. Because of the different physical dimensions of the two setups, modifications to the tubing for the simulated exhaust and the pneumatic high-temperature switching valves (HTSV) were altered.

Initially EmeraChem donated several oxidation catalyst samples to the project with various loadings ranging from 25, 50, 75, and 100 g-Pd / $ft^3$. In the first RFOCR system set-up, the oxidation catalyst sample used had a precious metal loading of 100 g-Pd / $ft^3$. This catalyst sample was three inches long, 7/8 of and inch thick and had a cell density of 300 cells / $in^2$ (cpsi).

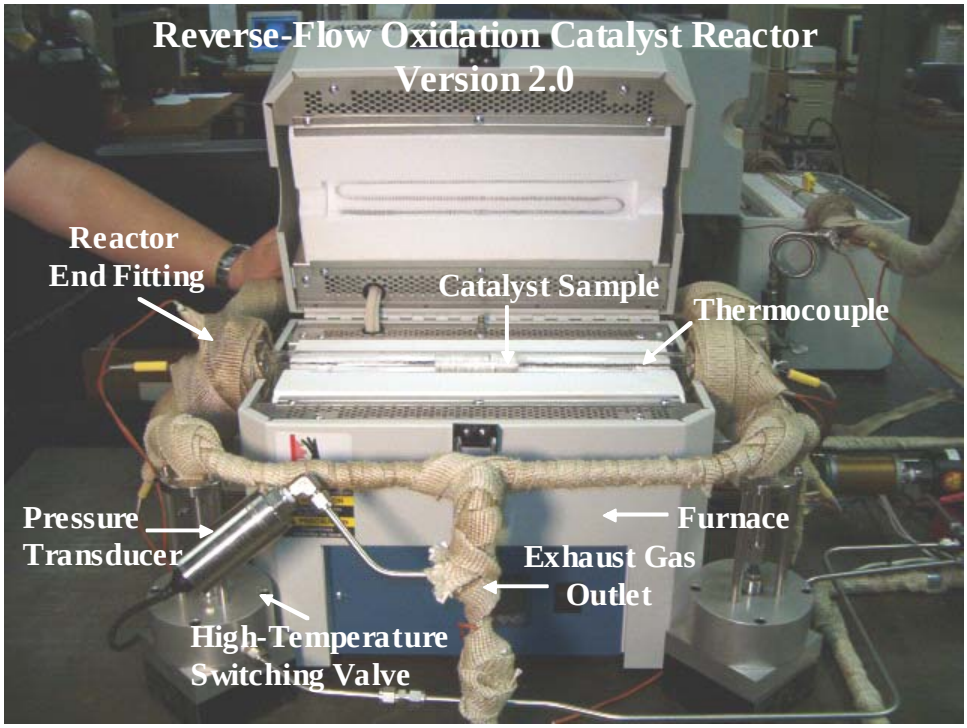


**Figure 6 Reverse Flow Oxidation Catalyst Reactor**

Unfortunately, the initial catalyst sample used was damaged in the process of completing the modifications the RFOCR system. For continuity, a fresh 100 g-Pd / $ft^3$ catalyst sample was used again to compare the experimental data between the initial and present RFOCR system set-ups. A picture of the experimental set-up with the fresh catalyst in place can be seen in Figure 6**.** The catalyst, as described in the 2004 Project Annual Report, is placed at the mid-point of the reactor and is wrapped with FiberFrax to prevent the simulated exhaust gas from "slipping" around the catalyst sample. Five thermocouples are installed into the RFOCR to determine both end temperatures of the sample and the temperature at ¼, ½, and ¾ the length of the catalyst.

The final modification to the RFOCR system was the reactor end fittings. The fittings, seen in Figure 7, were modified to prevent the exhaust mixture from escaping at the reactor end fitting. The previous set-up was very similar to the present set-up shown in Figure 7 with the exception of the graphite ferrule. Due to the high temperatures that the system attained the O-rings would fatigue and fail. The failure would cause leaks at the reactor end fittings and as a result of the mixture leak, the emission data collected was inaccurate.

This component failure was resolved by replacing the reactor end fitting completely. While the basic design is very similar, using a graphite ferrule to seal the reactor allows the RFOCR system to obtain high temperatures without sacrificing the reactor end fittings integrity. The reactor end fittings may also be carefully removed from the reactor tube without damaging or destroying the graphite ferrule. This advantage allows the service of damaged thermocouples or the replacement the catalyst sample inside the reactor tube without having to replace the end fitting.

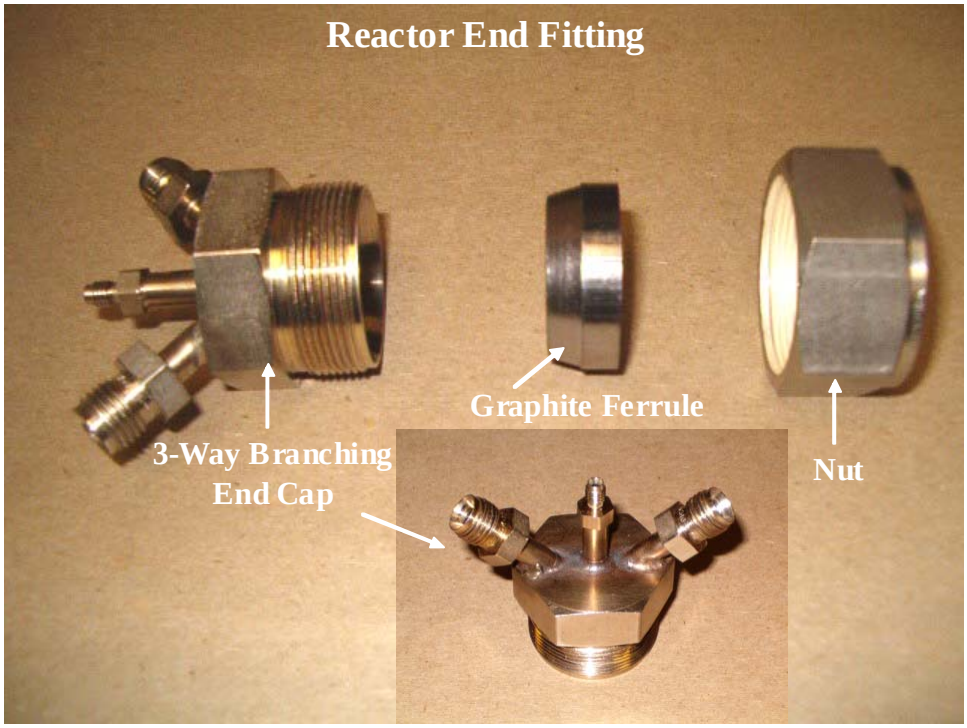


**Figure 7 Reactor End Fitting**

Lean NOx Trap Catalyst Reactor Modifications

Several modifications were made from the original LNT design. A fuel injection system (FIS) was added to evaluate the performance of regeneration using direct fuel injection. As shown in Figure 8, the FIS has four major components: a pressure regulator and pressure gage, an amplifier, a piezoelectric valve, and a rotameter. The pressure of fuel is precisely regulated since the fuel flow rate through the piezoelectric valve is strongly dependent on the pressure. A small change of pressure during the experiment induces a large change in the amount of fuel injected. The amplifier increases the voltage of input signal from the LabView control program to control the piezoelectric valve. The voltage range of the input signal from LabView is 0 to 5V, whereas the amplified voltage of output signal to the piezoelectric valve is 0 to 100V. The output signal is linearly proportional to the input signal. The Maxtek MV-112 piezoelectric valve regulates the precise amount of fuel to be injected into the reactor. The response time of the piezoelectric valve is 2 milliseconds and is fast enough to neglect time lag within FIS. Flow range of the valve is 0 to 500 cc/m at standard pressure, but it can be increased to a higher pressure condition (max 50psi). To measure the fuel flow rate from the piezoelectric valve, A Dwyer rotameter was used. The rotameter has a range between 0 and 4717 cc/m.

In the original configuration, the LNT catalyst sample was placed at the mid point of the quartz tube. Glass beads were filled in the inlet to maintain a uniform temperature profile. Using K-type thermocouples it was found that a temperature was approximately 20º lower at the inlet than that at the outlet. As a result, the catalyst sample was repositioned towards the exit side of the reactor and more glass beads were added. In this manner, the simulated exhaust gases would have adequate time to be heated up to the desired temperature. Heavy insulation was also added to the lines to minimize the heat lose to the surroundings.

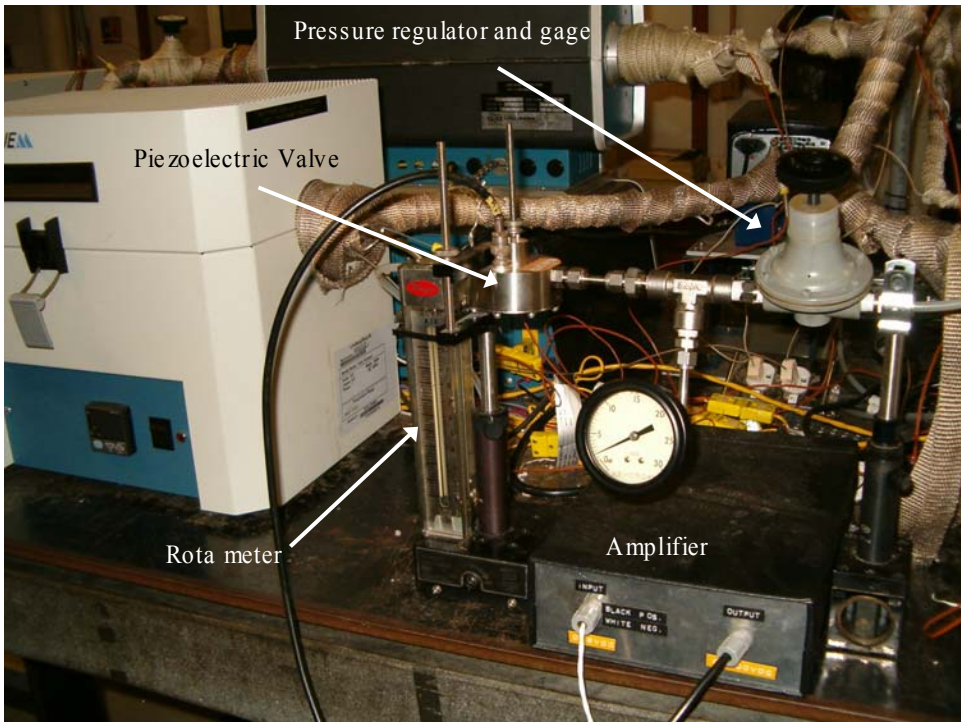


**Figure 8 The Components of Fuel Injection System**

Reverse Flow Reactor Model Modifications

*Reaction Kinetics*

To develop the code for the reverse flow oxidation, considering the surface reaction between methane and oxygen over palladium, it is necessary to know the reaction kinetics. It is important to have the correct values of the decisive parameters like the activation energy, the specific rate constants, and the pre-exponential term. Furthermore when the oxidation of methane over palladium in the presence of $CO_2$ and water vapor is considered, it is necessary to find the effects of all these constituent gases on the reaction as well as finding the reaction order. And finally it is important to find the heat energy involved in the reaction to determine the reaction rate and predict the correct reaction mechanism that would represent the actual reaction.

A detailed review of related literature gave the activation energy for the oxidation of methane over palladium but does not tell anything about the specific rate constants involved with the reaction. In order to supply the input values for the model code and to conduct experiments using the BFR, it was necessary to know the specific rate. To do so the reactor is run in a differential mode. This method employs both a global and a detailed chemical kinetic approach to the heterogeneous and homogeneous oxidation mechanisms. Some of the main factors that are considered in this mode are the length of the catalyst, the catalyst loading, the reactor temperature, the composition of the gases, the methane conversion, and the space velocity. A preview of each of these parameters is explained below.

While the temperature is one of the basic parameter that defines the kinetics and the reaction rates, the length of the catalyst is very important as well. To minimize the effects of temperature variation, it is necessary to maintain a uniform temperature through out the length of the catalyst. This is made easier by using a small length of catalyst. A longer catalyst will have a definite temperature variation along the length of sample. One more reason for having a smaller catalyst length is to keep the conversion down. Because the conversion process is exothermic in nature,

keeping the conversion as low as 10% helps to minimize the effect of any temperature rise. It is necessary to maintain a constant temperature as the reaction rates are exponentially dependent in the temperature. The literature review revealed that experiments are done at temperatures varying from 300°C to 600°C. It has been found that conducting experiments with a wide temperature range results in more accurate kinetics

One of the other important criteria is the space velocity. While the space velocity determines the residence time of the gases in the catalyst; it becomes necessary to have a proper control of it As mentioned earlier, it is necessary to have a low conversion to minimize the effect of temperature. What's more, to low of a space velocity has an increased residence time which allows the reaction a longer time to occur resulting in increased conversion. The increased conversion results in a larger temperature difference thus resulting in the uncertainty of the accuracy of the determined kinetics. So the space velocity is kept high to minimize the residence time and to lower the conversion. Due to convection increasing the flow rate also has an affect on the temperature. But keeping the catalyst sample short and preheated close to the temperature of the reactor that effect can be minimized.

To study the effect of catalyst loading, samples loaded to 100, 150 and 200g/ cubic feet per foot palladium can be used. Using helium as an inert gas , the effect of constituent gases in the feed stream can be studied using methane, oxygen, carbon dioxide and water vapor. A generalized concentration of these gases is shown in Table 1. below. The gas species concentrations are varied one at a time so that the effect of that particular gas can be found.

**Table 1 Different Species Concentration for the Differential Mode**

| Species (%) | $CH_4$ | $O_2$ | $CO_2$ | $H_2O$ | He |
|---|---|---|---|---|---|
| $CH_4$ | 0.3 – 5.7 | 5 | 0 | 0 | Balance |
| $O_2$ | 1 | 0.5 - 8 | 0 | 0 | Balance |
| $CO_2$ | 1 | 5 | 0.3 – 1.7 | 0 | Balance |
| $H_2O$ | 1 | 5 | 0 | 0.3 – 3.5 | Balance |

By utilizing the method of excess, it is possible to determine the relationship between reaction rate and the concentration of the species. The reaction mechanism shown in the 2004 Annual report to find the global reaction rate is considered again. Initially just methane and oxygen are flowed through the catalyst with the above concentrations along with helium or an other inert gas. We know that

$$-r_{CH_4} = kC_{CH_4}^{\alpha} C_{O_2}^{\beta}$$

Where both α and β are unknown, the reaction could be first run in an excess of $O_2$ so that $C_{O2}$ remains essentially unchanged during the course of the reaction and

$$-r_{CH_4} = k' C_{CH_4}^{\alpha}$$

Where

$$k' = kC_{O_2}^{\beta} \approx kC_{O_2 o}^{\beta}$$

So after determining α, the reaction is carried out in the excess of A, for which the rate law is approximated as

$$-r_{CH_4} = k'' C_{O_2}^{\beta}$$

This can be used to find the value of β. Then a similar run with carbon dioxide and water vapor can be run to find the reaction order of those species. The order is found by plotting the change in concentration with time along the y axis and the concentration along the x axis. The slope of this graph gives the order of the reaction with respect to that species. A similar plot can be done for all the species to find the order.

To find the above it is necessary to know the reaction rate. This is found out using the formula given below

$$-r_{CH_4} = \frac{F_{CH_4 o} X}{W}$$

Where $F_{CH_4 o}$ is the volumetric flow rate of the methane, X is the conversion percentage and W is the mass of the catalyst which is known from the catalyst loading.

*FORTRAN Compiler*

The previous report had a brief introduction about the need for a compiler and about the Compaq Visual FORTRAN Compiler. The code that was previously used had lots of subroutines which required more linking and so a visual compiler was more suitable. It was easy to traverse between subroutines and simpler to debug. There were some problems with the numerical handling of the compiler. It repeatedly gave errors or wrong results due to the high math involved within the code and the poor number handling capacity. The current code has one main program and a solver for ordinary differential equation. So the Intel FORTRAN compiler for Linux was used. This compiler is used along with the VI editor.

The current code works perfectly for the forward flow. Test runs conducted with the kinetics of propylene over platinum corresponded well to the literature. Once the kinetics for oxidation of methane over palladium was obtained, it was incorporated into the code to obtain the results for the forward flow. With an input file that has all the required parameters, the program has the option of running it either in unidirectional flow or with reverse flow. This option is setup in the input file. This can also be used to determine the temperature and conversion with the kinetics of methane over palladium. The input file also has parameters like temperature at which the simulation is to be done, the flow rate, the composition, and all the other required input parameters.

Figure 9 shows the temperature profile along the length of the catalyst at varying time. It is seen from the graph that the temperature starts increasing from the tail end of the catalyst and the peak moves towards the entrance as time proceeds. This is the trend of curve that has been observed in literature. Figure 10 shows the conversion of all the gases. As said before these are for propylene over platinum and it is just to show how the results are obtained from the code.

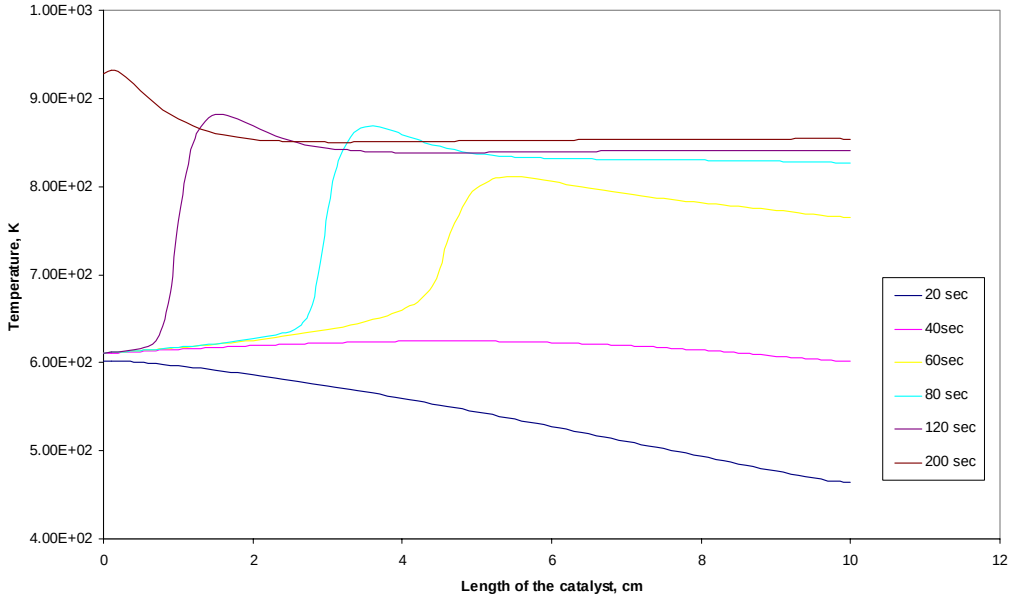


**Figure 9 Temperature Profile along the Length of Catalyst as a Function of Time**

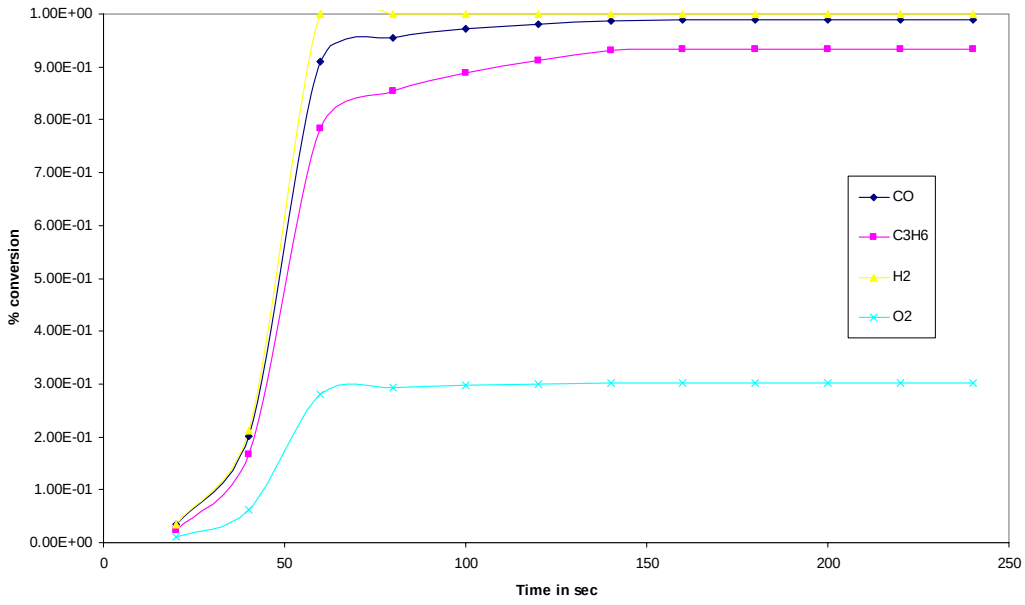


**Figure 10 Conversion of Different Species as a Function of Time**

The current code for the reverse flow has to be debugged. There is a convergence error with the Newton iteration method. This method is used to predict the temperature and concentration at each node and has to converge to the specified tolerance level. When the flow is reversed after a particular time, the inlet temperature, when reversed, is too high compared to the forward flow. Since the temperature difference is so high, the initial guess that is required to solve the Newton method is way off from what it has to be and so the value does not converge to a preset tolerance. Varying the tolerance to suit this problem is not a good method to debug the problem as it affects

the accuracy of the results obtained. Several different methods were tried to rectify this convergence problem. One such method is called the global Newton method. This method has a subroutine which checks each iteration. Once the iteration does not converge to the set tolerance and diverges, that particular iteration is omitted and the entire iteration is started with a different initial guess. By doing this we see through that we always converge. Unfortunately this method could not be used at this time due to code incompatibility.

One of the other methods considered was the bisection method. In this method, the extreme values are considered and the range is made closer and closer until it reaches the required value. This is a very reliable method but it is a very time consuming process. Considering the number of nodes and the number of iterations required this method would slow down the program too much and as the tolerance limit set smaller, it further increases the time required to complete. So this method was not incorporated either. Some of the other methods like the Broydens method and the secant method are currently being reviewed for the feasibility of incorporating one into this code.

Reverse-Flow Oxidation Catalyst Reactor Progress

As previously stated, the objective of the RFOCR is to prove that the reverse-flow configuration increases THC conversion and to optimize the system for maximum THC conversion. Below are several representative plots of experimental data to date. Further experimental data can be found in the Appendix section of this report. The RFOCR results are categorized into three major groups: the effects of varying switching time, exhaust gas mixture space velocity (flowrate), and temperature. The exhaust gas mixture concentrations for the RFOCR experiments remain constant and are shown in Table 2.

**Table 2 Typical Exhaust Gas Mixture**

| Gas Concentrations | Concentration |
|---|---|
| $H_2O$ Vapor (%) | 10 |
| O2 (%) | 6 |
| CO2 (%) | 6 |
| CO (%) | 0.5 |
| NOx (ppm) | 0 |
| CH4 (ppm) | 2000 |
| H2 (%) | 0 |

*Varying Switching Time*

The switching time increments are defined as the amount of time the exhaust mixture is allowed to flow in one direction. For example, a switching time of 15 seconds implies that the gas stream flows in the forward-flow direction for 15 seconds and then the gas flow direction is switched to the reverse-flow direction for 15 seconds. To date all experiments were performed with symmetric switching time duration.

In Figures 11 to 13 below, the temperature, concentration, and space velocity all remain constant. The RFOCR furnace temperature is 500°C, methane concentration is 2000ppm, and the space velocity is 20,000 $hr^{-1}$. It is immediately apparent that the reversing the flow through the catalyst does have a significant impact on the THC conversion. As seen in these figures it appears there is little affect on THC conversion between having a 15 or 20 second switching time duration. Both appear to have an approximate THC conversion of 90% at a space velocity of 20,000 $hr^{-1}$. A switching time duration of thirty seconds appeared to lower THC conversion to an approximate value of 87%. Through simple comparisons as these it is believed possible to determine a more suitable time duration scheme for maximum THC conversion. At the present time, shorter switching time durations are being further investigated in order to maximize THC conversion efficiency.

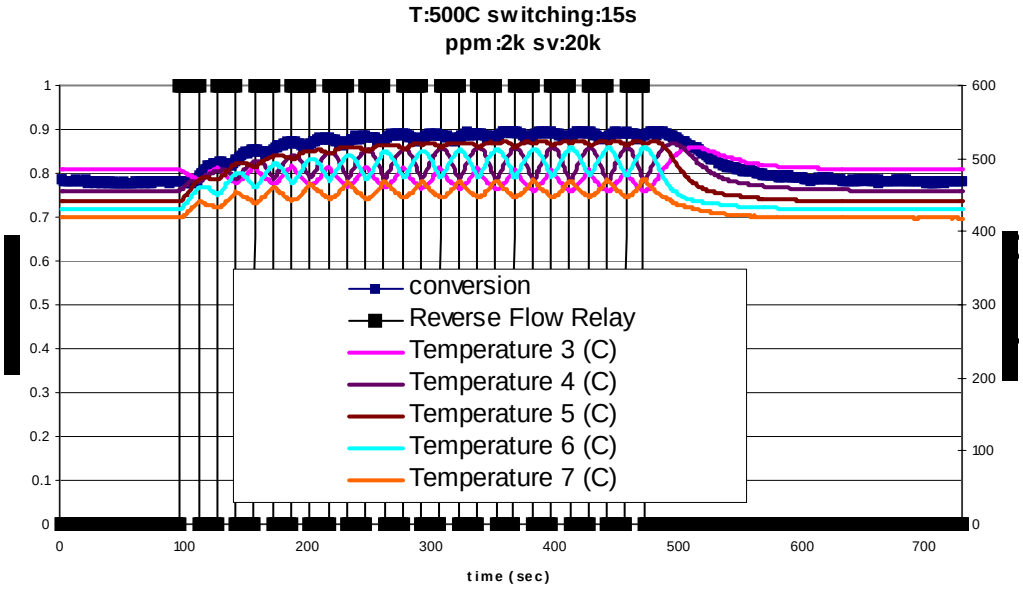


**Figure 11 RFOCR Temperature Profile and Conversion Percentage**

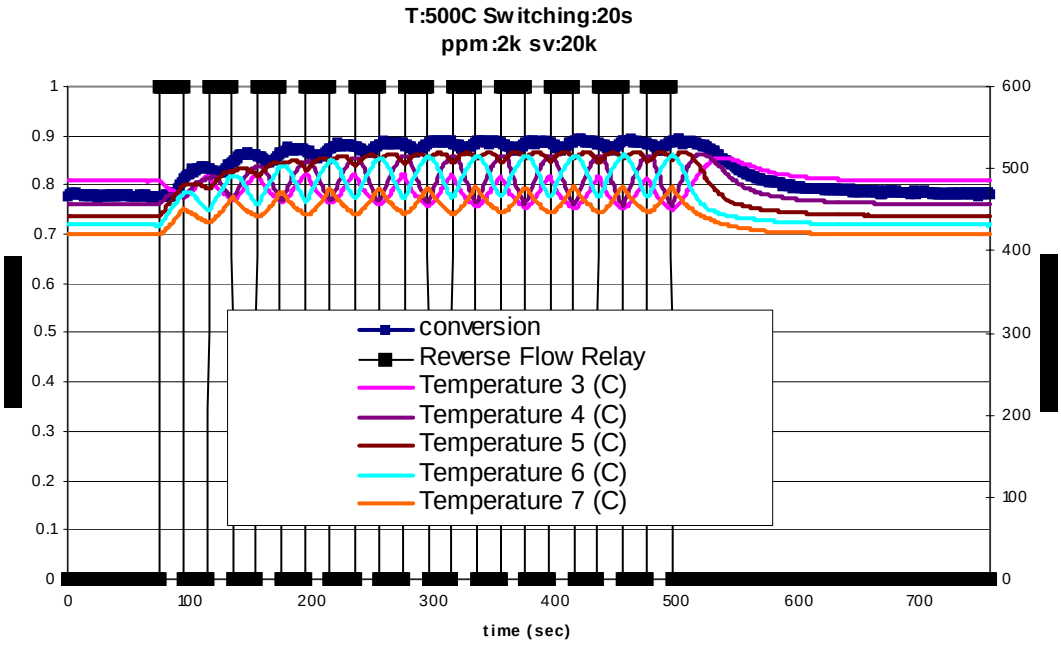


**Figure 12 RFOCR Temperature Profile and Conversion Percentage**

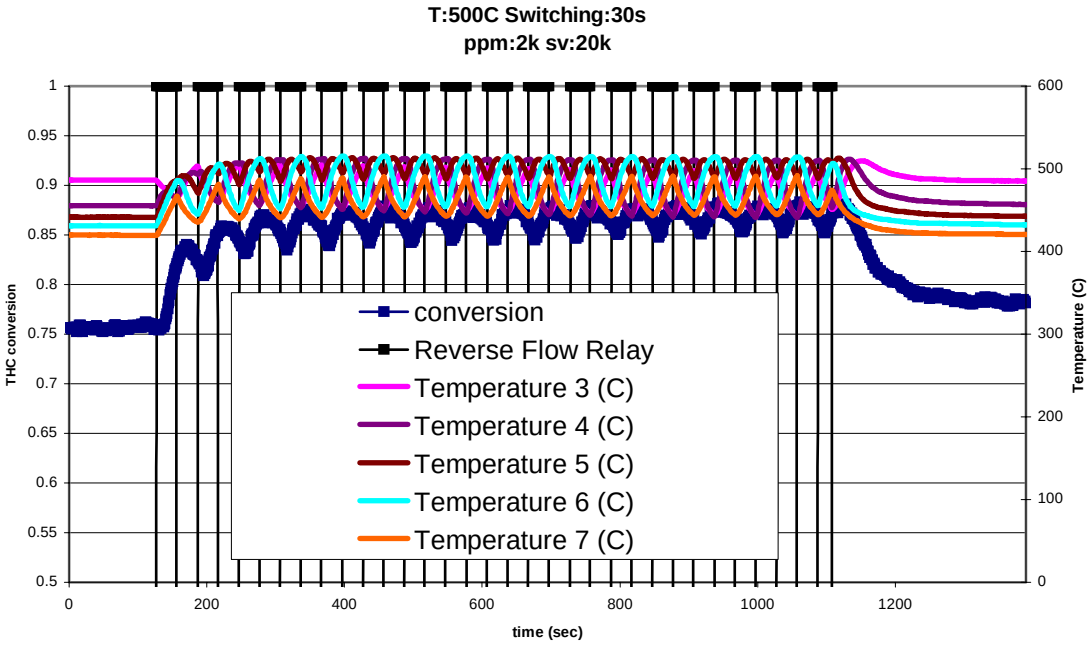


**Figure 13 RFOCR Temperature Profile and Conversion Percentage**

In Figures 14 to 16 the temperature, switching time, and exhaust concentration are the same as the previous plots above. However, the space velocity is increased to 40,000 $hr^{-1}$. When THC conversion is compared with the plots of 20,000 and 40,000 $hr^{-1}$ it is clear that increasing the simulated exhaust gas flowrate THC conversion decreases. At a space velocity of 40,000 $hr^{-1}$ an average THC conversion of 70% is obtained. This conversion is approximately 20% lower than the same experiment with a space velocity of 20,000 $hr^{-1}$. As in the first set of 20,000 $hr^{-1}$ plots, the set of 40,000 $hr^{-1}$ plots show a slight advantage in the shorter duration switching time in THC conversion.

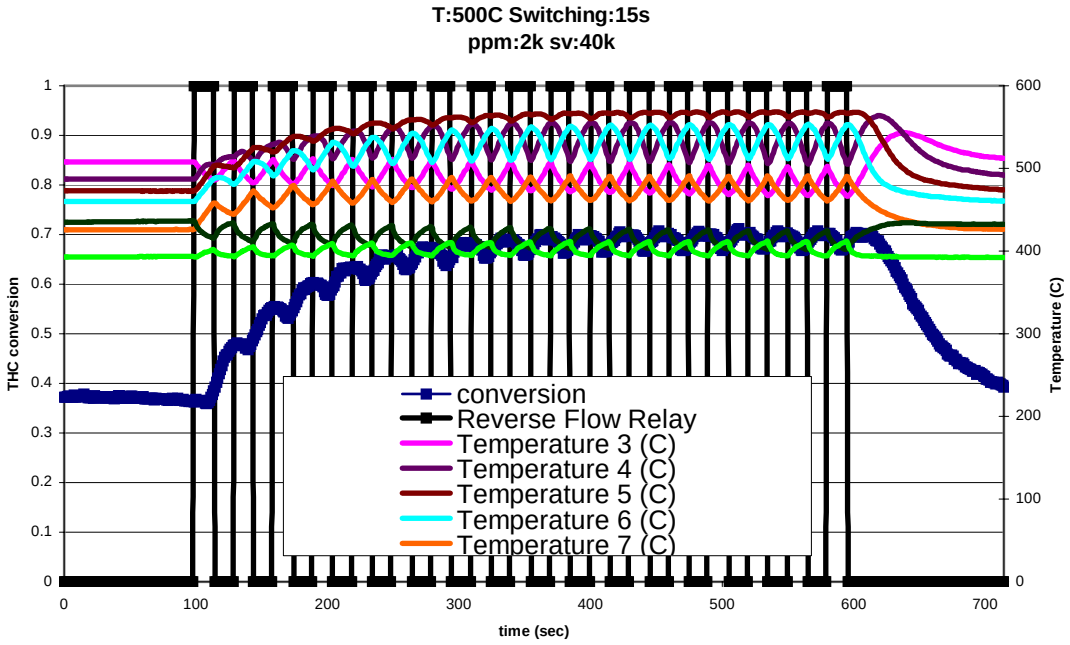


**Figure 14 RFOCR Temperature Profile and Conversion Percentage**

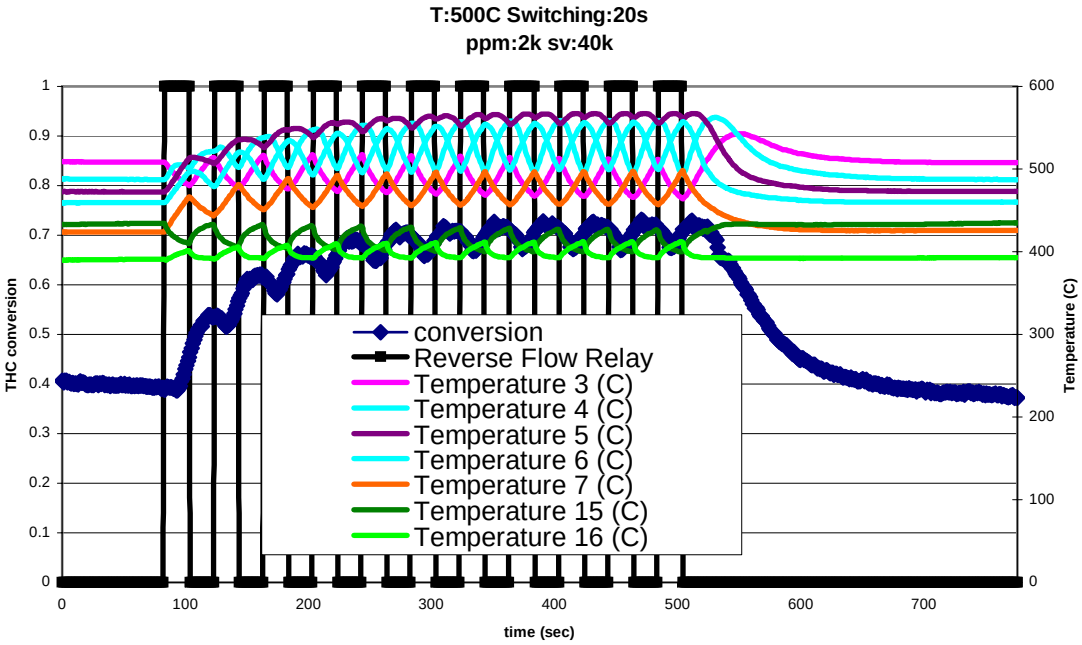


**Figure 15 RFOCR Temperature Profile and Conversion Percentage**

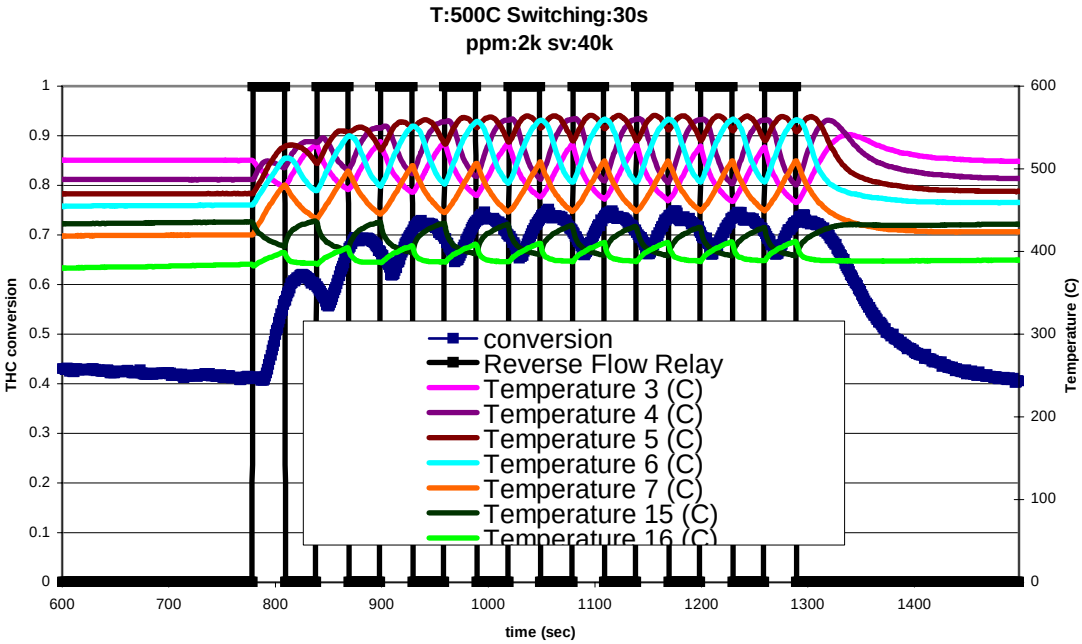


**Figure 16 RFOCR Temperature Profile and Conversion Percentage**

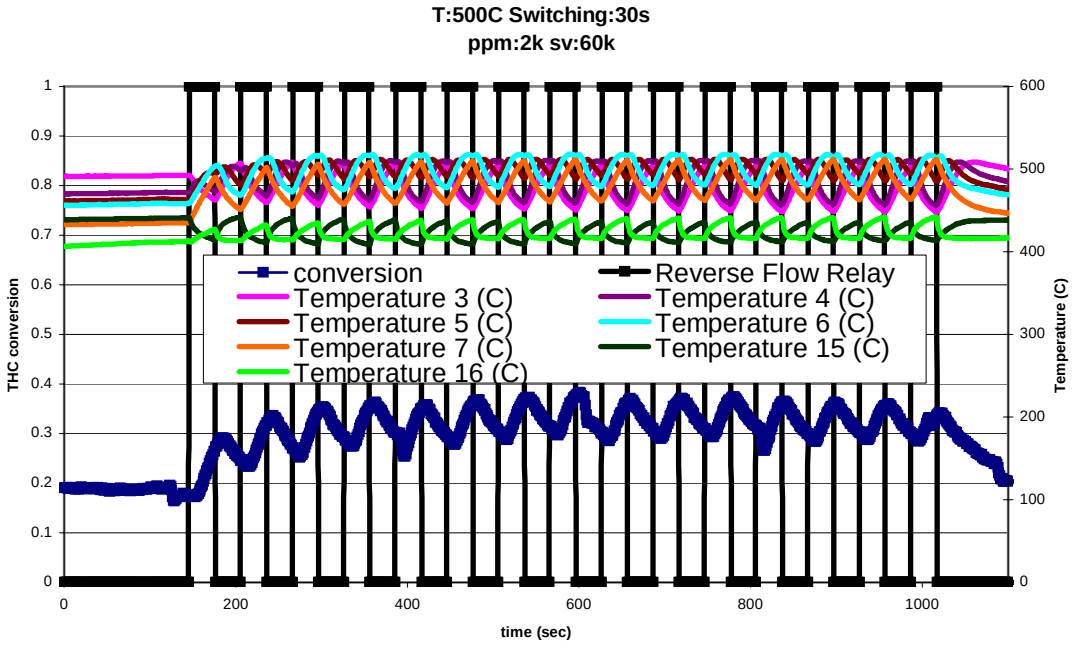


**Figure 17 RFOCR Temperature Profile and Conversion Percentage**

Figure 17 shows the results at a furnace temperature of 500°C, a switching time of 30 seconds, and a space velocity of 60,000 $hr^{-1}$. It can be seen the dramatic affect that space velocity has on THC conversion in this plot. The 20,000, 40,000, and 60,000 $hr^{-1}$ space velocity plots, at a switching duration of thirty seconds, have a THC conversion of 87%, 68%, and 35%, respectively. Comparison of these results shows that in order to achieve a maximum THC conversion a RFOCR configuration should be at shorter switching time durations and lower space velocities

*Varying Temperature*

In Figures 18 to 21 the effects of temperature on THC conversion is plotted. Space velocity, switching time duration, and mixture concentration are all held constant for this set of plots. Here the RFOCR furnace is varied from 400-550°C in 50°C increments. Figure 20 shows that at a relatively low temperature that reversing the flow through the catalyst reactor has little or no affect on THC conversion. THC conversion for a furnace temperature of 400, 450, 500, and 550°C is approximately 5%, 20%, 55%, and 85%, respectively.

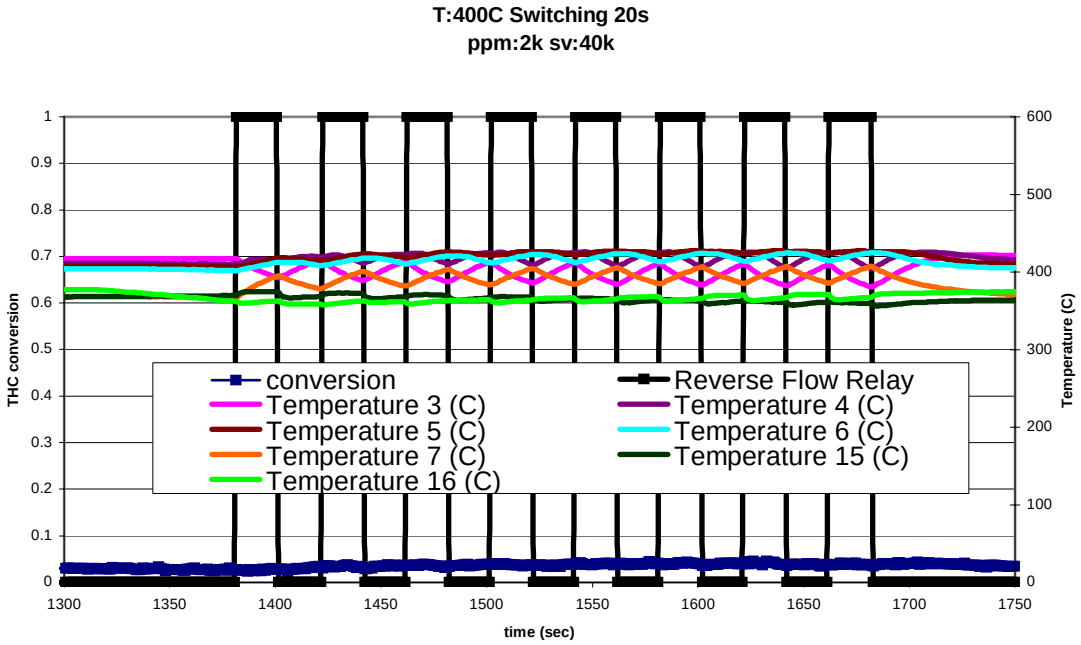


**Figure 18 RFOCR Temperature Profile and Conversion Percentage**

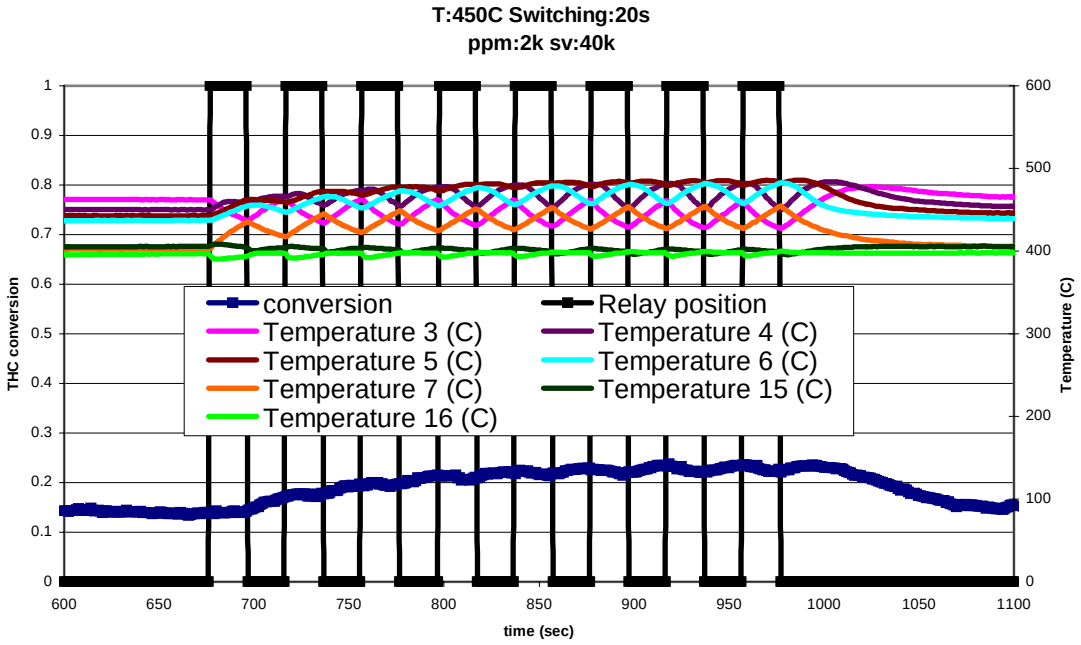


**Figure 19 RFOCR Temperature Profile and Conversion Percentage**

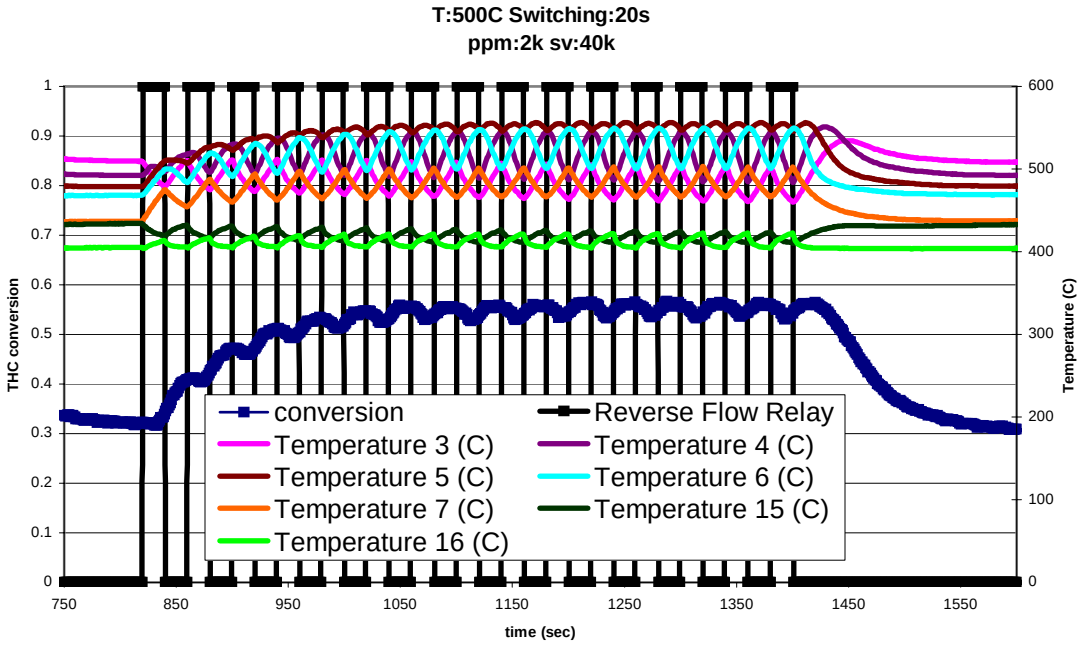


**Figure 20 RFOCR Temperature Profile and Conversion Percentage**

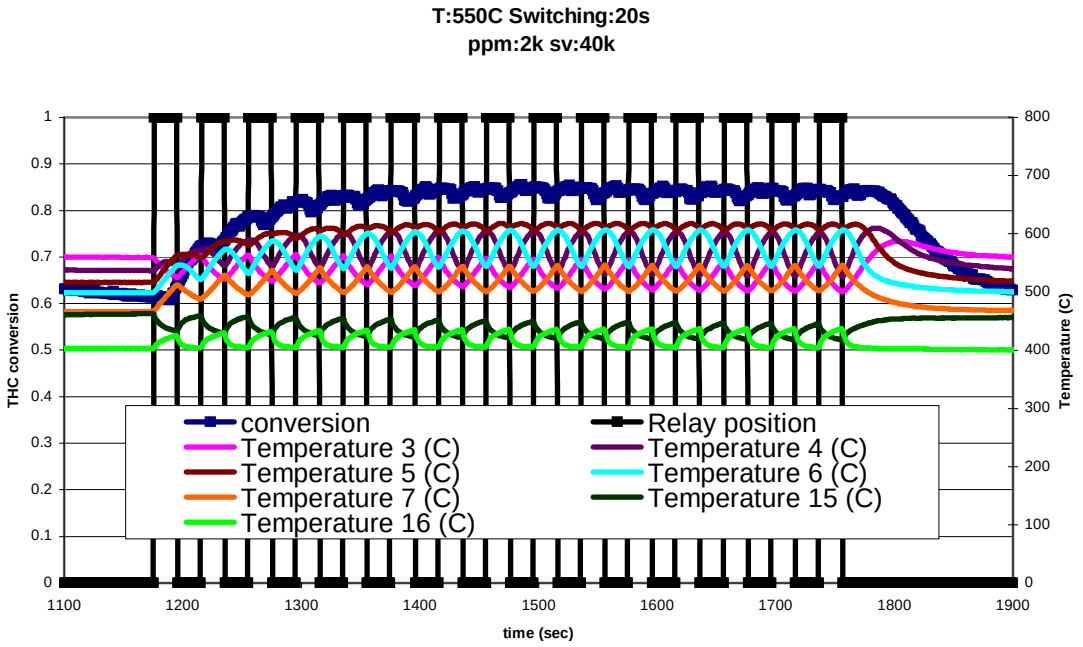


**Figure 21 RFOCR Temperature Profile and Conversion Percentage**

## Conceptual Design of a Partial Flow LNT Regeneration and Gas Divider System Review

System Concept

The difficulties of using methane as a reductant in LNT strategies necessitates the development of a $NO_x$ reduction catalyst coupled with an oxidation catalyst in a system capable of maintaining a high reaction temperature. A possible solution of maintaining a high reaction temperature in the converter is to use a reversing flow catalytic converter, which is capable of maintaining temperatures superior to the adiabatic temperature rise. Periodic flow reversal oxidation is a heat trap that performs active heat recovery on the top of the heat retention capability of the catalyst bed. The conception of the catalyst with reciprocating flow was discussed theoretically and verified experimentally[1, 3-6], but the problem of the deep investigation of more appropriate operational regimes of the such kind of reciprocating system over a broad range of conditions is not solved yet. The idea of the reversing flow catalyst is quite simple. The feed is periodically switched between the two ends of the catalytic converter. The operation of the reverse flow catalytic converter is controlled using valves, as shown schematically in the Fig. 22.

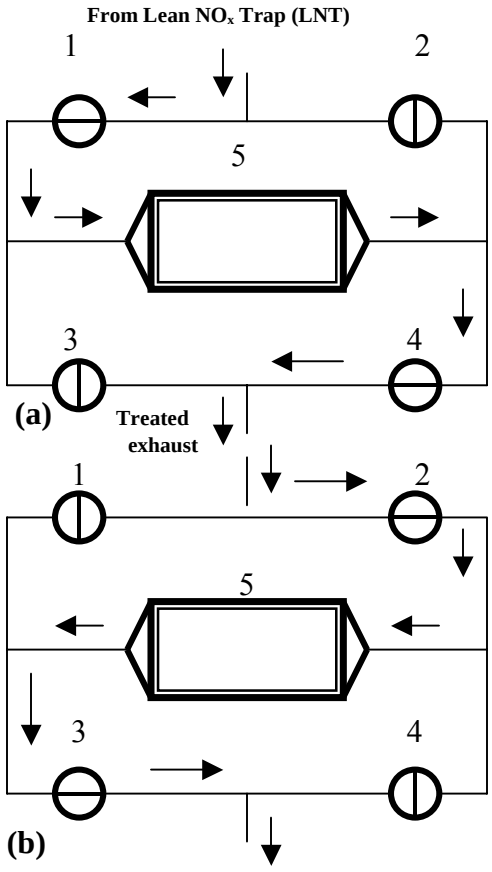


**Figure 22 Schematic of rotating gas divider**

In the Figure 22 (a) the control valves 1 & 4 are opened and engine exhaust flows to the catalytic converter from left to right (forward flow mode). In Figure 22 (b) the control valves 2 & 3 are opened and engine exhaust flows to the catalytic converter from right to left (reverse flow mode). Total time of the cycle equals to the sum of the times of the forward and reverse mode.

Such a concept provides a heat trap effect that can be used to achieve and maintain an enhanced reactor temperature as compared to a single direction flow mode operation. Figure 23 (a) illustrates a reactor temperature profile that might be observed in conventional unidirectional flow operation due to exothermic reaction. The temperature initially rises slowly as the reaction commence, and then more sharply as the heat released in the reaction accelerates the rate owing to the exponential temperature dependence of the rate constant. If the temperature pattern is established (Figure 23 (b)), the reverse mode can be used to take advantage of the high temperatures near the exit top reheat the reactor feed. During the reverse mode the energy, stored in the catalytic converter during the forward mode, is effectively used to preheat the feed, that provides the opportunity to achieve the temperatures higher than the adiabatic temperature rise, based on the fresh feed inlet temperature. Depending on the duration of the modes one can achieve the autothermal converter operation at feed temperatures below those required for autothermal operation with unidirectional flow. In such a case, a quasi-steady –state operation may be achieved in which the reactor temperature profile has maximum near the center of the reactor (Figure 23 (e)).

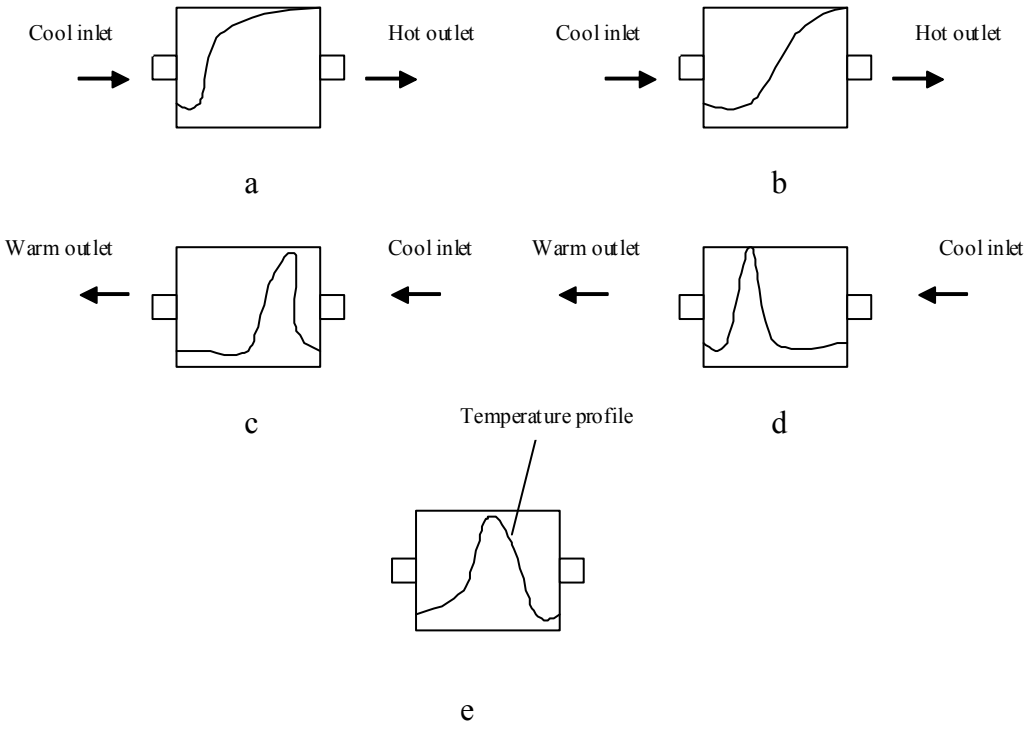


**Figure 23 The heat trap effect for reverse flow catalytic converter (a, b – forward mode; c, d – reverse mode, e - temperature profile at the quasi-steady-state**

Four-Way Single Diversion Valve Conceptual Schematic and Operation

The four-valve arrangement shown in Figure 22 may prove to be a less favorable system for vehicle installations. Because it is reasonable to expect a high level of leakage of exhaust gases with the current industrial shut-off valves, alternative design concepts had also been proposed to use rotary catalyst substrates [8]. Although the integrated design set forth in traditional rotary design was a conceptual improvement, the complication involved inhibited its use in automotive applications. An improved method [5] that combines both previous concepts is a "four-way single valve" system shown in the Figure 24.

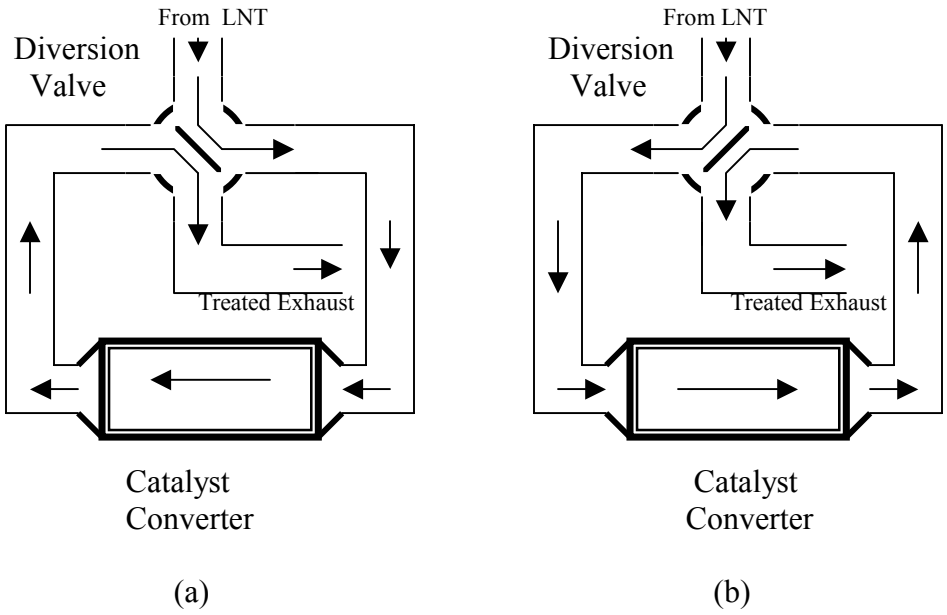


**Figure 24 Four-way single valve system: (a) - forward mode; (b) reverse mode**

The advantages of this conceptual scheme are a relatively simple design, the opportunity to minimize the leakage, and it requires a small operational torque, which is required for the valve's rotor rotation. The reverse flow catalyst mechanism (PRFCM), showed in Fig. 24 consists from three main systems, a catalytic converter (CC), four-way single diversion valve (FWSDV) and exhaust pipe system (EPS).

As was discussed before, the FWSDV seems to be an attractive option for the reverse flow catalyst design. The conceptual schematic of the FWSDV handles the reverse flow with two cylinders organized in a rotor (inner cylinder) and stator (outer cylinder) configuration. The stator has four openings arranged at right angles. The four fixed path options are the exhaust gas inlet from the LNT; to/from the oxidation catalyst and a system outlet. The rotor, which sits inside the stator acts as a divider to direct the flow of the exhaust gas. The rotor also has four path options. However, a divider plate placed across the middle separates the rotor in half. Furthermore there are four perforated openings each machined between a regular opening. In total, each side of the divider has two openings and two perforated openings alternating with each other. With the rotor placed inside the stator and with no offset, exhaust gas can enter from the LNT and is directed into the oxidation catalyst. As it exits the oxidation catalyst it re-enters the other side of the stator/rotor assembly and is directed out of the system as treated exhaust. A close-up view can be seen in Figure 25.

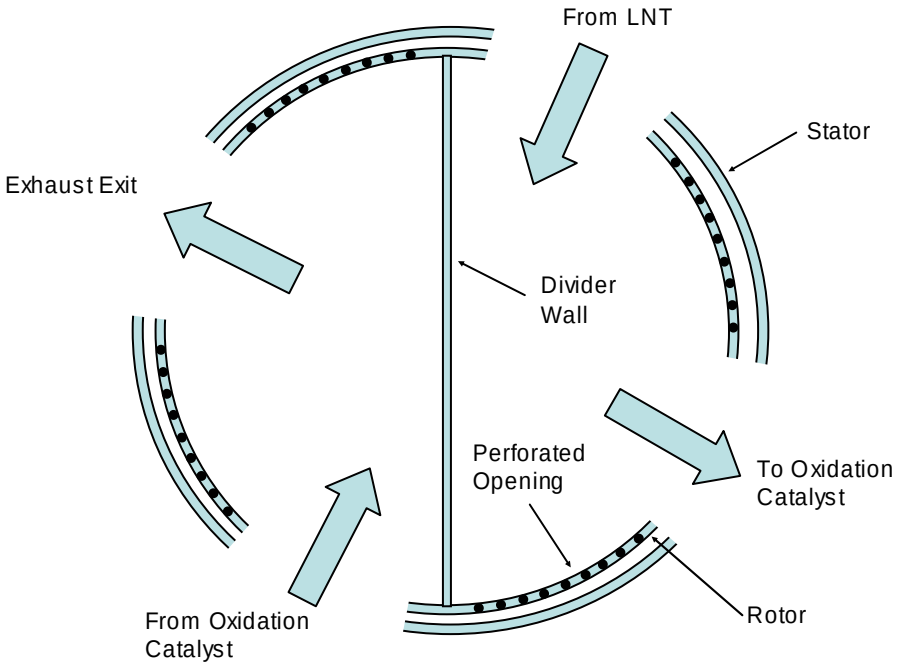


**Figure 25 Exploded View of the Stator and Rotor Assembly**

As the rotor is rotated, the flow directions are reversed and the oxidation exit becomes the entrance. The perforated openings provide a smooth transition period from forward and backward flow modes, minimizing the back pressure during the mode switching. At the same time, they prevent the leakage of the gases between the neighbor openings of the stator. To further prevent leakage, the gap between the rotor and stator walls will be minimized, yet have low enough friction to provide a smooth transition. The system can be operated in two modes, the rotor can rotate in only one direction (unidirectional) or back and forth (unidirectional). A detailed explanation of each is described in the next section.

*Unidirectional Rotation*

The total cycle of the RFC can be represented in two steady-state flow modes and transient transitional modes. Starting with no offset (0 degree), exhaust enters the assembly from the LNT and is directed to the entrance of the oxidation catalyst. This mode can be represented as Mode A. After some operation time period, the exit of the catalyst substrate is heated due to chemical reactions. At this time, the rotor is rotated to direct the LNT exhaust into the exit of the oxidation catalyst. The total motion for this operation requires that the rotor be rotated 90 degrees. During this rotation, a perforation in the rotor wall allows some exhaust to enter the rotor/stator assembly. This "slip" of exhaust is designed to reduce the back pressure effect on the engine. This transition period can be represented as Mode B. After the rotor as rotated 90 degrees, the exhaust from the LNT is now directed into the exit of the oxidation catalyst where it momentarily utilizes the reversed thermal profile to increase the catalytic reaction. This steady-state mode is represented as Mode C. As the temperature profile inside the catalyst returns to a normal profile, the rotor is again rotated another 90 degrees through a second perforation. This transient mode is represented as Mode D. As the rotor travels towards 360 degrees total rotation, the system returns to Mode A with no rotor/stator offset. A diagram of this action is represented in Figure 26. Figure 27 shows the predicted flow rate through the system for each mode.

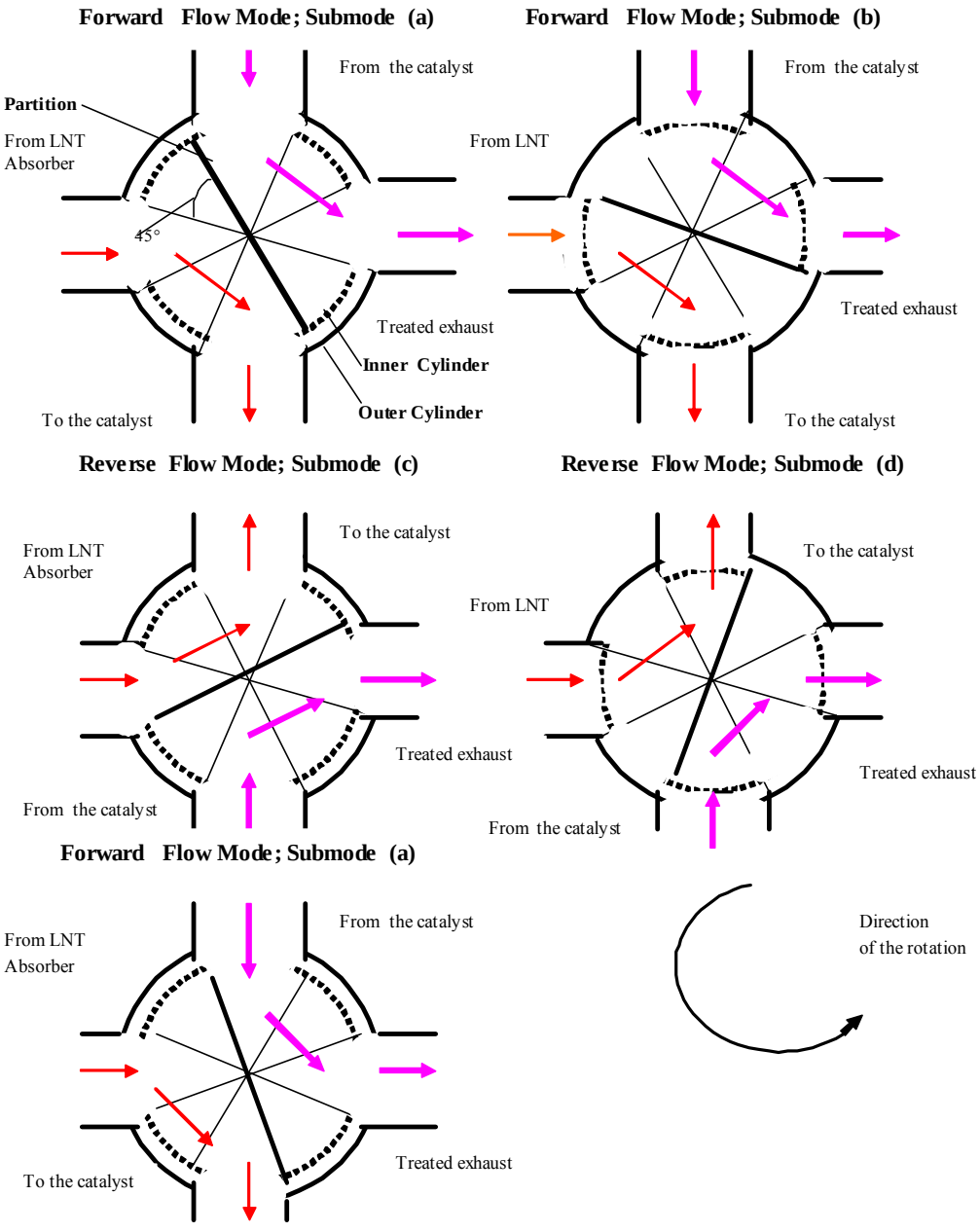


**Figure 26 Four-Way Single Diversion Valve Conceptual Schematic with Unidirectional Rotation**

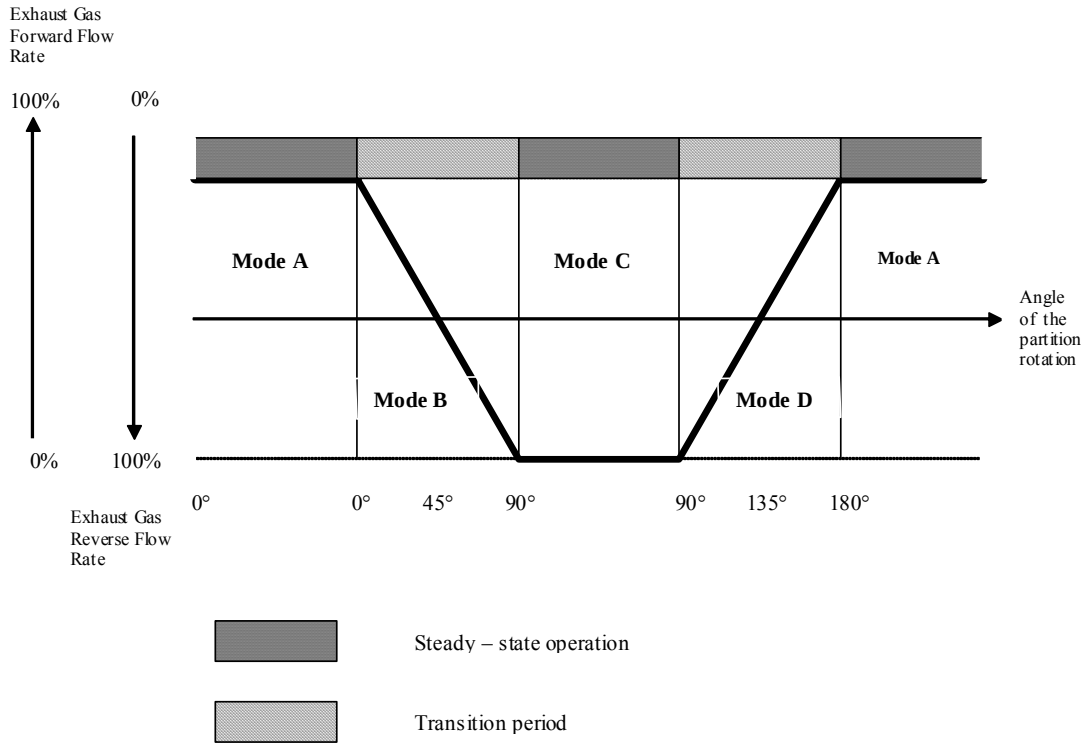


**Figure 27 Flow Rate/Rotation Diagram for Four-Way Single Diversion Valve with Unidirectional Rotation**

*Multidirectional rotation*

In addition to the unidirectional rotation option of the FWSDV, a multidirectional operation can be used. It differs from the previous option in that the rotor would rotate in two directions. When compared to the unidirectional method, the operation of Modes A, B, and C are the same. However at the end of Mode C, instead of rotating in the same direction towards Mode D, the rotor will reverse direction and travel back through the perforated Mode B to Mode A. For comparison Mode D can re-represented as Mode B'. A diagram of the operation can be seen in Figure 28 and a diagram of the flow rate effects can be seen in Figure 29.

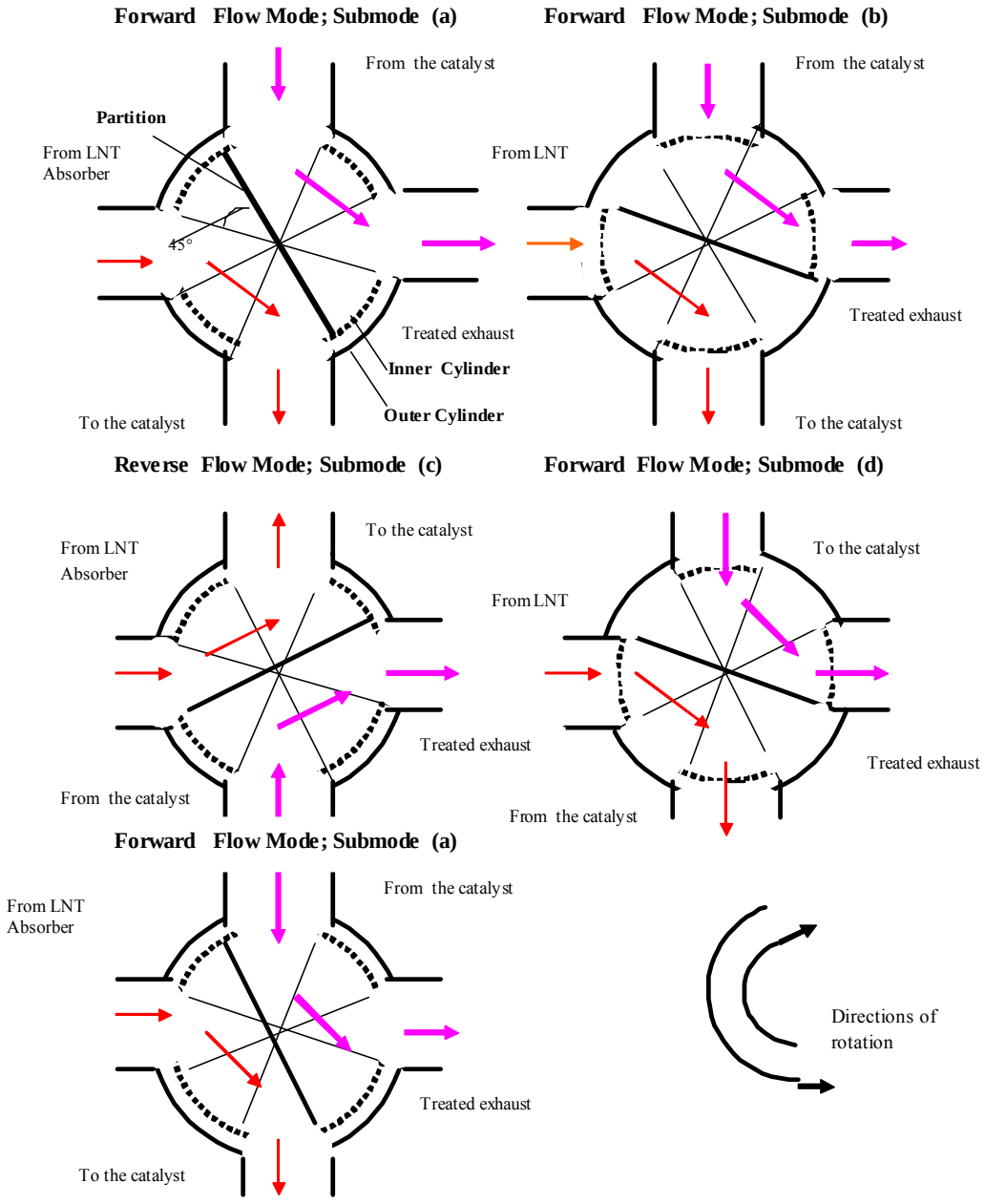


**Figure 28 Four-Way Single Diversion Valve Conceptual Schematic with Multidirectional Rotation**

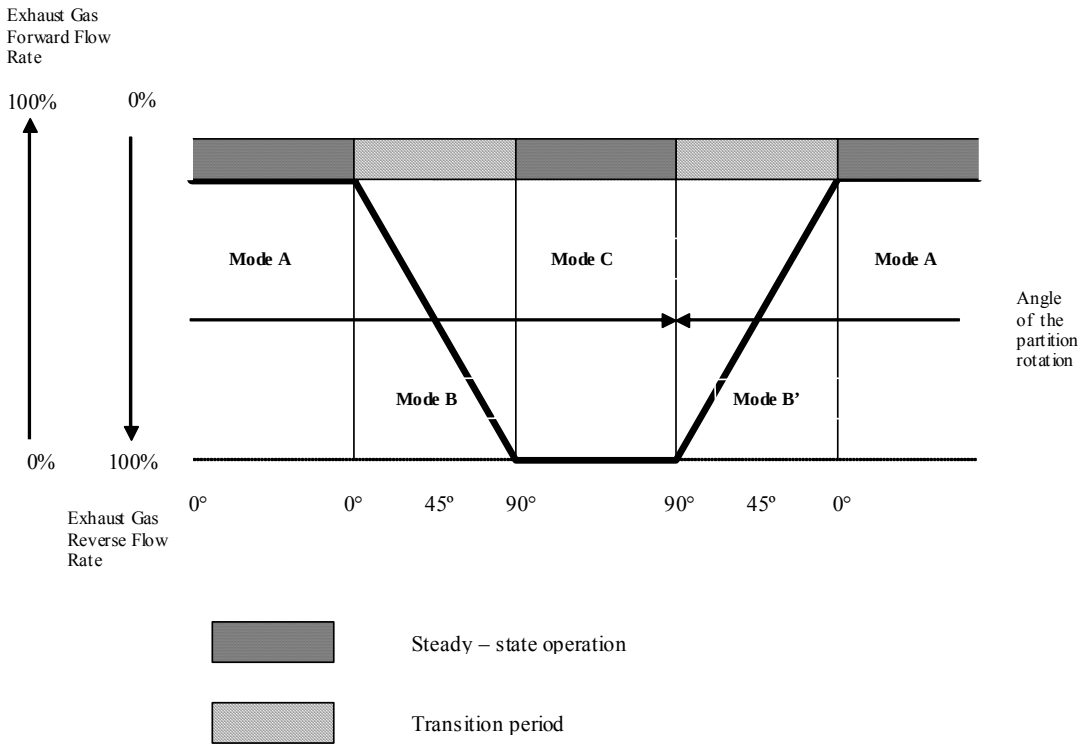


**Figure 29 Flow Rate/Rotation Diagram for Four-Way Single Diversion Valve with Multi-directional Rotation**

## Conceptual Design of a Partial Flow LNT Regeneration and Gas Divider System Progress

Estimation of the Main Dimensions of the Periodical Reverse Flow Catalyst Mechanism

*Catalyst Space Velocity Calculation*

The Space Shared Lean NOx Trap and Reverse Flow Catalyst Mechanism should be sized for the testing with CG-280 natural gas engine that has the exhaust parameters shown in Table system: There are several oxidation catalysts available for various applications but studies and experiments show that the Palladium catalyst has high conversion ratio for methane. Refer [3] Palladium catalyst with alumina wash coat is recommended for methane oxidation. The standard size of 9.5 inches diameter and 6 inches length of Palladium catalyst is used and the space velocity for this kind of catalyst equals 50,000 $hr^{-1}$ . So, the standard residence time for the entire catalyst brick could be calculated as:

$T_{rs} = 1 / 50{,}000 = 0.00002$ hr

**Table 3 Natural Gas Engine Exhaust Parameters**

| | | | Rated Power | Peak Torque |
|---|---|---|---|---|
| Exhaust gas flow rate | $V_e$ | Liter/sec | 817 | 539 |
| Exhaust gas temperature | $T_e$ | $^0C$ | 643 | 587 |
| Exhaust pipe diameter | $D_e$ | Inches | 4 | 4 |

The original space velocity of the system with the mentioned catalyst brick could be calculated for rated power as:

$SV_{643} = V_e / Vc = 422{,}235.95\ hr^{-1}$

Where, Vc is the catalyst volume; $SV_{643}$ is the space velocity for outlet gas temperature condition.

Recalculating the original space velocity at standard temperature (25 $^0C$) yields:

$SV_{25} = SV_{643} / (\rho_{25} / \rho_{643}) = SV_{643} / (916.15\ K / 298.15\ K) = 137{,}410.8\ hr^{-1}$

The original residence time could be calculated as $1 / 137{,}410.8\ hr^{-1} = 0.000007277$ hr, that is less than standard residence time for the existing catalyst brick of 0.00002 hr. However with an arrangement of two catalysts in line, the original space velocity equals to:

$SV_{25\,(2)} = SV_{25} / 2 = 68{,}705.4\ hr^{-1}$

and original residence time equals to:

$T_{ro} = 1 / 68{,}705.4\ hr^{-1} = 0.0000145549$ hr

This is more than the standard residence time for two catalysts bricks arranged in line at 0.00001 hr.

Calculations at peak torque conditions demonstrate the following results:

$SV_{643} = V_e / Vc = 278{,}563.17\ hr^{-1}$,

$SV_{25} = SV_{643} / (\rho_{25} / \rho_{587}) = SV_{643} / (860.15\ K / 298.15\ K) = 96{,}559.038\ hr^{-1}$

The original residence time could be calculated as $1 / 96{,}559.038\ hr^{-1} = 0.000010356$ hr, which is less than standard residence time for the existing catalyst brick.

For two bricks in line:

$SV_{25\,(2)} = SV_{25} / 2 = 48{,}279.519\ hr^{-1}$

and the original residence time equals to:

$T_{ro} = 1 / 48{,}279.519\ hr^{-1} hr^{-1} = 0.0000207127$ hr,

This again is more than standard residence time for two catalysts breaks arranged in line at 0.00001 hr.

In conclusion, calculations show that two 6" × 9 ½" catalyst breaks could provide the appropriate CH4 oxidation for both rated power and peak torque conditions.

*Calculation of the Dimensions of the Rotor and Stator Openings*

As shown in the Fig. 25, the FWSDV is required to have four manifolds. An engine of this rating usually requires four inch exhaust piping. Taking this in to consideration, it cajn be expected that the FWSDV diameter could reach up to 14-15 inches. In order to decrease the diameter of the FWSDV two approaches were considered:

i. to decrease the area of the openings in two times
ii. to switch the round shape of the openings to the elliptical one.

The cross section area of the engine's 4-inch exhaust manifold equals to 81,032 $cm^2$. With the maximum exhaust gas velocity at rated power, the maximum exhaust flow rate can be calculated to be could be estimated at rated power regime (that corresponds to the maximum flow rate of the exhaust gases) exhaust gas flow rate as:

liters/sec / 0.81032 $dm^2$ = 100.8 m/s

Following the first approach, the cross section area of the valve's manifolds should be roughly of 40.5 $cm^2$ that corresponds to the diameter of the round opening of 7.2 cm. The ellipse with the same cross section area could have the following dimensions of the axes: 10.8 cm and 4.8 cm. The velocity of the exhaust gases through the existing elliptical opening will be of 201.6 m/s. The FWSDV rotor has four perforated openings (Fig. 4). As will be shown later each perforated

opening consists of 43 round holes with diameter of 0.8 cm. So exhaust gas velocity could be calculated as:

$Vexh = 812 \text{ liters/sec} \times 4 / (3.14 \times 0.08^2 \text{ dm}^2 \times 43) = 375.87 \text{ m/s}$

Thermodynamic calculations of the fuel-lean combustion of natural gas and air with an equivalence ratio of 1.7 were performed in order to estimate the velocity of sound in the exhaust gases and compared with the calculated velocity of the gases that pass through the perforated opening. The following conditions were used for the estimation of the sound velocity:

Temperature of combustion products: T=1642 K;

Molecular mass of combustion products: $\mu$=28.2

Specific heat ratio: $\gamma$=1.272

Taking into account the relaxation of the combustion products temperature up to 643 $^0$C ($\approx$ 946 K), the velocity of sound is calculated to be:

$a = (\gamma \times R \times T/\mu)^{1/2} = 595.62$ m/s

From this it is concluded that the velocity of the exhaust gases in the perforated opening will not exceed the velocity of sound. As a result, the dimensions for the stator's and rotor's regular and perforated openings were established. In addition, these dimensions became the base for the estimation of the rough outer diameter of the valve, which is to be 165 mm.:

Ellipse's axes: 108 mm × 48 mm;

The diameter of the holes in the perforated opening: 8mm;

The quantity of holes: 43.

*Permissible Valve Leakage Calculation*

Inherent to the reverse flow valve design is that a small amount of exhaust gas will by pass the oxidation catalyst untreated during the flow reversal. In order to still meet future federal regulations, a calculation needed to be performed to determine the allowable leakage rate. Since the reversing valve is after the NOx adsorber, we are only interested in the effect of the oxidation catalyst. Therefore only the leakages of HC and CO are studied and since the ARES goal is geared toward stationary natural gas engines, the emission regulations set forth in the Code of Federal Regulation Part 40 for non-road engine are used. New terminology in the CFR allows lean burn natural gas fueled engines to be classified and tested as compression ignition engines. Therefore the following calculations were made using the Tier 4 regulations for non-road engines in the 175 $\leq$hp $\leq$ 750 hp range. These emission standards are to take effect in the 2011 to 2013 timeframe. The Tier 4 says that the emission reductions can be achieved through the use of control technologies; including advanced exhaust gas after treatment. The allowable limits are given as follows:

NMHC → 0.14 gms/hp-hr.

CO → 2.6 gms / hp-hr.

Data are obtained corresponding to the engine speed of 1800 rpm and the leakage calculations are made for various engine speeds (10%, 25%, 50%, 75% and 100%).

Since the leakage is largely affected by exhaust flow and engine backpressure, the leakage (both volumetric and mass flow) rates are calculated at rated speed and load conditions. To match other ARES work on the test engine, an engine speed of 1800 rpm is used for these conditions. At rated conditions. the exhaust composition downstream of LNT (Lean Nox Trap) is 1117 ppm of HC and 546 ppm of CO. With the engine at 100% load (252 hp), the amount of Hydrocarbon (HC) and Carbon monoxide (CO) allowed from emission standards in terms of grams per minute is calculated as

HC = 0.588 $\frac{gms}{\min.}$ and 10.92 $\frac{gms}{\min.}$ respectively. Now, it is required to find out the amount of HC and CO that are allowed to by pass the catalyst for the same engine load and speed. The calculation involves various steps including finding out the volumetric flow rate, temperature, partial pressure, density and mass flow rate of the exhaust compositions.

Step 1: Finding out the volumetric flow rate of HC and CO:

Knowing the diameter and the length of catalyst the total volume for 2 catalysts is found to be 0.4922 cubic feet. The space velocity corresponds to 1800 rpm is 68,409 $hr^{-1}$. Now, the Exhaust flow rate = space velocity X Volume of catalysts

= 68,409 X 0.4922

= 561.1818 cubic feet per minute.

Volumetric flow rate = mole fraction X exhaust flow rate

(Volumetric flow rate) $_{HC}$ = 1117 x $10^{-6}$ X 561.1818

= 0.0177 cubic meter per minute.

(Volumetric flow rate) $_{CO}$ = 546 x $10^{-6}$ X 561.1818

= 0.3064 cubic meter per minute.

Step 2: Partial pressure of HC and CO:

The pressure of the exhaust composition down stream of the LNT is 2 atm. So the partial pressure of Hydro carbon (HC) and Carbon monoxide (CO) is calculated as follows:

Pp (HC) = 16.7 x 1117 x $10^{-6}$ = 0.01865 psi = 128.587 $N/m^2$

Pp (CO) = 16.7 x 546 x $10^{-6}$ = 0.00912 psi = 62.868 $N/m^2$.

Step 3: Density of HC and CO:

The density of HC is $\rho_{HC} = \frac{Pp(HC)}{R_{HC} \times T}$ and the density of CO is $\rho_{CO} = \frac{Pp(CO)}{R_{CO} \times T}$.

The temperature of HC and CO downstream of LNT is 873 K and the gas constants for HC and CO are 0.6395 J/gm- K and 0.297 J/gm- K respectively. Now,

Density of HC is $\rho_{HC} = \frac{128.587}{0.6395 \times 873}$ = 0.2303 grams per cubic meter.

Density of CO is $\rho_{CO} = \frac{62.868}{0.297 \times 873}$ = 0.2425 grams per cubic meter.

Step 4: Mass flow rate for HC and CO:

a. Mass flow rate of HC is $\dot{m}_{HC} = \rho_{HC}$ x (Volumetric flow rate) $_{HC}$

= 0.2303 x 0.0177

= 0.00407 grams per minute

b. Mass flow rate of CO is $\dot{m}_{CO} = \rho_{CO}$ x (Volumetric flow rate) $_{CO}$

= 0.2425 x 0.3064

= 0.002104 grams per minute

Step 5: Leakage rate:

It is required that the mass flow rate allowed from the CFR should be greater than or equal to the mass flow rate of the gas coming out of the system, which is given by

$$\overset{*}{m}_{law} \geq \overset{*}{m}_{(outofcatalyst)} + \overset{*}{m}_{(pastthecatalyst)}$$

$$\geq (1 - \text{conversion efficiency})\ \overset{*}{m}_{engine} + \overset{*}{m}_{(leakage)}$$

Leakage rate for HC:

$$\overset{*}{m}_{(leakageHC)} \leq -(1 - \text{conversion efficiency})\ \overset{*}{m}_{engine}$$

$$\leq 0.5\ \overset{*}{m}_{law}\ 88 - (1 - 0.90) \text{ x } 0.00409$$

$$\leq 0.5875 \text{ grams per minute}$$

Leakage rate for HC:

$$\overset{*}{m}_{(leakageCO)} \leq \overset{*}{m}_{law} - (1 - \text{conversion efficiency})\ \overset{*}{m}_{engine}$$

$$\leq 60.48 - (1 - 0.90) \text{ x } 0.002104$$

$$\leq 10.919 \text{ grams per minute}$$

Thus, it is calculated that the maximum leakage that is allowed to by pass the catalyst for Hydrocarbon (HC) is 0.5875 grams per minute and that of Carbon monoxide (CO) is 10.919 grams per minute

## Four-Way Single Diversion Valve Design

### *Valve Assembly Description*

The concept of multidirectional rotation was used to simplify the design of the valve drive system. The design of the diversion valve consists of two cylinders, one rotating inside the other, which is stationary. A partition plate is welded to the inner cylinder and the alternating rotation of inner cylinder causes periodic flow reversal. The valve assembly also includes a top plate, a top cap, a top flange, a gasket and a steel washer. A diagram of the four-way single diversion valve is provided in Figure 30.

To simplify construction, the outer cylinder (1) and inner cylinder (2) are fabricated from standard dimensional pipe available through retail. Although the gap between the inner and outer cylinders is very small, the leakage through this gap can have an effect on the system performance. To accommodate the required seal and the rotation of the valve a labyrinth type seal will be used. Furthermore at the center of the outer cylinder, an arrangement for sleeve seating is provided on which the inner cylinder will rest and rotate. This prevents the direct surface-to-surface contact between the inner and outer cylinder and hence avoids possible wearing during rotation.

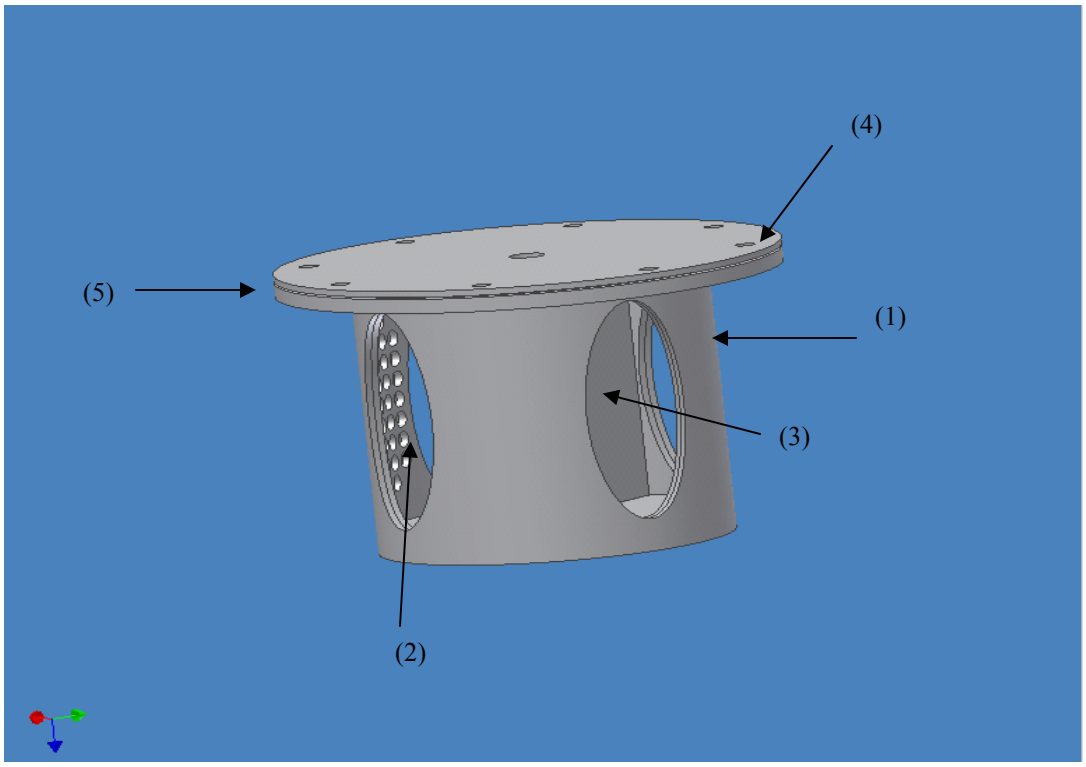


**Figure 30 Four-Way Single Diversion Valve – (1)Outer cylinder; (2) Inner cylinder; (3) Partition Plate; (4) Top cap; (5) Top flange**

*Description of the Outer Cylinder*

For the outer cylinder, the outer diameter is 166.275mm and the inner diameter is 160.275mm. Four elliptical openings are provided at 90-degree increments in order to facilitate both forward and reverse flow. A small seating arrangement lip is provided near the upper surface of the outer cylinder. This has been provided to maintain accuracy when assembling the flange and other parts. Figure 31 shows the snap shot of the outer cylinder.

As a requirement for assembly, a flange will be seated around the top of the outer cylinder at the flange seating (item 2 in Figure 31). The flange is provided in order to connect the outer cylinder with a assembly top cap. The flange is also provided with a seating arrangement for a copper gasket and a steel washer used to seal the assembly. The steel washer provides a small gap between the plate and the cap and leaves room for the valve to rotate. Figure 32 shows the top flange

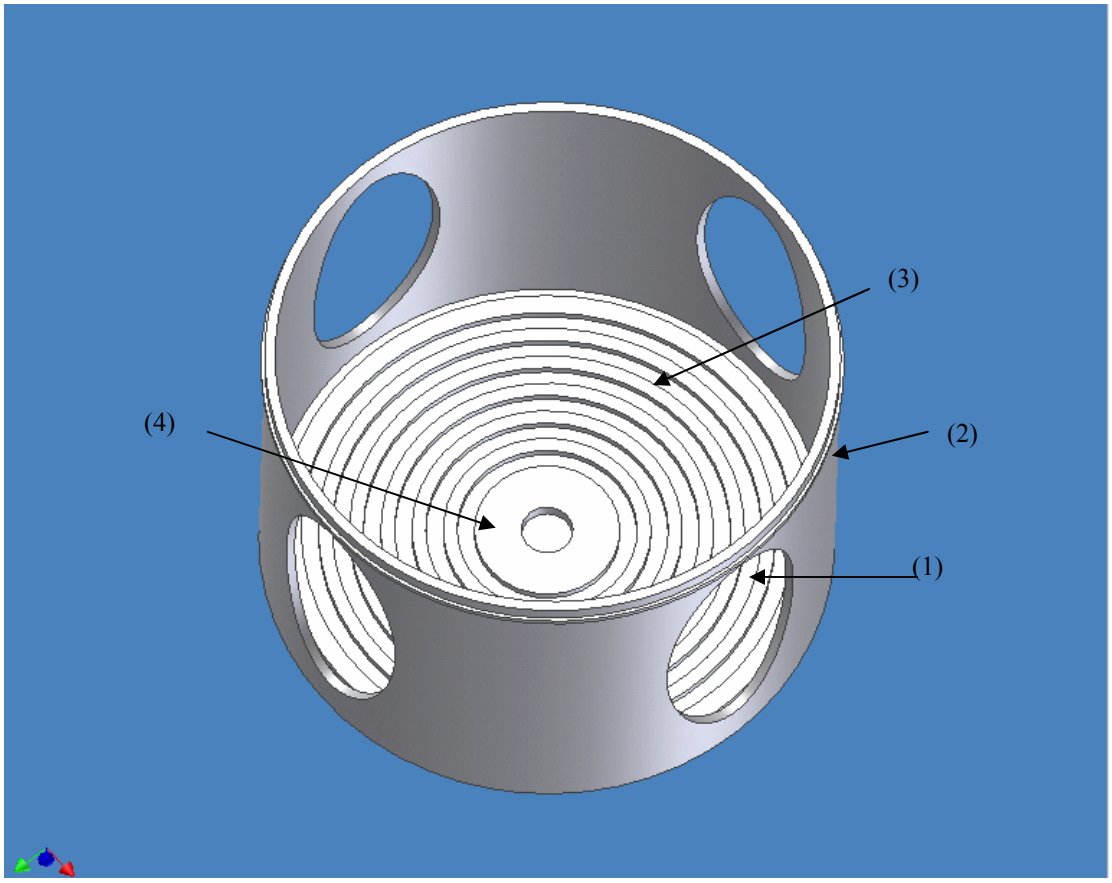


**Figure 31 Outer Cylinder/Stator – (1) Elliptical hole; (2) Flange seating; (3) Labyrinth sealing; (4) Sleeve seating**

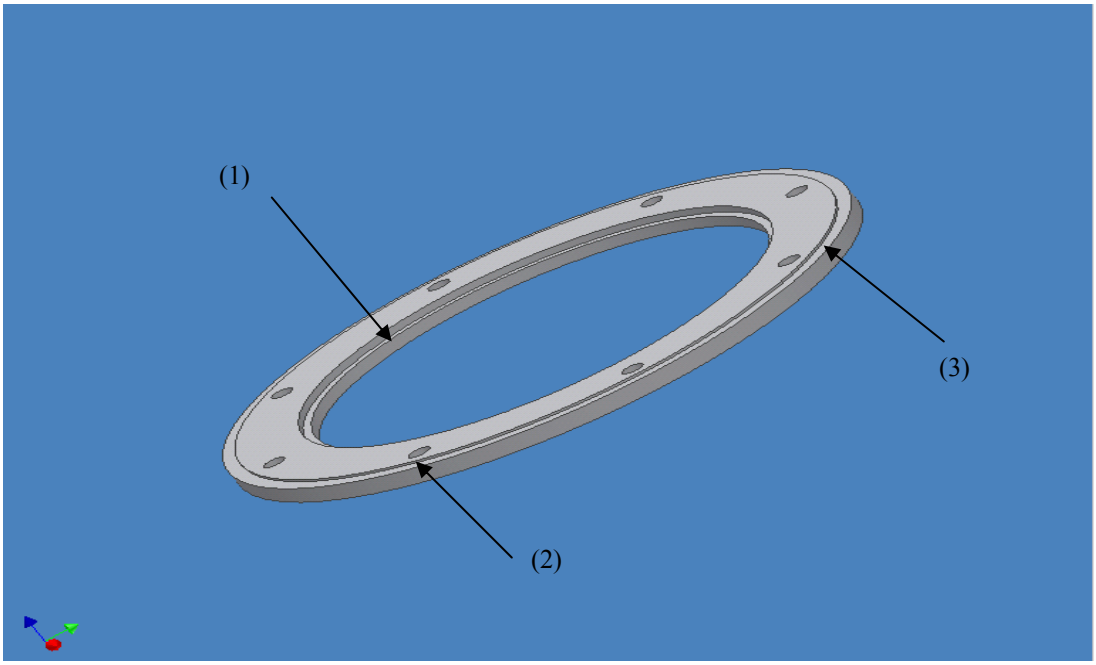


**Figure 32 Flange – (1) Flange Seating; (2) Assembly Bolt Holes; (3) Gasket Groove**

*Description of Inner Cylinder*

While the outer cylinder remains stationary, the inner cylinder rotates 90 degrees alternatively to provide the full cycle that includes one forward and one reverse mode. As with the outer ctlinder, the inner cylinder has four elliptical holes and four perforated opening. The elliptical patterns are provided in order to avoid the complete blockage of the exhaust gas while the inner cylinder is rotating inside the outer cylinder. For clarity, the snap shot of inner cylinder is provided in Figure 33.

A base plate (item 4 in Figure 33) is positioned flush with the bottom of the inner cylinder and provides a slot for the partition plate. This plate will be press fit into the inner cylinder. The bottom of the base plate provides the top surface of the lower labyrinth seal. Once the lower plate is in place, the partition plate is press fit into its slot. To complete the inner cylinder assembly, a top plate is press fit flush with the top of the inner cylinder and the partition plate. A diagram of the top plate can be seen in Figure 34.

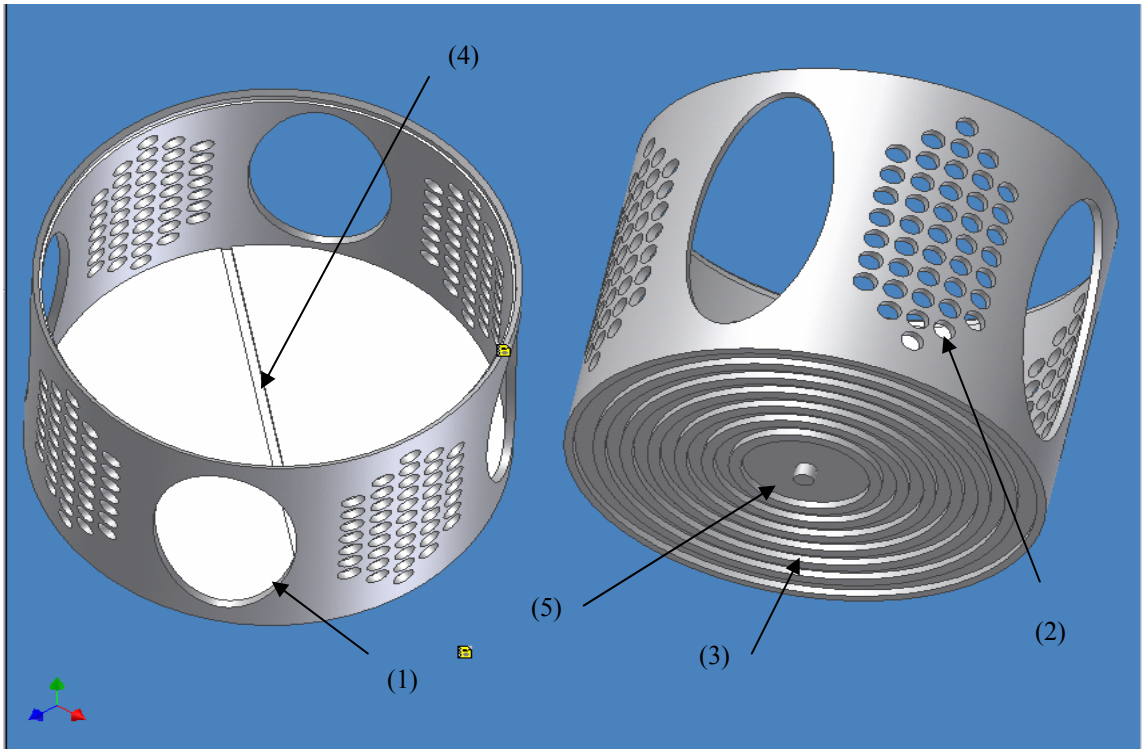


**Figure 33 Inner Cylinder – (1)Elliptical opening; (2) Perforated in elliptical opening; (3) Labyrinth sealing; (4) Lower Base plate with groove for partition plate; (5) Projection to maintain gap**

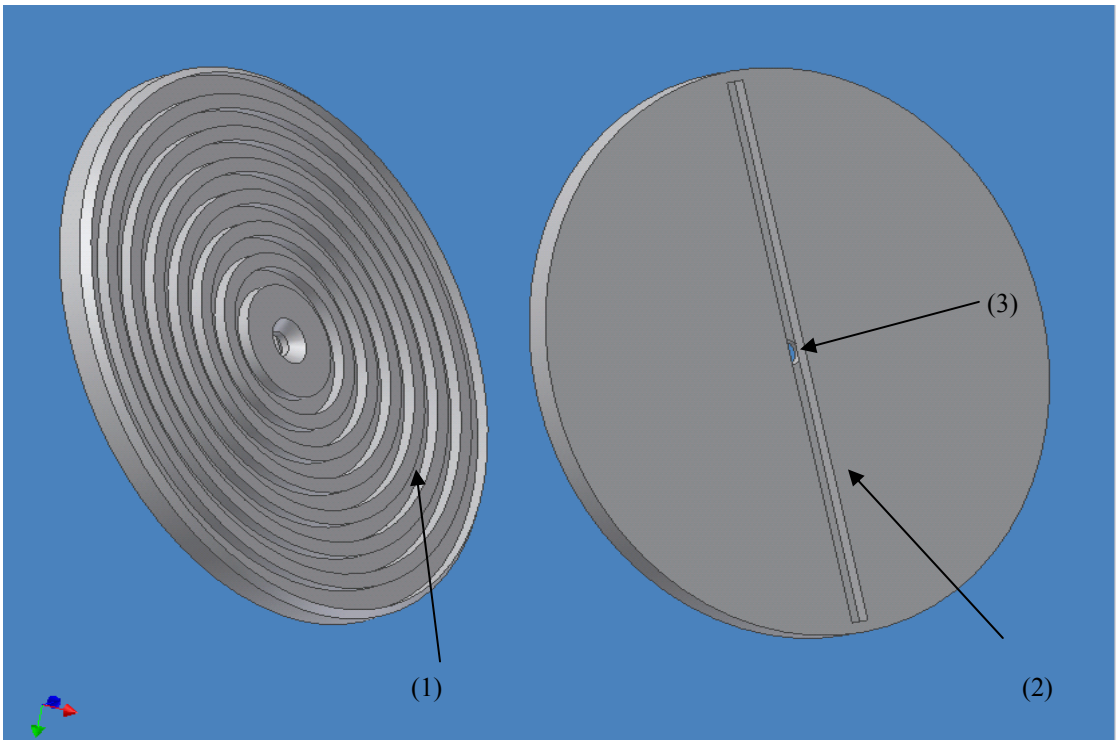


**Figure 34 Top Plate - (1) Labyrinth sealing; (2) Slot for partition plate; (3) Shaft Hole**

*Description of the Top Cap*

After the inner cylinder has been assembled and the placed inside the outer cylinder assembly a top cap plate is bolted to the flange of the outer cylinder. The plate is shown in Figure 35. The labyrinth sealing surface on the bottom side of the top cap is mated with the sealing surface on the top of the inner cylinder to provide a leak proof seal. A circular hole is provided at the center and is where the rotation shaft passes through to the inner cylinder. The other end of the shaft is connected to the cylinder piston arrangement and will be discussed in the next section. However a sectional view of the assembled valve can be seen in Figure 36

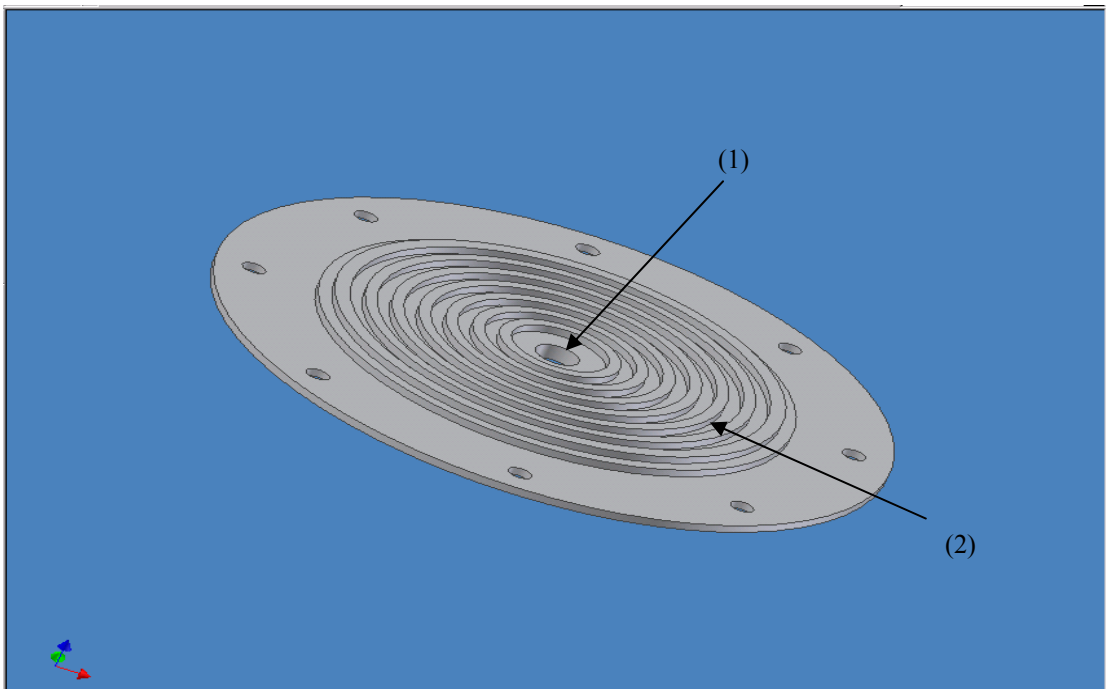


**Figure 35 Top Cap - (1) Hole for Rotation Shaft; (2) Labyrinth Sealing**

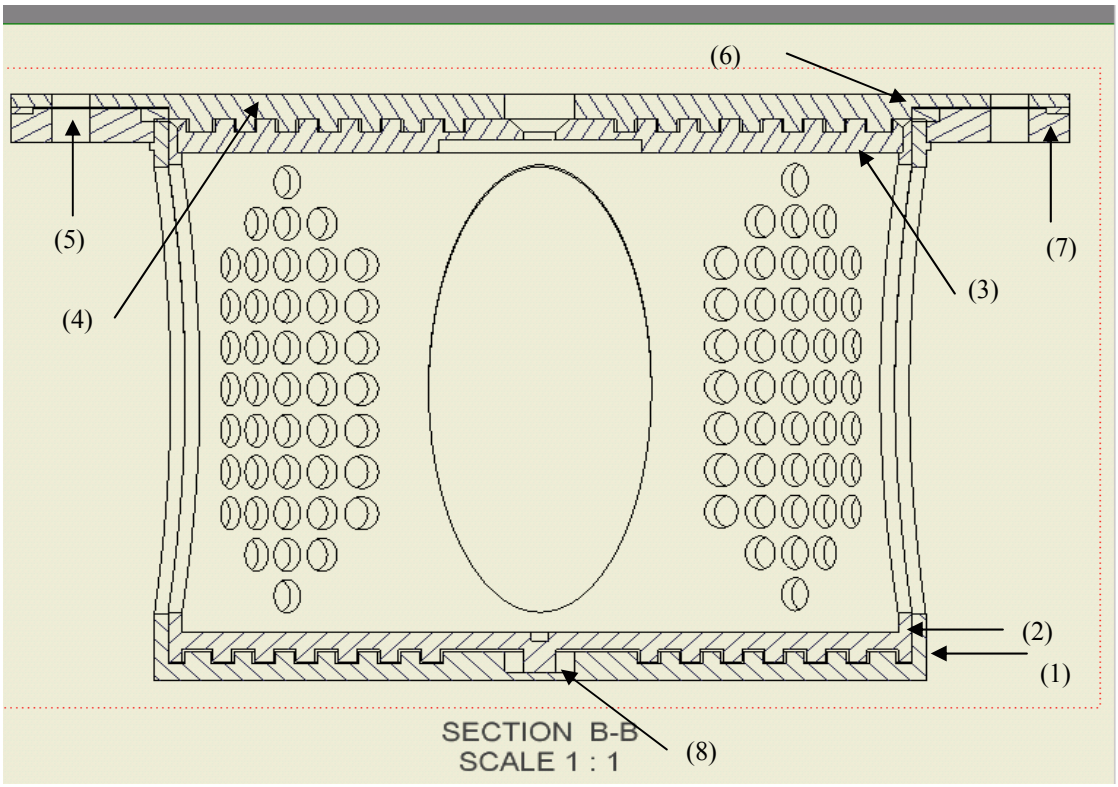


**Figure 36 Valve Assembly - (1) Outer Cylinder; (2) Inner Cylinder; (3) Top Plate; (4) Top Cap; (5) Assembly Bolt Holes; (6) Copper Gasket; (7) Steel Washer**

*Description of Elliptical-to-Circular Pipe Connector*

Since the valve openings are elliptical, an adapter is required to go from circular exhaust pipe to the elliptical opening. The specially fabricated pipe connector has a circular opening at one end and elliptical opening at another end. The exhaust pipe is connected to the circular opening using standard Marman flanges and the elliptical opening is welded with the outer cylinder of the valve. Four such pipe connectors are used, two at the inlets to the valve and two at the outlets from the valve. Figure 37 shows the pipe connector.

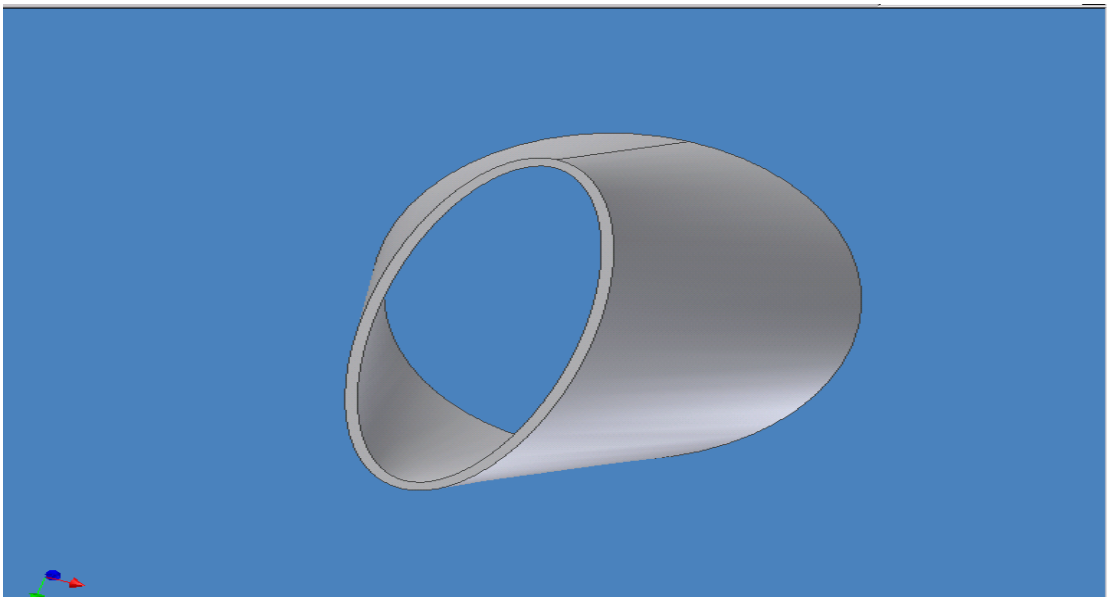

**Figure 37 Pipe Connector**

*Operation of Valve Drive Mechanism*

The multidirectional rotation of the valve is achieved through a reciprocating mechanism. The mechanism consists of an air piston and a drive arm. The piston end is connected to the rotational shaft, which is connected to the inner cylinder of the four way single diversion valve. Figure 38 shows the schematic diagram of the assembly and the estimated dimensions of the piston stroke based on the dimension of the valve, the valve's rotation and dimensions of the air cylinder. The linear movement of the piston rotates the inner cylinder and each full stroke of the piston rotates the inner cylinder 90 degrees.

Since the air cylinder turns from the axial position during the displacement of piston, tie rods are used to connect the piston end to the arm. The male tie rod is connected to the steel arm and the female tie rod is connected to the piston rod. The two tie rods are coupled so that the piston cylinder arrangement rotates the steel arm 90 degrees. Therefore the steel arm makes alternate rotation through 90 degree in both clock wise and anti-clock wise direction, which in turn rotates the inner cylinder of the valve through 90 degree alternatively. The inner cylinder shaft is fabricated with two steps, one having the diameter of 0.275 inches for the length of 2.00 inches. This end goes through the hole in the top cap and is secured to the top plate. The other end has the diameter of 0.50 inch for the length of 0.75 inches. A steel coupler is fabricated that couples the shaft with the steel arm. For clarity, the pictures of the shaft, coupler and the steel arm are provided in Figure 39. Figure 40 shows the complete motion control arm assembled.

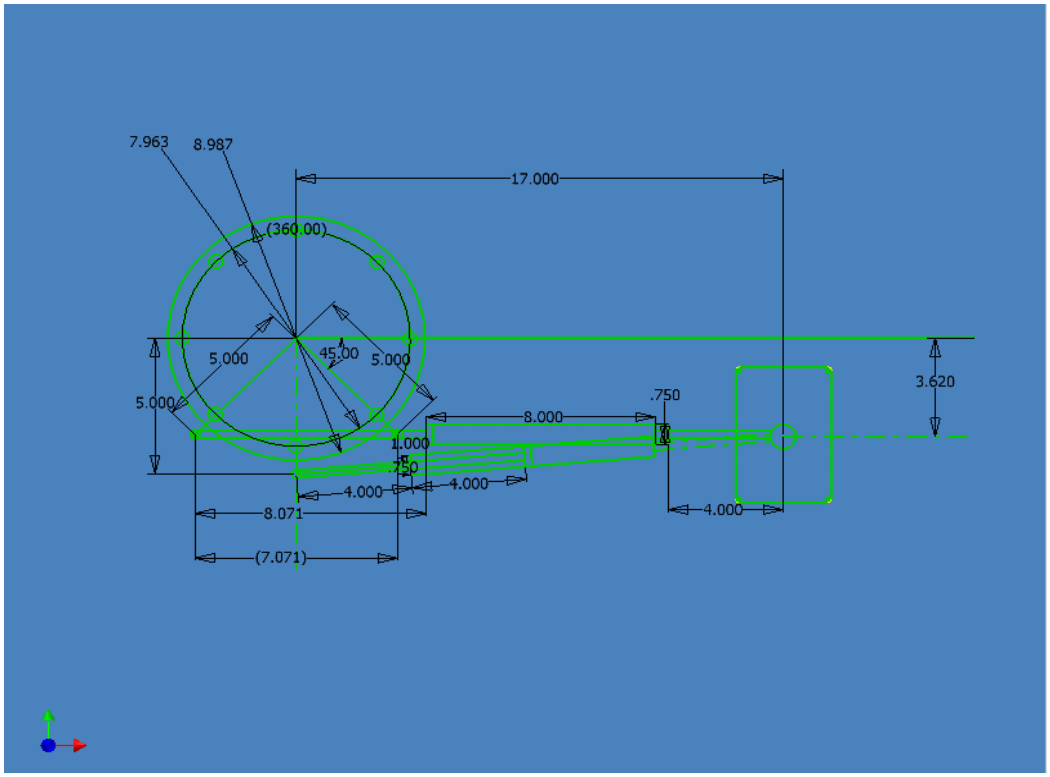


**Figure 38 Schematic Diagram of the Motion Control Mechanism**

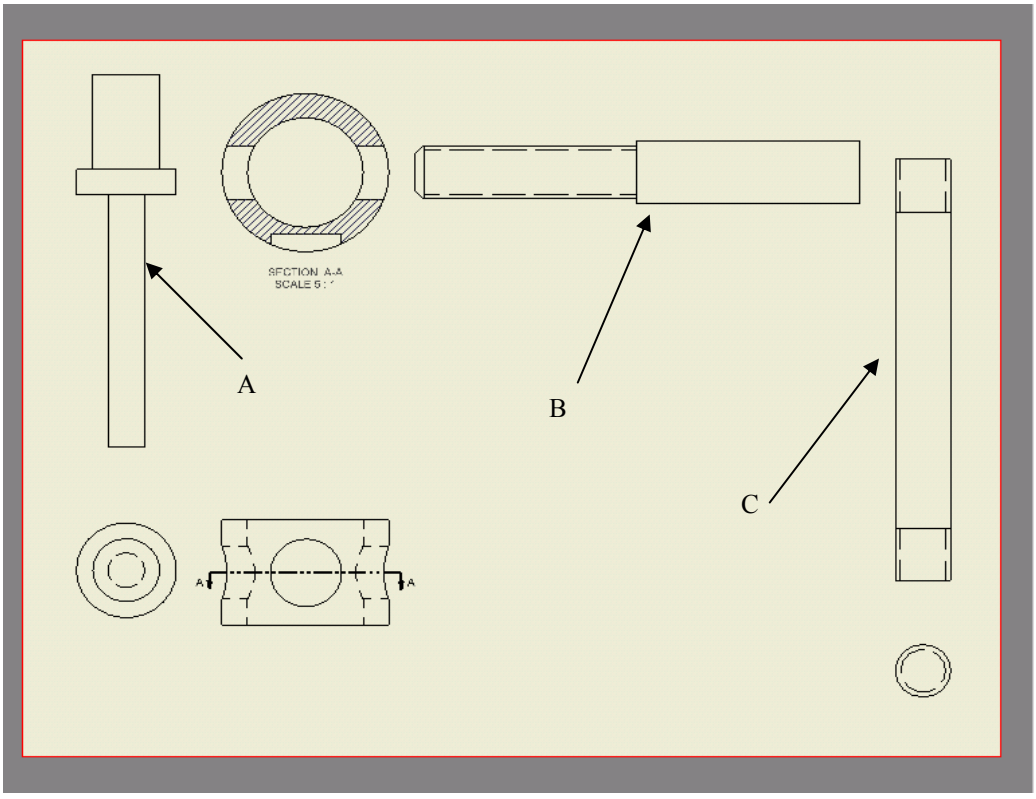


**Figure 39 (A) Shaft; (B) Coupler; (C) Steel arm**

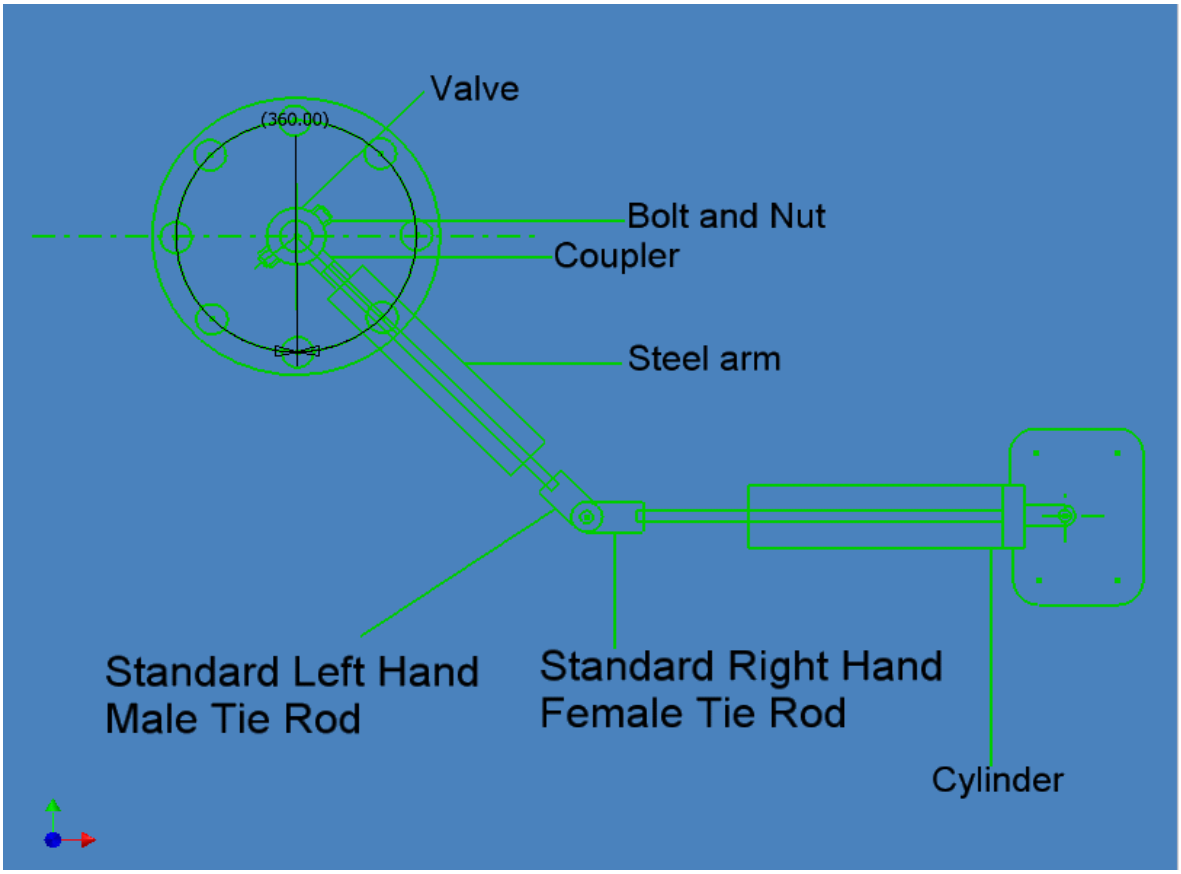


**Figure 40 Schematic of Assembled Motion Control Arm**

## Lean Burn Natural Gas Engine Testing and $NO_x$ Reduction Strategy Review

Test Bed Development

The test bed was developed to allow both The University of Tennessee and the Oak Ridge National Lab (ORNL) to evaluate their unique LNT systems, applied to a lean burn natural gas engine. The development of the test bed, including installation of the engine and setup of all controls and data acquisition for LNT management, has been completed and was reported in Report 1. Table 4 shows a summary of the engine specifications. While this engine is not in the size range of interest to the ARES program it serves as a practical starting point for assessing the catalyst technology.

**Table 4 Cummins Engine Specifications**

| C Gas Plus General Engine Data | | |
|---|---|---|
| Name | C Gas Plus | |
| Model | CG-280 | |
| Type | 4 Cycle; In-Line 6 Cylinder | |
| Bore x Stroke (mm) | 114 x 135 | |
| Displacement (L) | 8.3 | |
| **General Performance Data** | **Peak Power** | **Peak Torque** |
| Engine Speed (rpm) | 2400 | 1400 |
| Engine Power (kW) | 209 | 169 |
| Engine Torque (N-m) | 831 | 1153 |
| Inlet Air Flow (L/sec) | 293 | 205 |
| Exhaust Gas Flow (L/sec) | 817 | 539 |
| Exhaust Gas Temperature (C) | 643 | 587 |
| Nominal Fuel Consumption (kg/hr) | 47 | 34 |
| Inlet Air Restriction (mm H2O) | 445 | |
| Exhaust Restriction (mm Hg) | 102 | |

Currently the LNT system for ORNL and UTK is installed on the test bed to allow for an initial catalyst evaluation and development of regeneration parameters. This LNT system consists of a dual path $NO_x$ adsorbing catalyst system shown below in Figure 41. One leg of the dual path system is regenerated while the other is in the adsorption stage. Methane is injected into the exhaust stream ahead of the catalyst to create the fuel rich environment necessary for regenerating the LNT, and a set of pneumatically actuated exhaust brake valves are used to control the space velocity. The catalyst system consists of an oxidation, reformer and LNT catalyst developed by EmeraChem.

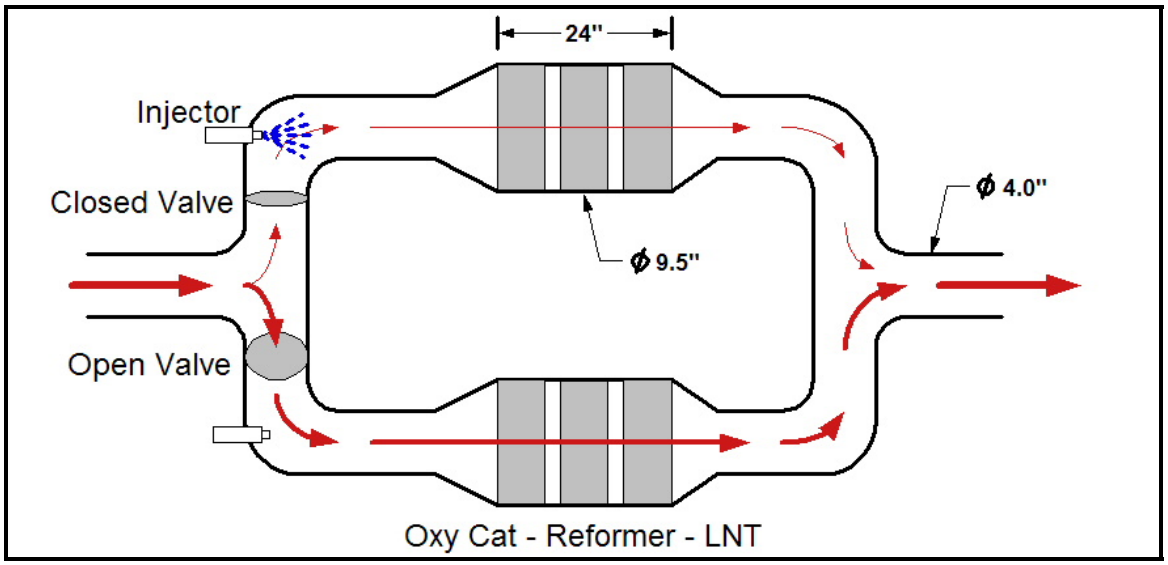


**Figure 41 Dual leg Catalyst System Schematic**

Initial Engine Baseline

The baseline performance and emissions of the 8.3-liter natural gas engine have been characterized at a matrix of operating points. Some initial catalyst volume estimates have been made based on exhaust flow, NOx level and temperature data. Baseline results were also used to determine the validity of translating data from bench flow studies to full-scale engine data. This baseline data also allowed us to investigate the scalability of the 8.3-liter engine compared to the larger genset engines of interest to the ARES program. Figure 42 shows a matrix of engine out NOx levels for the C Gas Plus.

Development of LNT Regeneration Strategy

Methane will be used as the reducing agent for the LNT. Before the storage sites of the catalyst become saturated methane will be injected into the exhaust directly upstream of the catalyst. Control over the injection rate will allow for control of the exhaust composition entering the catalyst. In addition, during regeneration the space velocity must be controlled across the catalyst to allow enough time for $NO_x$ release and subsequent reduction. This was accomplished by throttling the exhaust flow with a set of exhaust brake valves.

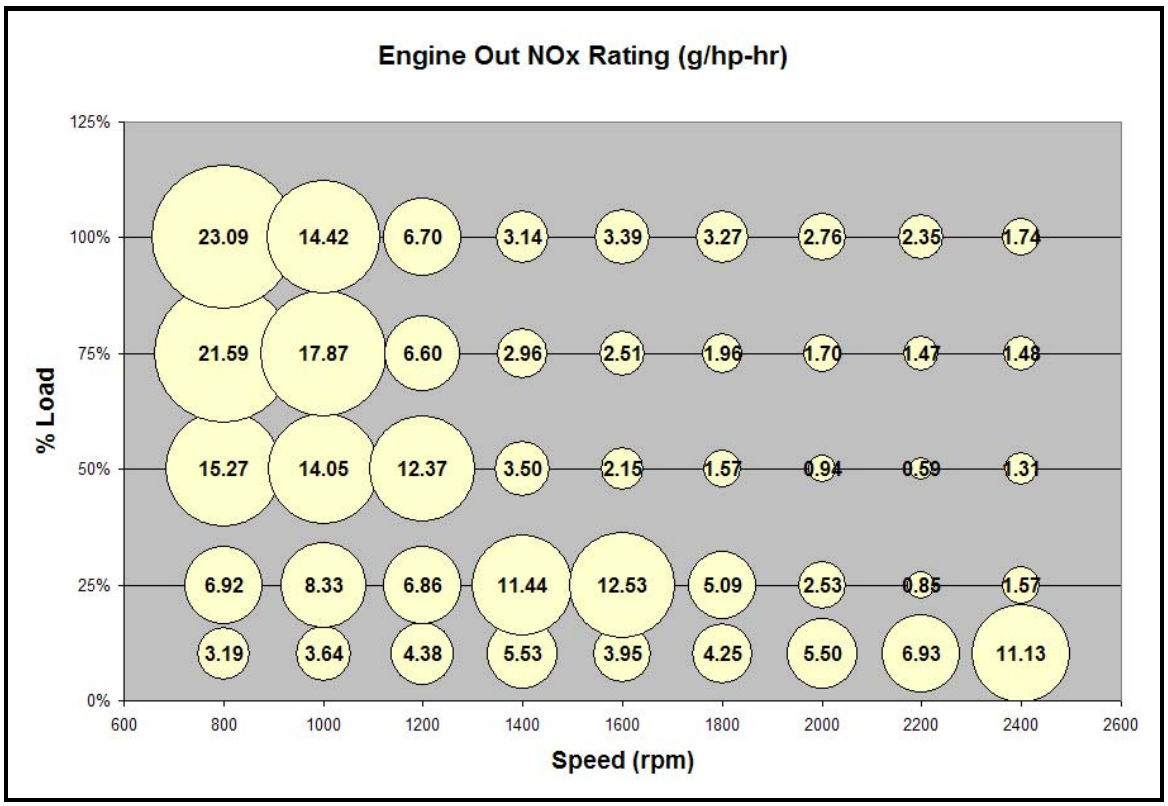


**Figure 42 NOx Rating**

## Lean Burn Natural Gas Engine Testing and $NO_x$ Reduction Strategy Progress

Exhaust Aftertreatment System

Aftertreatment of lean burn natural gas NOx was achieved through implementation of a dual path NOx adsorbing catalyst system as shown in Figure 43. The dual path system allows for NOx reduction by managing the LNT catalyst on a time-shared schedule. By periodically alternating the flow, the catalyst leg can flow the majority of the exhaust while in its adsorption mode. When it is time to regenerate the catalyst, the majority of the flow is diverted through the bypass leg. Restricting the flow across the catalyst during regenerating serves two purposes; the lower catalyst space velocity allows enough time for the release and reduction of stored NOx and the lower mass flow rate of lean exhaust gasses reduces the amount of reductant needed to create the correct stoichiometry for regeneration. This consequently reduces the fuel penalty.

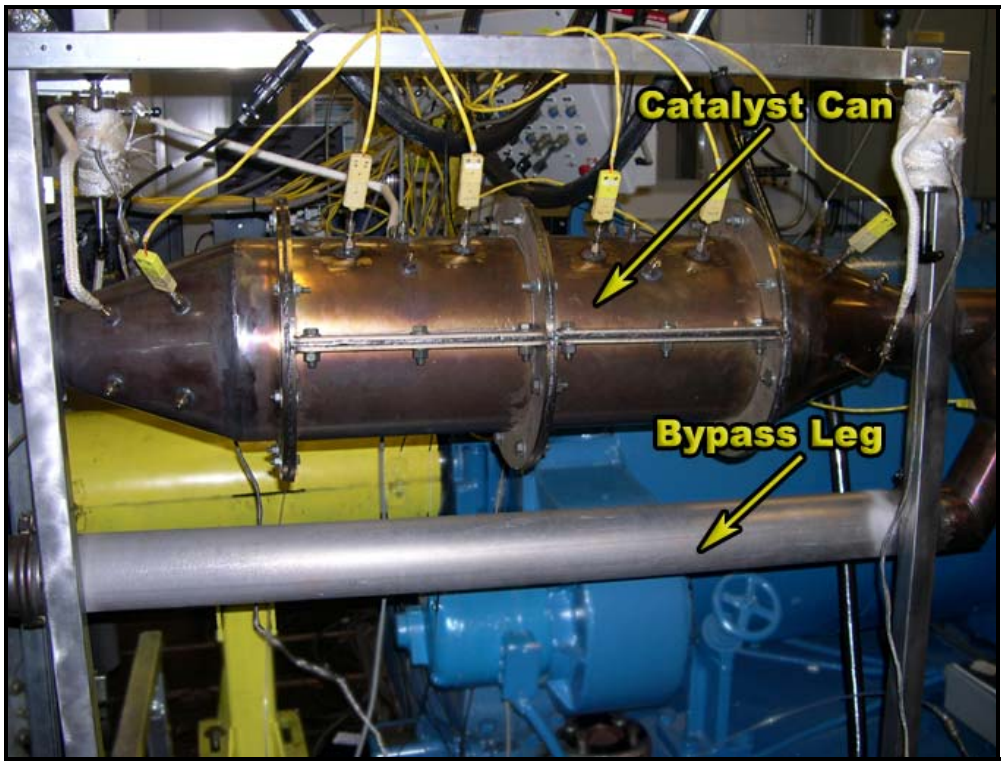


**Figure 43 Exhaust Aftertreatment System Photograph**

For the purpose of simplifying the experiment, only one leg of the system contains catalyst bricks. In an actual application, both legs of the system would contain catalysts. However, the single chamber system was used here to evaluate the lean NOx trap's ability to store and reduce NOx as well as the reforming catalyst's ability to break down methane into a usable source for regeneration. Projections of the conversion efficiencies and fuel penalties for a two chamber system were made from measurements of the one chamber system.

For this research, the same compressed natural gas supplied to the engine was used as the reducing agent. Shown in Figure 43, a pair of automotive injectors introduced the reductant directly upstream of the catalyst can. The injectors were actuated by a 75 Hz square wave signal. Adjusting the duty cycle of this signal controlled the amount of reducing agent introduced. The natural gas supplied was primarily methane. However, efficient regeneration of an LNT requires hydrogen or carbon monoxide in an oxygen free environment. Thus, an oxidation catalyst and reforming catalyst, placed upstream of the LNT, served to burn out the excess oxygen from the lean exhaust and reform the methane to a usable source for regeneration.

The oxidation catalyst, reforming catalyst and two lean NOx trap catalyst bricks were each 9.5" in diameter by 6" in length. Each of the catalysts, developed by EmeraChem, were deposited on a cordierite honeycomb with 300 cells/in$^2$. The LNT catalyst contained a loading of 1.6 g/in$^3$ $Al_2O_3$, 100 g/ft$^3$ of Platinum and 0.14 g/in$^3$ of barium oxide. The oxidation catalyst had a coating of 1.8 g/in$^3$ alumina and 50 g/ft$^3$ of palladium metal. The reformer catalyst was prepared with a 1.59 g/in$^3$ 6:1 Platinum-Rhodium washcoat with a precious metal loading of 40 g/ft$^3$ and 3.9% cerium oxide on alumina. An additional 20 g/ft$^3$ of Rhodium was deposited on the surface

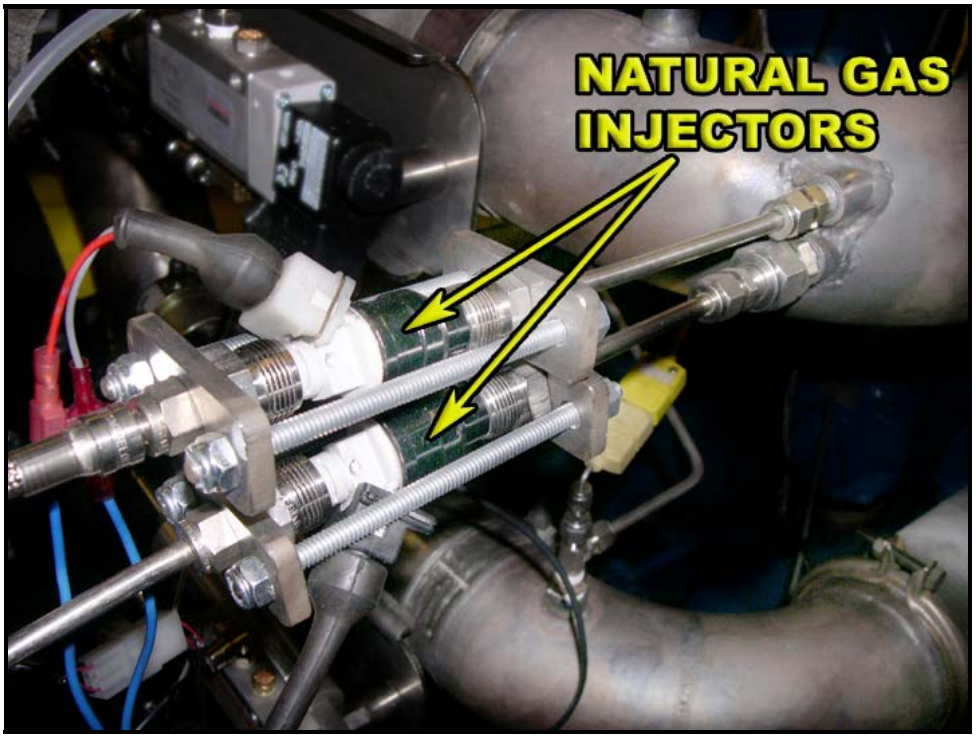


**Figure 44 Natural Gas Injectors**

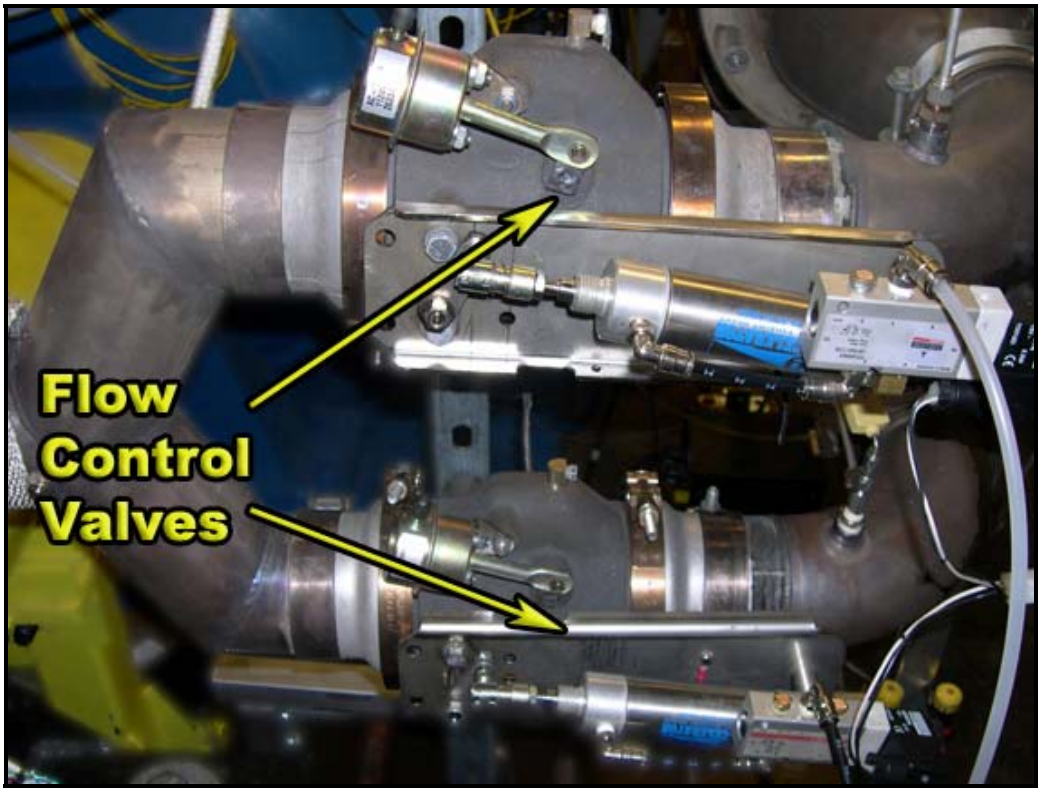


**Figure 45 Flow Control Valves**

A set of pneumatically actuated exhaust brake valves designed by US Gear was used to control the flow of the exhaust gasses. Shown in Figure 45, one valve is mounted in each leg of the exhaust system and are alternately opened and closed to redirect the exhaust flow. A computer based control system controlled the auxiliary fuel injection and exhaust valves and allowed the capability of either manual or automatic control of the system.

Complete Baseline Testing

Following the development of the experimental test bed, the first objective was to fully characterize the engine through a series of baseline tests. These tests would serve to provide pertinent performance and emissions data necessary for the development of the exhaust aftertreatment system. While the 210 kW engine does not fall into the .5 to 6.5 MW range of interest to the ARES program, it serves as a practical starting point for assessing the catalyst technology. Thus, baseline testing not only evaluates the performance and emissions characteristics, but it was also necessary to determine the scalability of the 8.3 liter engine compared to larger gensets of interest to ARES. A complete set of baseline data also serves to support further experimental results and aids in the comparison to other published data. In accordance with ARES goals, baseline testing was focused on a fixed speed of 1800 rpm. The baseline map was then extended to include a full load torque curve from 800 to 2400 rpm as well as a 45-point test matrix. This chapter serves to outline the details and present the results of all baseline testing. In addition, estimations of the catalyst's performance are made for certain test modes.

Before conducting baseline tests, a procedure was followed for engine warm up and calibration of the emissions analyzers. The same engine warm up procedure was followed throughout the research to maintain consistency and to ensure repeatability of results. Following engine warm up, the inlet and exhaust restrictions at rated conditions were set at 17.5" $H_2O$ and 4" Hg. The following list outlines the standard engine warm up procedure as specified in CFR 40, Part 89, Subpart E (89.407), for constant speed engines:

For constant-speed engines:

Operate the engine at minimum load for 2 to 3 minutes.

Operate the engine at 50 percent load for 5 to 7 minutes.

Operate the engine at maximum load for 25 to 30 minutes.

Start test cycle within 20 minutes of the end of the warm up. A mode begins when the speed and load are stabilized within ±2%. A mode ends when valid emission sampling for that mode ends. For a mode to be valid, the speed and load requirements must be maintained continuously during the mode. The torque modal points were calculated from the torque value with the engine warm and at rated conditions. All data was recorded during a minimum of the last 60 seconds of each mode. The emissions instruments were turned on at least one hour before calibration. Each analyzer was first zeroed with purge air, then calibrated with bottled span gasses. The span drift was checked at the end of testing to ensure zero and span difference did not exceed ±3% of full scale as specified by CFR 40, Part 89, Subpart E (89.408).

The first step in the baseline test procedure was to generate a 9 point full load torque curve from 800 rpm to 2400 rpm. This full load curve was then used to determine the 45-point test matrix for baseline testing. Modes for the test matrix included 10%, 25%, 50%, 75% and 100% load for each of the 9 speeds used to develop the full load torque curve. After warm up, testing began at

the highest speed and load point then moved through each of the 5 load points at this fixed speed. Data was collected at five-minute intervals between each mode to allow temperatures and engine out emissions to stabilize. Each mode in the test matrix was logged for 120 seconds at a sampling frequency of 10 Hz. The full test matrix is shown in Table 3.1.

**Table 5 Baseline Test Matrix**

| | Torque (ft-lbs) | | | | | | | | |
|---|---|---|---|---|---|---|---|---|---|
| | 800 rpm | 1000 rpm | 1200 rpm | 1400 rpm | 1600 rpm | 1800 rpm | 2000 rpm | 2200 rpm | 2400 rpm |
| 100% | 468 | 546 | 665 | 841 | 809 | 753 | 712 | 630 | 580 |
| 75% | 351 | 410 | 499 | 631 | 607 | 565 | 534 | 473 | 435 |
| 50% | 234 | 273 | 333 | 421 | 405 | 377 | 356 | 315 | 290 |
| 25% | 117 | 137 | 166 | 210 | 202 | 188 | 178 | 158 | 145 |
| 10% | 47 | 55 | 67 | 84 | 81 | 75 | 71 | 63 | 58 |

The exhaust flow, brake specific fuel consumption (BSFC), brake mean effective pressure (BMEP) and the NOx rating were calculated using the experimental data. The equations and assumptions used for calculating each of these are described below. The bubble plots in Figures 46 through 52 represent emissions maps of the engine. All other pertinent data collected during baseline testing is summarized in Tables 6 through 16.

The overall NOx rating for an engine is calculated in accordance with CFR 40, Part 89, Subpart E, where the NOx rating for each of five modes is weighted and summed per the weighting factors shown in Table 17. Using the NOx rating data for 1800 rpm from Table 14, the engine's rating is 1.73 g/hp-hr. The goal for the ARES program is to achieve a NOx rating of 0.1 g/hp-hr. Using this engine as an example, the exhaust aftertreatment system must reduce the NOx levels by greater than 94% to meet this goal.

$$\dot{V}_{exh} = \dot{V}_{fuel} + \dot{V}_{air}$$

$$\dot{V}_{fuel} = \frac{\dot{m}_{fuel} * SV}{MW_{fuel}}$$

*Where*:

$\dot{V}_{exh}$ = *calculated volumetric exhaust flow* $(\frac{Liters}{min})$

$\dot{V}_{fuel}$ = *calculated volumetric fuel flow* $(\frac{Liters}{min})$

$\dot{V}_{air}$ = *measured volumetric inlet air flow* $(\frac{Liters}{min})$

$\dot{m}_{fuel}$ = *measured mass fuel flow* $(\frac{lb}{min})$

$SV$ = *standard volume* $(22.414 \frac{Liters}{mole})$

$MW_{fuel}$ = *molecular weight* $(16.499 \frac{g}{mole})$

$$NOx\ Rating = \frac{\dot{m}_{NOx}}{P}$$

$$\dot{m}_{NOx} = \frac{X_{NOx} * \dot{V}_{exh} * MW_{NO_2}}{SV}$$

*Where*:

$NOx\ Rating$ = *calculated NOx rating* $(\frac{g}{hp-hr})$

$\dot{m}_{NOx}$ = *calculated mass NOx flow* $(\frac{g}{hr})$

$P$ = *measured power* $(HP)$

$X_{NOx}$ = *measured NOx concentration* $(ppm)$

$MW_{NO_2}$ = *molecular weight* $(46\frac{g}{mole})$

$$BMEP = \frac{2 * P}{N * V_{swept}}$$

*Where*:

$BMEP$ = *calculated brake mean effective pressure* $(bar)$

$P$ = *measured power* $(kW)$

$N$ = *measured engine speed* $\left(\frac{rev}{sec}\right)$

$V_{swept}$ = *engine swept volume* $(.0083\,m^3)$

$$BSFC = \frac{\dot{m}_{fuel}}{P}$$

*Where*:

$BSFC$ = *calculated brake specific fuel consumption* $(\frac{lb}{hp-hr})$

$\dot{m}_{fuel}$ = *measured mass fuel flow* $(\frac{lb}{hr})$

$P$ = *measured power* $(HP)$

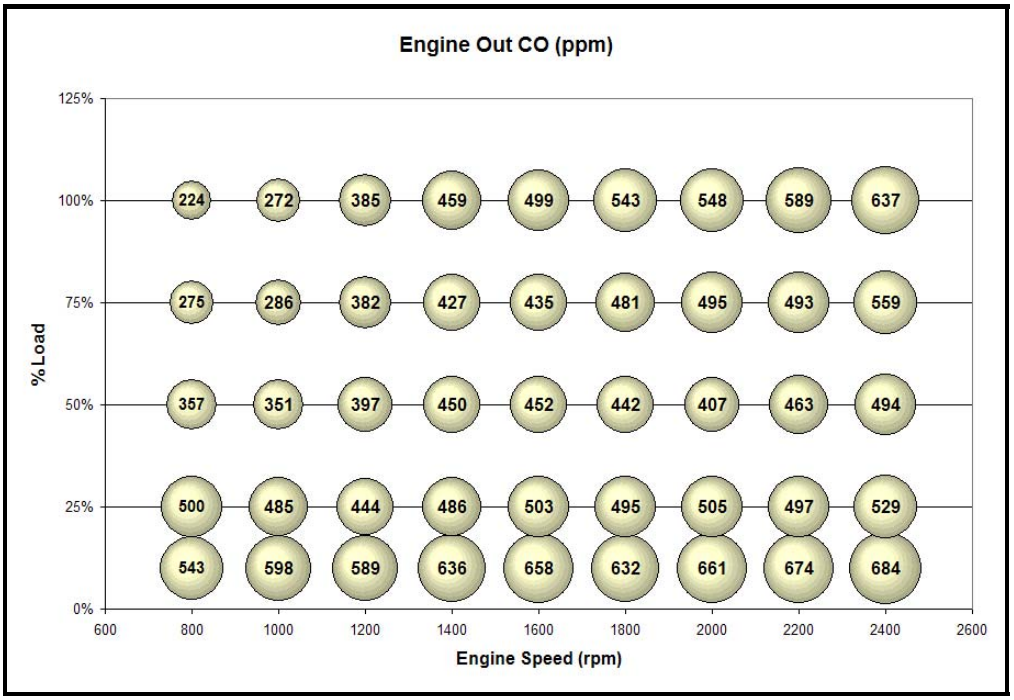


**Figure 46 Engine CO Map**

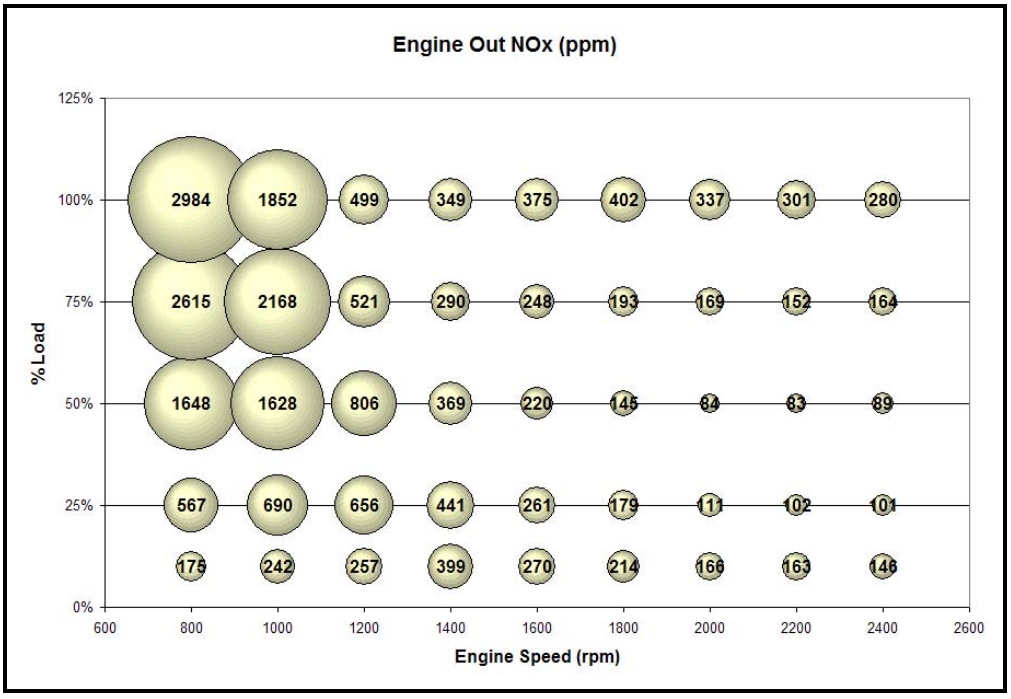


**Figure 47 Engine NOx Map**

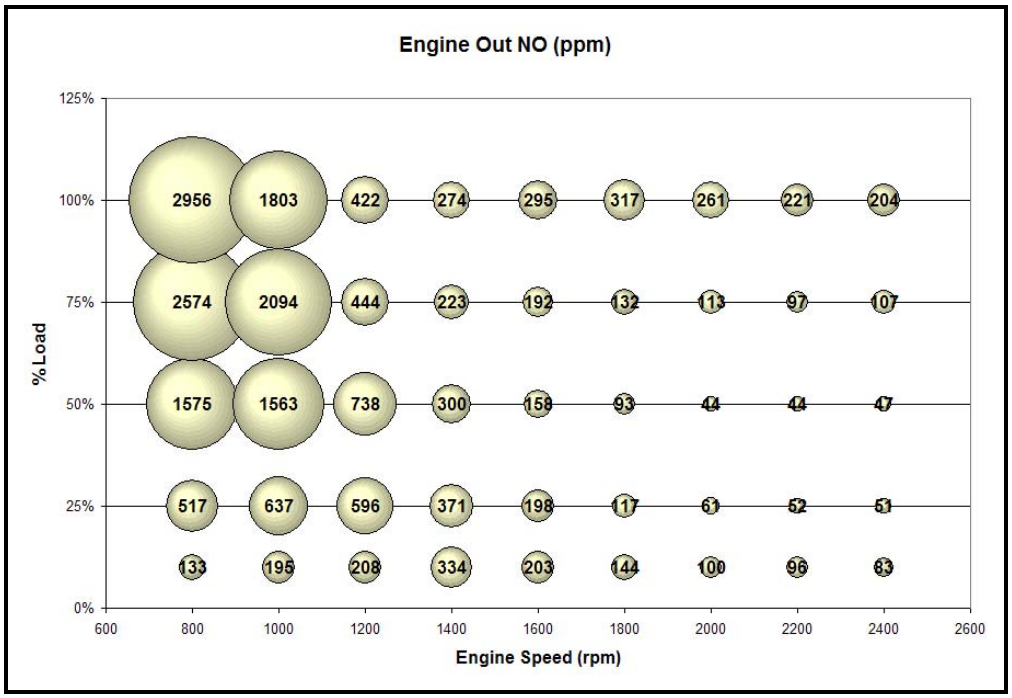


**Figure 48 Engine NO Map**

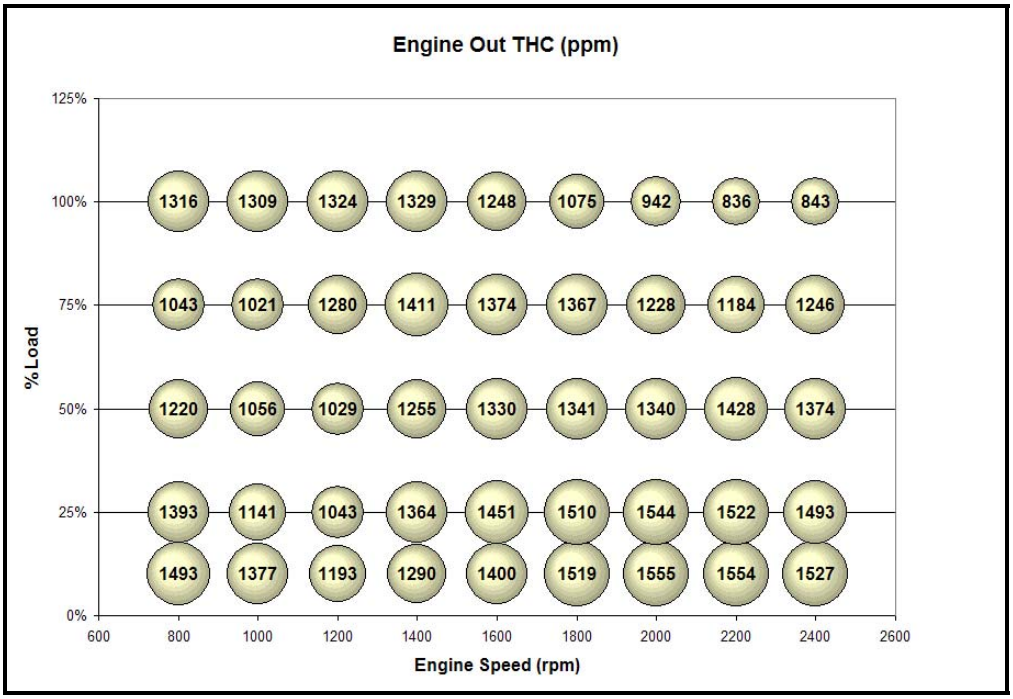


**Figure 49 Engine THC Map**

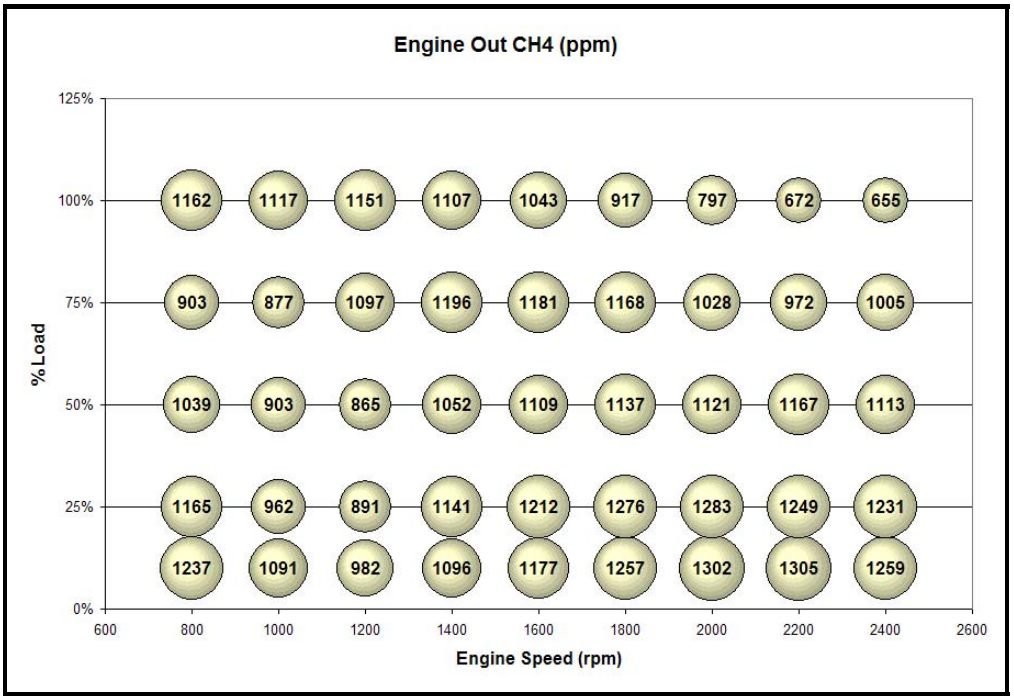


**Figure 50 Engine Methane map**

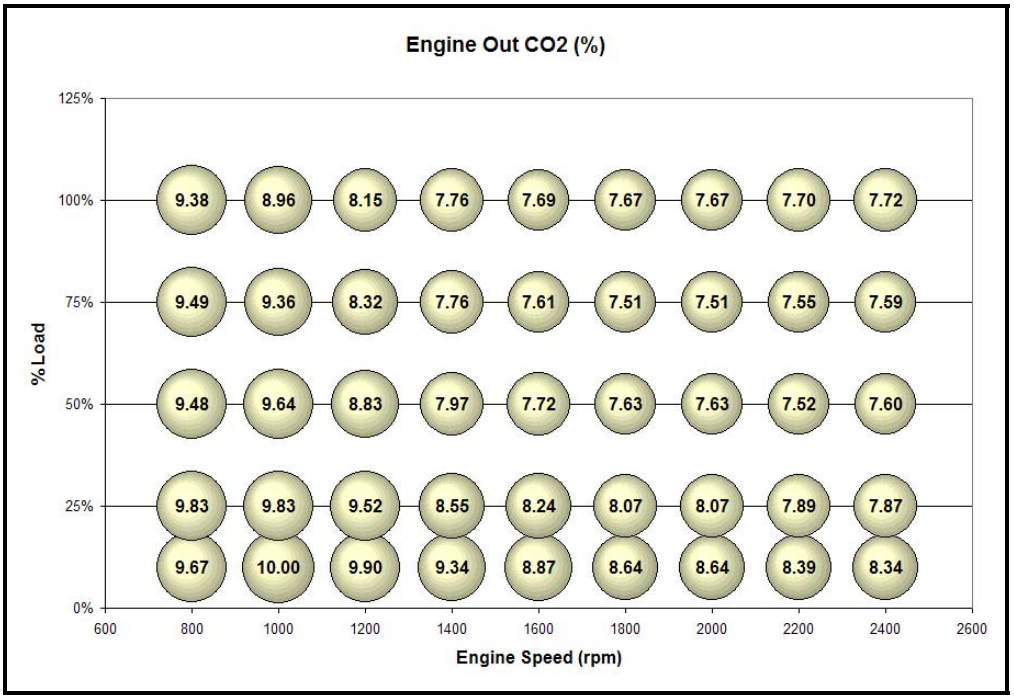


**Figure 51 Engine CO2 Map**

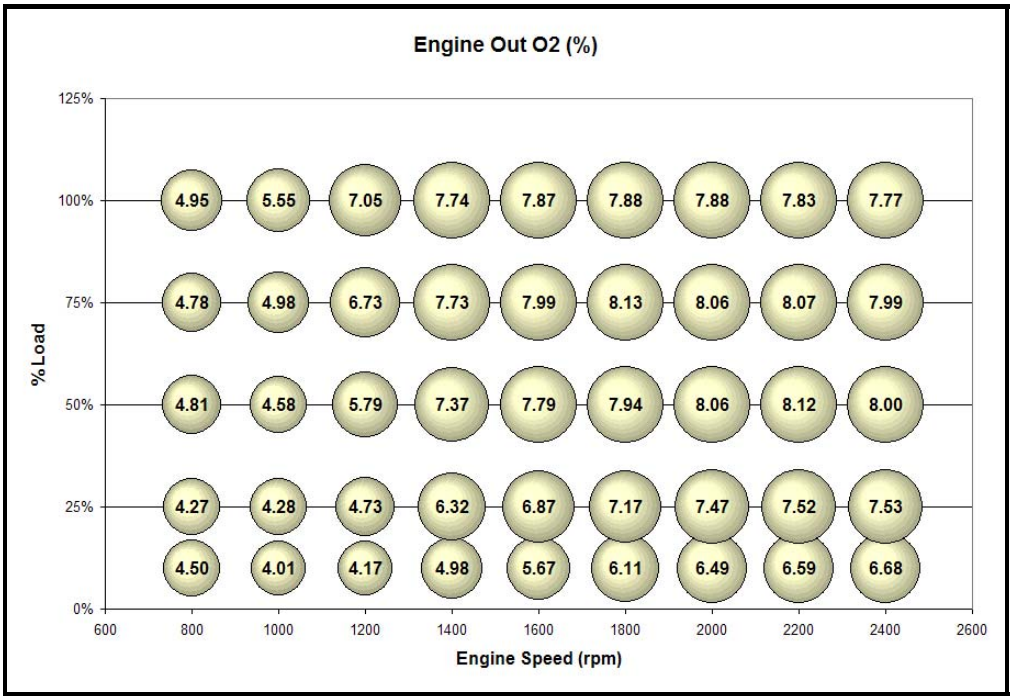


**Figure 52 Engine O2 Map**

**Table 6 Baseline Power Map**

| Power (hp) | | | | | | | | | |
|---|---|---|---|---|---|---|---|---|---|
| | 800 rpm | 1000 rpm | 1200 rpm | 1400 rpm | 1600 rpm | 1800 rpm | 2000 rpm | 2200 rpm | 2400 rpm |
| 100% | 66 | 95 | 137 | 213 | 239 | 252 | 264 | 276 | 276 |
| 75% | 50 | 71 | 103 | 161 | 179 | 188 | 198 | 209 | 208 |
| 50% | 33 | 48 | 69 | 106 | 121 | 126 | 131 | 138 | 138 |
| 25% | 16 | 24 | 34 | 53 | 59 | 61 | 65 | 67 | 68 |
| 10% | 7 | 10 | 13 | 22 | 24 | 25 | 26 | 27 | 27 |

**Table 7 Baseline Boost Pressure Map**

| Boost Pressure (psig) | | | | | | | | | |
|---|---|---|---|---|---|---|---|---|---|
| | 800 rpm | 1000 rpm | 1200 rpm | 1400 rpm | 1600 rpm | 1800 rpm | 2000 rpm | 2200 rpm | 2400 rpm |
| 100% | 2.79 | 5.70 | 11.63 | 21.21 | 21.34 | 20.04 | 19.65 | 19.49 | 18.09 |
| 75% | 1.61 | 3.24 | 7.33 | 13.91 | 14.13 | 13.99 | 14.21 | 14.73 | 14.35 |
| 50% | 0.63 | 1.50 | 3.47 | 7.58 | 9.38 | 9.74 | 10.85 | 11.80 | 12.44 |
| 25% | 0.01 | 0.28 | 0.88 | 2.38 | 3.27 | 4.23 | 5.60 | 6.70 | 7.68 |
| 10% | -0.16 | -0.05 | 0.12 | 0.52 | 0.87 | 1.31 | 1.87 | 2.42 | 3.27 |

**Table 8 Baseline Inlet Air Flow Map**

| Inlet Air Flow (scfm) | | | | | | | | | |
|---|---|---|---|---|---|---|---|---|---|
| | 800 rpm | 1000 rpm | 1200 rpm | 1400 rpm | 1600 rpm | 1800 rpm | 2000 rpm | 2200 rpm | 2400 rpm |
| 100% | 112 | 158 | 268 | 446 | 498 | 524 | 563 | 602 | 615 |
| 75% | 95 | 122 | 191 | 338 | 377 | 403 | 437 | 477 | 491 |
| 50% | 81 | 97 | 130 | 207 | 252 | 282 | 324 | 356 | 372 |
| 25% | 70 | 78 | 91 | 119 | 137 | 153 | 176 | 194 | 211 |
| 10% | 64 | 69 | 75 | 85 | 95 | 103 | 113 | 123 | 136 |

**Table 9 Baseline Fuel Flow Map**

| Fuel Flow (lb/hr) | | | | | | | | | |
|---|---|---|---|---|---|---|---|---|---|
| | 800 rpm | 1000 rpm | 1200 rpm | 1400 rpm | 1600 rpm | 1800 rpm | 2000 rpm | 2200 rpm | 2400 rpm |
| 100% | 23.5 | 33.2 | 47.8 | 72.4 | 81.0 | 86.5 | 93.4 | 100.5 | 103.7 |
| 75% | 18.5 | 25.7 | 37.1 | 56.2 | 62.7 | 67.7 | 73.8 | 80.3 | 83.2 |
| 50% | 13.7 | 19.0 | 26.5 | 38.4 | 44.6 | 49.0 | 54.7 | 59.1 | 62.3 |
| 25% | 8.8 | 12.2 | 16.6 | 22.8 | 26.1 | 28.8 | 32.6 | 35.7 | 38.5 |
| 10% | 6.2 | 8.5 | 10.8 | 14.1 | 16.3 | 18.2 | 20.5 | 22.8 | 25.4 |

**Table 10 Baseline Exhaust Flow Map**

| Exhaust Flow (L/min) | | | | | | | | | |
|---|---|---|---|---|---|---|---|---|---|
| | 800 rpm | 1000 rpm | 1200 rpm | 1400 rpm | 1600 rpm | 1800 rpm | 2000 rpm | 2200 rpm | 2400 rpm |
| 100% | 3421 | 4826 | 8066 | 13367 | 14921 | 15739 | 16901 | 18070 | 18481 |
| 75% | 2882 | 3709 | 5798 | 10159 | 11320 | 12101 | 13130 | 14338 | 14749 |
| 50% | 2439 | 2938 | 3960 | 6245 | 7600 | 8483 | 9740 | 10685 | 11160 |
| 25% | 2061 | 2326 | 2741 | 3594 | 4144 | 4619 | 5313 | 5871 | 6382 |
| 10% | 1875 | 2040 | 2227 | 2562 | 2844 | 3094 | 3416 | 3728 | 4113 |

**Table 11 Baseline BSFC Map**

| BSFC (lb/hp-hr) | | | | | | | | | |
|---|---|---|---|---|---|---|---|---|---|
| | 800 rpm | 1000 rpm | 1200 rpm | 1400 rpm | 1600 rpm | 1800 rpm | 2000 rpm | 2200 rpm | 2400 rpm |
| 100% | 0.355 | 0.349 | 0.349 | 0.341 | 0.338 | 0.343 | 0.354 | 0.364 | 0.376 |
| 75% | 0.371 | 0.362 | 0.361 | 0.348 | 0.350 | 0.360 | 0.373 | 0.385 | 0.400 |
| 50% | 0.414 | 0.398 | 0.384 | 0.362 | 0.370 | 0.389 | 0.417 | 0.429 | 0.450 |
| 25% | 0.553 | 0.514 | 0.486 | 0.430 | 0.445 | 0.472 | 0.502 | 0.533 | 0.570 |
| 10% | 0.954 | 0.849 | 0.814 | 0.646 | 0.680 | 0.740 | 0.778 | 0.847 | 0.929 |

**Table 12 Baseline BMEP Map**

| BMEP (bar) | | | | | | | | | |
|---|---|---|---|---|---|---|---|---|---|
| | 800 rpm | 1000 rpm | 1200 rpm | 1400 rpm | 1600 rpm | 1800 rpm | 2000 rpm | 2200 rpm | 2400 rpm |
| 100% | 8.90 | 10.25 | 12.31 | 16.37 | 16.12 | 15.09 | 14.23 | 13.52 | 12.38 |
| 75% | 6.73 | 7.65 | 9.23 | 12.43 | 12.07 | 11.25 | 10.67 | 10.22 | 9.34 |
| 50% | 4.44 | 5.14 | 6.20 | 8.16 | 8.12 | 7.55 | 7.07 | 6.76 | 6.22 |
| 25% | 2.16 | 2.57 | 3.06 | 4.07 | 3.95 | 3.65 | 3.49 | 3.29 | 3.04 |
| 10% | 0.88 | 1.08 | 1.20 | 1.69 | 1.62 | 1.47 | 1.42 | 1.32 | 1.23 |

**Table 13 Baseline Exhaust Back Pressure Map**

| Exhaust Back Pressure (psig) | | | | | | | | | |
|---|---|---|---|---|---|---|---|---|---|
| | 800 rpm | 1000 rpm | 1200 rpm | 1400 rpm | 1600 rpm | 1800 rpm | 2000 rpm | 2200 rpm | 2400 rpm |
| 100% | 0.67 | 0.78 | 1.03 | 1.57 | 1.80 | 1.99 | 2.23 | 2.52 | 2.59 |
| 75% | 0.64 | 0.72 | 0.88 | 1.23 | 1.38 | 1.54 | 1.71 | 1.94 | 1.98 |
| 50% | 0.62 | 0.67 | 0.75 | 0.91 | 1.01 | 1.12 | 1.26 | 1.37 | 1.42 |
| 25% | 0.60 | 0.63 | 0.67 | 0.72 | 0.76 | 0.79 | 0.85 | 0.90 | 0.93 |
| 10% | 0.58 | 0.60 | 0.63 | 0.66 | 0.66 | 0.69 | 0.71 | 0.73 | 0.75 |

**Table 14 Baseline NOx Rating Map**

| NOx Rating (g/hp-hr) | | | | | | | | | |
|---|---|---|---|---|---|---|---|---|---|
| | 800 rpm | 1000 rpm | 1200 rpm | 1400 rpm | 1600 rpm | 1800 rpm | 2000 rpm | 2200 rpm | 2400 rpm |
| 100% | 19.02 | 11.57 | 3.62 | 2.70 | 2.88 | 3.09 | 2.66 | 2.43 | 2.31 |
| 75% | 18.58 | 13.96 | 3.62 | 2.24 | 1.93 | 1.53 | 1.38 | 1.29 | 1.43 |
| 50% | 15.01 | 12.36 | 5.70 | 2.67 | 1.71 | 1.20 | 0.76 | 0.79 | 0.89 |
| 25% | 9.00 | 8.29 | 6.49 | 3.69 | 2.27 | 1.67 | 1.12 | 1.10 | 1.18 |
| 10% | 6.22 | 6.06 | 5.30 | 5.75 | 3.94 | 3.32 | 2.65 | 2.78 | 2.69 |

**Table 15 Baseline Air to Fuel Ratio Map**

| Air to Fuel Ratio | | | | | | | | | |
|---|---|---|---|---|---|---|---|---|---|
| | 800 rpm | 1000 rpm | 1200 rpm | 1400 rpm | 1600 rpm | 1800 rpm | 2000 rpm | 2200 rpm | 2400 rpm |
| 100% | 20.5 | 21.4 | 23.1 | 24.3 | 24.6 | 24.8 | 24.9 | 25.0 | 25.3 |
| 75% | 20.1 | 20.8 | 22.9 | 24.1 | 24.6 | 24.7 | 24.8 | 24.9 | 24.8 |
| 50% | 19.9 | 20.2 | 21.0 | 23.6 | 24.1 | 24.4 | 24.6 | 24.6 | 24.5 |
| 25% | 19.7 | 19.9 | 20.5 | 20.7 | 20.6 | 21.9 | 22.8 | 23.6 | 23.6 |
| 10% | 19.3 | 19.5 | 19.8 | 20.5 | 21.3 | 21.5 | 21.4 | 20.9 | 20.7 |

**Table 16 Baseline Turbo Out Temperature Map**

| Turbo Out Temp (C) | | | | | | | | | |
|---|---|---|---|---|---|---|---|---|---|
| | 800 rpm | 1000 rpm | 1200 rpm | 1400 rpm | 1600 rpm | 1800 rpm | 2000 rpm | 2200 rpm | 2400 rpm |
| 100% | 527 | 579 | 604 | 586 | 590 | 604 | 621 | 638 | 656 |
| 75% | 519 | 573 | 599 | 598 | 600 | 614 | 630 | 645 | 655 |
| 50% | 489 | 543 | 580 | 585 | 590 | 606 | 636 | 640 | 649 |
| 25% | 453 | 506 | 553 | 564 | 574 | 586 | 604 | 615 | 624 |
| 10% | 411 | 455 | 507 | 539 | 549 | 569 | 586 | 595 | 614 |

**Table 17 Weighting Factors**

| Mode # | % of Full Load | Time in Mode (min) | Weighting Factors |
|---|---|---|---|
| 1 | 100% | 5 | 0.05 |
| 2 | 75% | 5 | 0.25 |
| 3 | 50% | 5 | 0.30 |
| 4 | 25% | 5 | 0.30 |
| 5 | 10% | 5 | 0.10 |

LNT Capacity Estimation

Baseline data is useful in predicting the performance of the lean NOx trap system at particular engine modes. Using baseline engine data along with bench flow reactor data provided by EmeraChem, estimates of the NOx storage capacity were made. The trapping capacity of the catalyst is highly dependent on temperature as was demonstrated by the bench flow reactor studies. Data from these studies gives the capacity of the catalyst after 10% and 50% NOx breakthrough ($\tau_{10}$ and $\tau_{50}$) over a range of temperatures. The conditions of the experiment along with bench flow data are listed in Tables 18 and 19.

Unfortunately, the catalyst temperatures on the engine test stand exceed the range of temperatures demonstrated in the bench flow study, thus the data was extrapolated to estimate capacities above

550 °C. The storage capacity was estimated, as a function of temperature, for 10%, 25%, 50%, 75% and 100% engine load at 1800 rpm. With knowledge of the catalyst's storage capacity (grams) and the engine's NOx flow rate (grams/sec), the 10% and 50% breakthrough times were estimated. Table 3.17 shows the results of these estimates based on a 14 liter LNT catalyst volume. Estimates for the 75% and 100% load points were not made, as interpolations of bench flow data showed trapping capacities falling off to zero at these temperatures.

**Table 18 Conditions for Bench Flow Study**

| Parameter | Bench Flow Value |
|---|---|
| LNT catalyst space velocity | 30,000 /hr |
| Oxidation catalyst space velocity | 60,000 /hr |
| Reformer catalyst space velocity | 60,000 /hr |
| Temperature | 400, 450, 500, 550° C |
| NOx | 500ppm |
| CO | 500ppm |
| H2O | 13.5% |
| CO2 | 6.7% |
| O2 | 6.0% |
| N2 | balance |

**Table 19 Results from Bench Flow Study**

| Temperature (C) | Capacity @ t10 (g/L) | Capacity @ t50 (g/L) |
|---|---|---|
| 400 | 2.1 | 3.5 |
| 450 | 1.4 | 2.5 |
| 500 | 0.6 | 1.3 |
| 550 | 0.3 | 0.4 |

**Table 20 LNT Capacity Estimations**

| % Load | 100% | 75% | 50% | 25% | 10% |
|---|---|---|---|---|---|
| Temperature (C) | 600 | 580 | 560 | 510 | 440 |
| NOx flow (g/sec) | 0.192 | 0.067 | 0.037 | 0.030 | 0.018 |
| t10 Capacity (g) | - | - | 1.96 | 7.56 | 21.56 |
| t50 Capacity (g) | - | - | 3.08 | 15.68 | 37.8 |
| t10 Time (sec) | - | - | 53 | 252 | 1198 |
| t50 Time (sec) | - | - | 83 | 523 | 2100 |

Development of Regeneration Parameters

With lean NOx trap technology, NOx is trapped on the barium oxide storage sites in a lean (excess oxygen) environment, forming barium nitrate. In a rich (oxygen depleted) environment, the stored NOx are released by reactions with excess CO and $H_2$ and is subsequently reduced over the catalyst's platinum loading. Injecting natural gas into the exhaust creates the conditions for the rich mode, termed "regeneration". The natural gas, which is primarily methane, reacts across an oxidation catalyst to burn out the excess oxygen. A reforming catalyst is then used to further promote the combustion of the highly stable methane into CO and $H_2$. In addition to controlling the exhaust composition during regeneration, it was also necessary to control the exhaust flow rate across the catalyst. Redirecting the majority of the exhaust through the bypass leg with a set of flow control valves did this. The ability to control both the exhaust composition and flow rate is critical to successful regeneration of the lean NOx trap. Therefore, a series of experiments were conducted to help gain insight into exhaust flow rates and compositions under various engine conditions and injection parameters. The first of these experiments was designed to determine the flow rate across the catalyst, during regeneration, for a range of engine conditions. The second experiment was to map out the exhaust composition for a range of engine conditions and injection parameters. The final experiment was to determine the oxidation efficiency of methane across the catalysts for a range of exhaust temperatures. This chapter serves to outline the methods and results for each of these experiments.

*Exhaust Flow Control*

Controlling flow through the dual leg exhaust system was crucial for management of the catalyst. When the NOx trap is in the adsorption stage the bypass leg must be closed off, thus directing most of the exhaust across the catalysts. Once the LNT begins to saturate, the majority of the lean exhaust gases must be redirected through the bypass leg and the reductant is injected. Diverting the majority of the exhaust for regeneration is crucial to LNT management for two reasons. It reduces the oxygen mass flow, thereby minimizing the amount of reductant needed, and consequently reducing the fuel penalty. It also reduces the space velocity across the catalyst, allowing enough time for release of the stored NOx and their subsequent reduction. In bench flow reactor studies conducted at EmeraChem, a space velocity of 5,000 /hr was used during regeneration. Based on a total LNT volume of 14 liters the exhaust flow rate would have to be throttled to 1167 liters/min to achieve similar conditions. The following experiment was used to map out the exhaust flow rate across the catalyst, while the flow control valve was used to restrict the flow.

With the flow control valve in the closed position, the portion of the exhaust that is allowed to pass is termed "slip flow". It was desired to know the rate of this slip flow under various engine conditions. Thus, an experiment was designed to estimate the volumetric slip flow rate by diluting the flow with nitrogen and measuring the change in the exhaust composition.

As shown in Figure 53, with the flow control valve partially closed, nitrogen was injected into the throttled exhaust stream at a fixed flow rate. The fraction of the exhaust flow, which crosses the flow control valve, was diluted by the injected nitrogen flow. The dilution ratio could be determined by taking exhaust samples upstream and downstream of the injection. The slip flow rate could then be calculated from the known nitrogen flow rate and the measured dilution ratio. The following control volume analysis (Figure 54) was used to derive an equation for the volumetric slip flow rate.

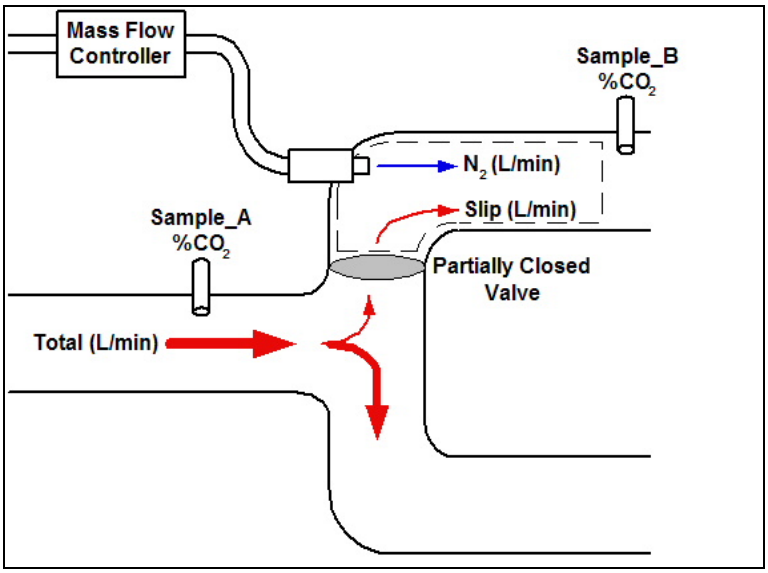


**Figure 53 Experimental Schematic for Slip Flow Estimations**

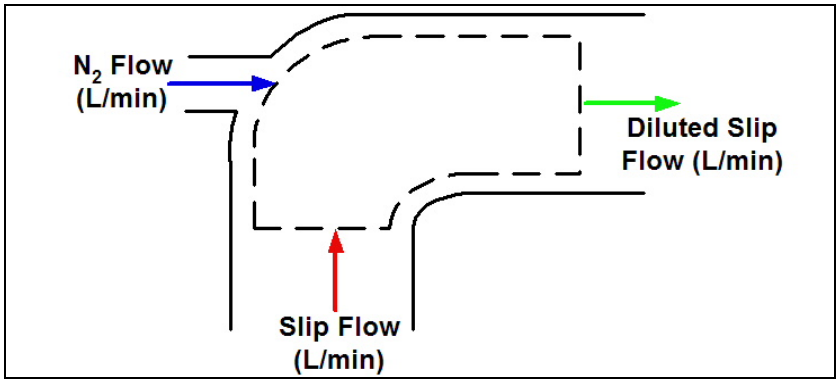


**Figure 54 Control Volume for Slip Flow Analysis**

The volumetric flow rate of $CO_2$ into and out of the control volume can be calculated as follows.

$$CO_2\_In\left(\tfrac{L}{\min}\right)=\%CO_2\_A\times\left[Slip\ Flow\left(\tfrac{L}{\min}\right)\right]$$

$$CO_2\_Out\left(\tfrac{L}{\min}\right)=\%CO_2\_B\times\left[Diluted\ Slip\ Flow\left(\tfrac{L}{\min}\right)\right]$$

$$=\%CO_2\_B\times\left[Slip\ Flow\left(\tfrac{L}{\min}\right)+N_2\ Flow\left(\tfrac{L}{\min}\right)\right]$$

Then an equation for the slip flow rate can be derived by equating the volumetric flow of $CO_2$ into and out of the control volume.

$$CO_2\_In\left(\tfrac{L}{\min}\right)=CO_2\_Out\left(\tfrac{L}{\min}\right)$$

$$\%CO_2\_A\times\left[Slip\ Flow\left(\tfrac{L}{\min}\right)\right]=\%CO_2\_B\times\left[Slip\ Flow\left(\tfrac{L}{\min}\right)+N_2\ Flow\left(\tfrac{L}{\min}\right)\right]$$

$$Slip\ Flow\ \left(\tfrac{L}{\min}\right)=N_2\ Flow\left(\tfrac{L}{\min}\right)\times\left[\frac{\%CO_2\_B}{\%CO_2\_A-\%CO_2\_B}\right]$$

These exhaust flow control experiments were used to determine the slip flow at 10%, 25%, 50%, 75% and 100% load for 1800 rpm. Measurements were taken at various nitrogen flow rates to verify repeatability of the test. Nitrogen flows were controlled with a Hastings mass flow controller. Bottled ultra high purity nitrogen was supplied to the mass flow controller at a constant 80 psi. The results of these tests are presented in Table 21 and Figure 55. Experimental results for estimating slip flow rates at 10% load are not presented, as they were highly inconsistent.

**Table 21 Exhaust Flow Rates During Adsorption and Regeneration**

| % Load | Slip Flow During Adsorption (L/min) | Slip Flow During Regeneration (L/min) |
|---|---|---|
| 100 | 14418 | 1298 |
| 75 | 11069 | 905 |
| 50 | 7814 | 603 |
| 25 | 4419 | 250 |

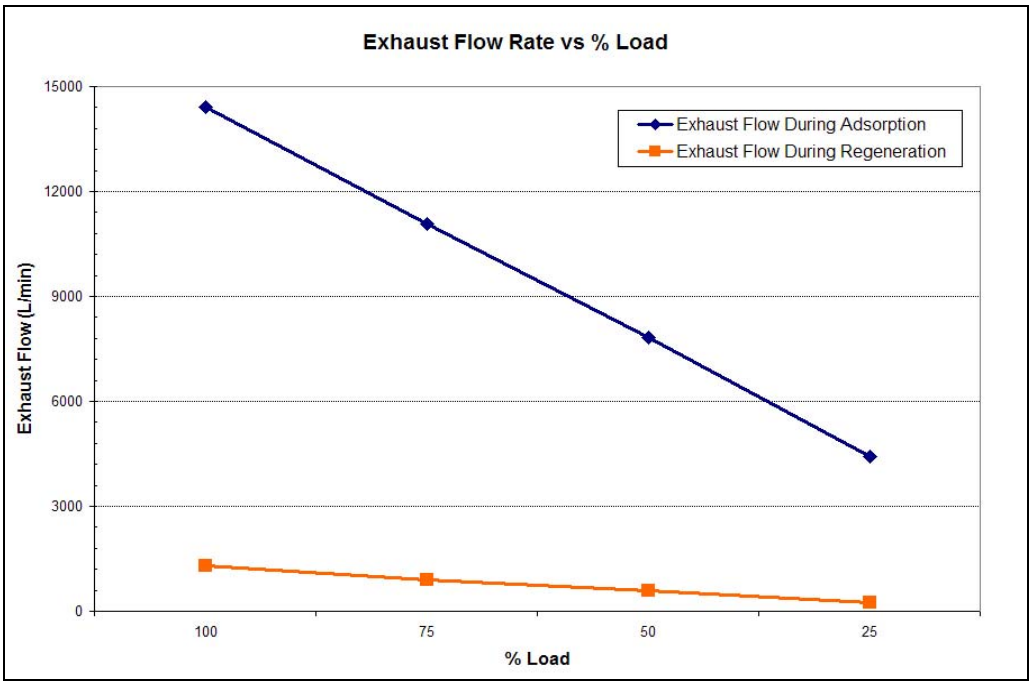


**Figure 55 Exhaust Flow Rates During Adsorption and Regeneration**

*Exhaust Composition Control*

As with controlling the flow rate across the catalyst, controlling the exhaust composition is also critical to regeneration. Enough reducing agent must be injected to fully burn out the excess oxygen and create the CO and $H_2$ necessary for regeneration. A universal exhaust gas oxygen sensor (UEGO) placed down stream of the injectors was used to determine the stoichiometry of the exhaust gasses entering the catalyst can. A stoichiometric air-fuel mixture for natural gas combustion has an A/F ratio of 17.2 while the lean burning C Gas Plus engine operates between 21.5 and 24.8 at 1800 rpm. In terms of lambda values, this is 1.25 to 1.44, where 1.00 represents a stoichiometric mixture and less than 1.00 would be rich. The goal of this experiment was to map out the injection parameters necessary to achieve lambda values of 0.5, 0.7 and 0.9 for each of the five load points at 1800 rpm. A 75Hz, 12-volt square wave signal was used to excite the injectors. The signal's duty cycle was the variable used to adjust the overall flow rate, thus controlling the exhaust composition. The following results present the number of injectors and the duty cycle used to achieve the desired equivalence ratio. As can be seen in Table 22, the two injectors at maximum duty cycle could not inject enough reductant to achieve the targeted equivalence ratio of 0.5 at 100% and 75% load. In addition, the fuel penalty was calculated, based on a cycling period of 25 second adsorption (lean operation) followed by a 5 second regeneration (rich operation) with a 3 second injection.

**Table 22 Exhaust Composition Control**

| 1800 rpm - 25 sec lean - 5 sec regen - 3 sec injection | | | | | |
|---|---|---|---|---|---|
| % Load | Number of Injectors | Duty Cycle % | Target Lambda | Actual Lambda | Fuel Penalty % |
| 100 | 2 | 95 | 0.5 | 0.70 | 2.22% |
| 100 | 2 | 95 | 0.7 | 0.70 | 2.22% |
| 100 | 2 | 35 | 0.9 | 0.90 | 0.80% |
| 75 | 2 | 95 | 0.5 | 0.57 | 3.17% |
| 75 | 2 | 65 | 0.7 | 0.70 | 2.09% |
| 75 | 2 | 25 | 0.9 | 0.90 | 0.82% |
| 50 | 2 | 72 | 0.5 | 0.49 | 3.29% |
| 50 | 2 | 38 | 0.7 | 0.70 | 1.71% |
| 50 | 2 | 18 | 0.9 | 0.90 | 0.70% |
| 25 | 2 | 27 | 0.5 | 0.48 | 2.32% |
| 25 | 2 | 16 | 0.7 | 0.70 | 1.29% |
| 25 | 1 | 8 | 0.9 | 0.91 | 0.53% |
| 10 | 1 | 13 | 0.5 | 0.50 | 1.58% |
| 10 | 1 | 8 | 0.7 | 0.72 | 0.80% |
| 10 | 1 | 6 | 0.9 | 0.90 | 0.42% |

*Methane Oxidation*

Successful regeneration of the LNT depends on the ability of the oxidation and reforming catalyst to combust methane with the excess oxygen present in the lean exhaust. The ability of the catalysts to combust the highly stable methane is partially dependent on the catalyst temperatures. Thus, at lower loads (i.e. lower temperatures), regeneration of the lean NOx trap may become more difficult. The following experiment was intended to assess the dependence of methane oxidation on catalyst temperatures. Exhaust methane concentrations were sampled at three locations as depicted in Figure 56, Oxi Cat In, Oxi Cat Out and LNT Out. These samples were taken at 8 different load points for 1800 rpm. This gave a range of catalyst temperatures from 550° to 413° C. Table 23 gives the reduction efficiencies through the oxidation catalyst and through the end of the aftertreatment system for this range of temperatures. Also shown in the table are the engine out methane concentrations in parts per million. As can be seen in Figure 57, the reduction efficiency begins to fall off below 500° C, and the oxidation catalyst becomes nearly ineffective below 450° C. The inability to regenerate the catalyst at lower temperatures presents a challenge for the application of the lean NOx trap aftertreatment system. This poor performance at lower temperatures coupled with the lower NOx storage capacity at higher temperatures creates a narrow temperature window for optimizing system performance. These temperature issues are further illustrated with testing presented in the next chapter.

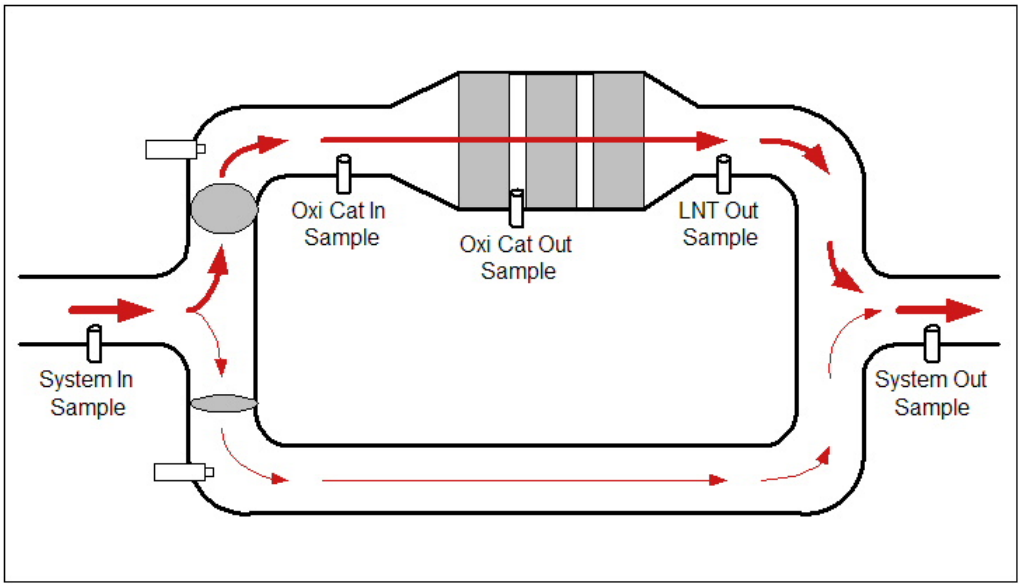


**Figure 56 Sample Positions for Methane Oxidation Study**

**Table 23 Methane Oxidation Results**

| Temp (C) | Oxi Cat Out CH4 Reduction | LNT Out CH4 Reduction | Engine Out CH4 (ppm) |
|---|---|---|---|
| 413 | 0.4% | 19.5% | 1180 |
| 452 | 6.7% | 26.9% | 1242 |
| 482 | 18.7% | 34.6% | 1212 |
| 508 | 26.7% | 35.3% | 1171 |
| 522 | 27.3% | 33.3% | 1219 |
| 538 | 26.0% | 35.3% | 1162 |
| 548 | 27.1% | 34.6% | 1134 |
| 550 | 28.8% | 33.2% | 1103 |

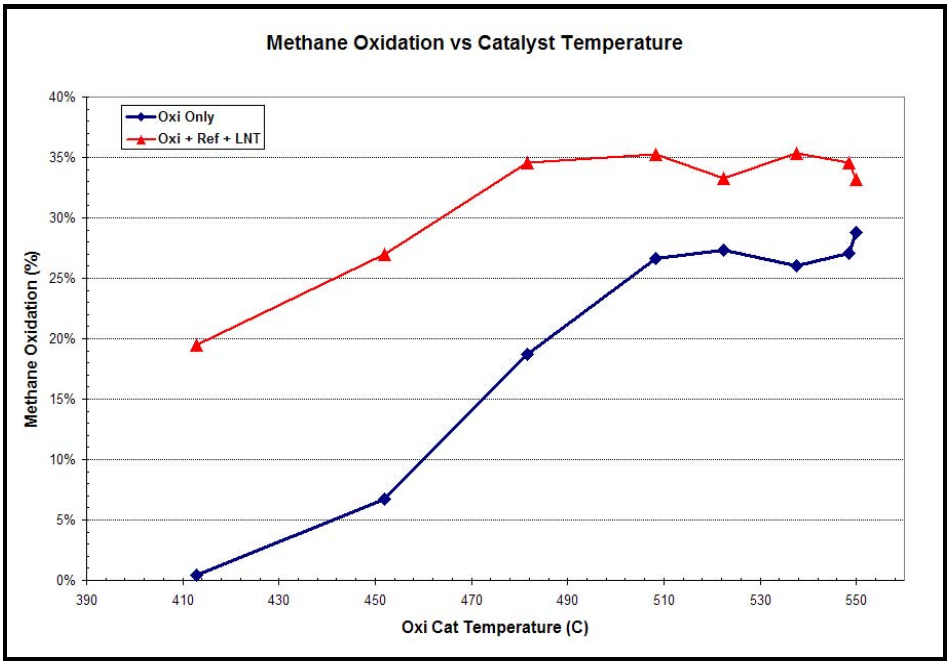


**Figure 57 Methane Oxidation vs. Catalyst Temperatures**

Lean NOx Trap Evaluation

The primary focus of this research was to evaluate the application of lean NOx trap catalysis to a lean burn natural gas engine. The key technical issues to be addressed were the utilization of natural gas for regeneration, as methane is difficult to catalytically combust, and the storage capacity of the catalyst under the high exhaust temperatures of natural gas combustion. As will be demonstrated in the following experiments, methane more readily reacts at higher temperatures, yielding better results for regeneration, while the LNT has higher storage capacities at lower temperatures. This leads to a narrow temperature window where the system will exhibit maximum performance. Testing of the aftertreatment system was conducted under steady state conditions at 1800 rpm with 10%, 25% and 50% engine loads; the catalyst temperatures under these conditions were 440, 510 and 560° C, respectively. Testing at 75% and 100% engine loads was avoided because high temperatures could potentially damage the catalysts. The remainder of this chapter serves to describe the procedures and results for these tests and concludes with an evaluation of the exhaust aftertreatment system.

*Lean NOx Trap Cycle*

Results of a typical test with the lean NOx trap system are shown in Figures 58 through 60. During this test, the engine was operated at 1800 rpm and 50% load. The catalyst was managed with 120 second sorption periods and 20 second regenerations. The exhaust flow rates were 297 scfm during sorption periods and 21 scfm during regeneration periods. This correlates to LNT space velocities of 36,042/hr and 2,550/hr based on 14 liters of catalyst. The 140 second catalyst management cycle, for which three periods are shown in the following figures, was repeated under steady state engine conditions. The first of these figures shows the NOx levels measured into and out of the dual leg system. Typical locations of the "system in" and "system out" sample points are shown in Figure 53.

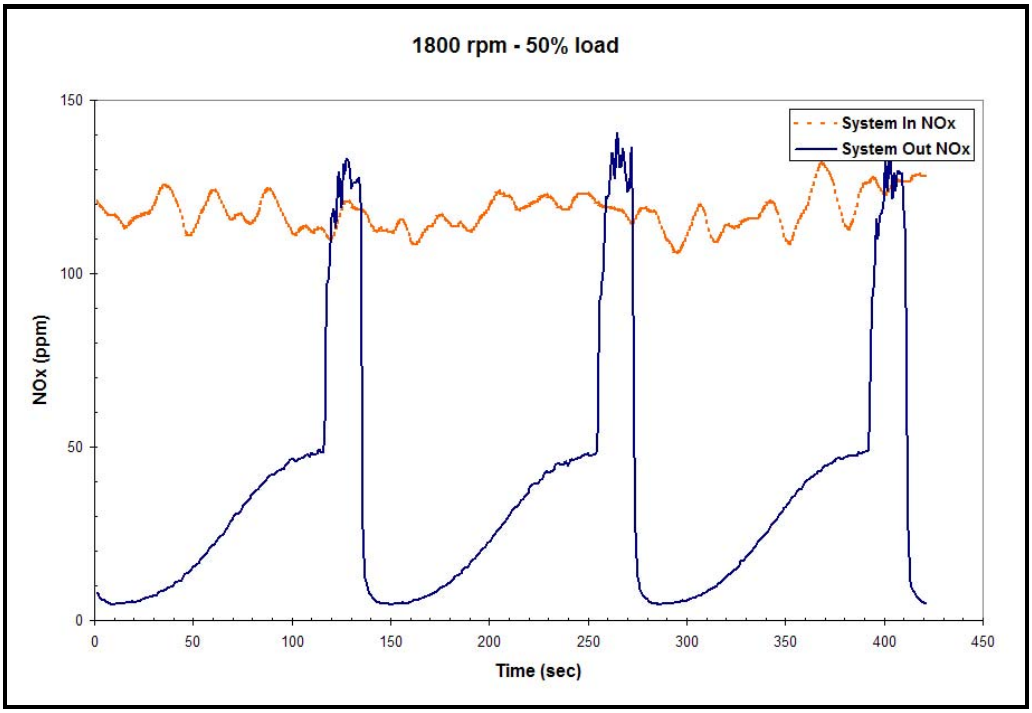


**Figure 58 Typical NOx Profiles**

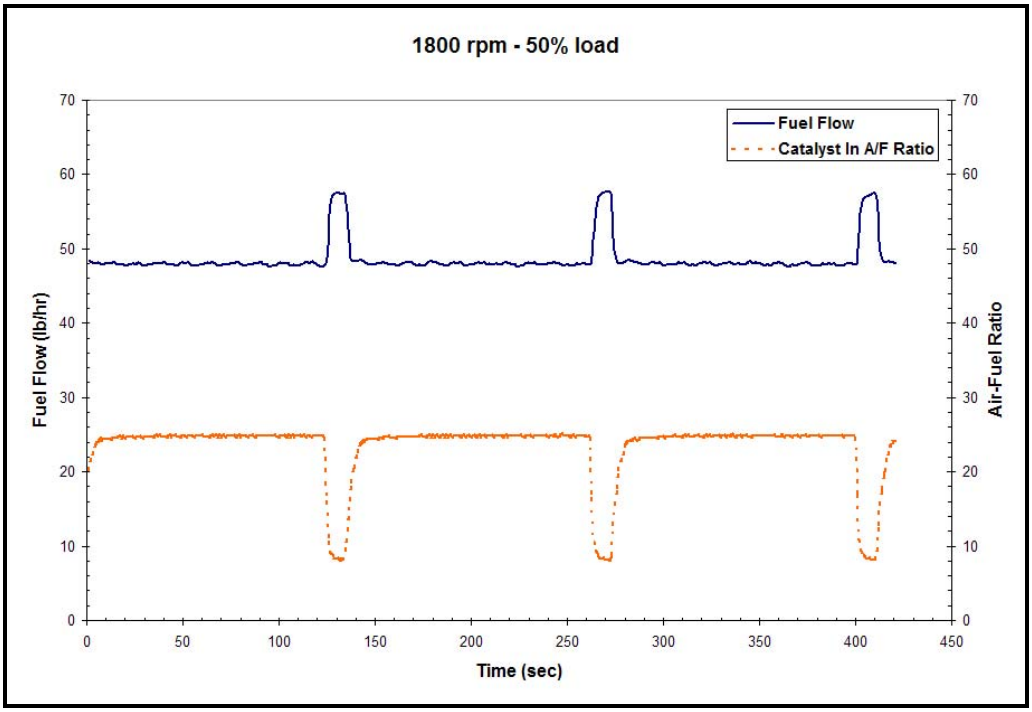


**Figure 59 Fuel Flow and Exhaust Stoichiometry**

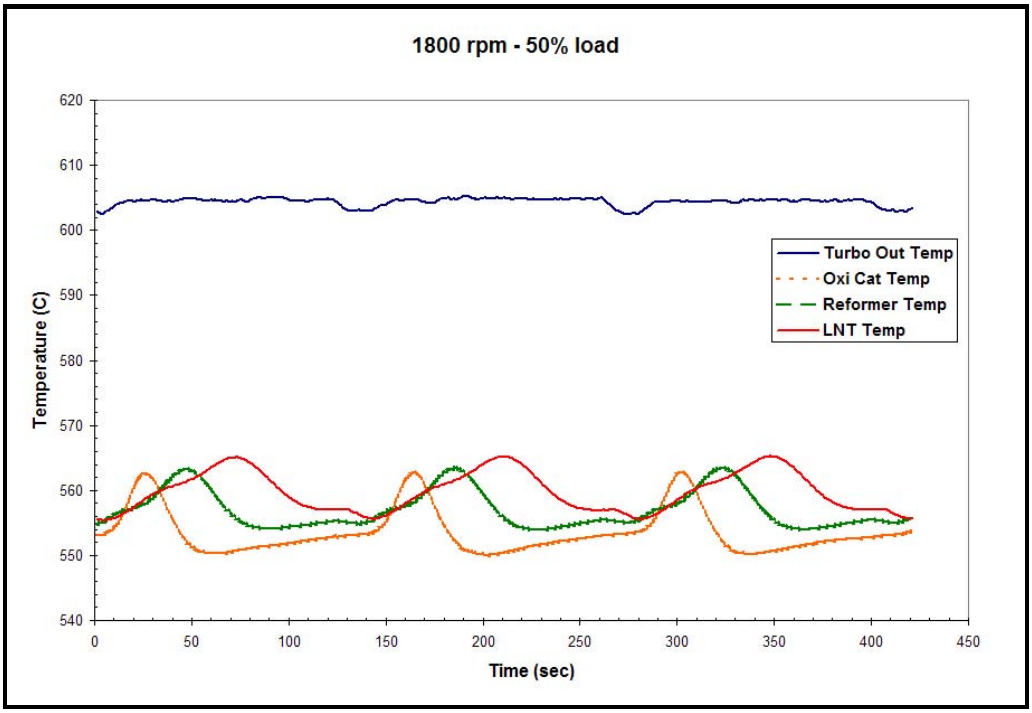


**Figure 60 Catalyst Temperatures**

The system in NOx levels average 120 ppm, while the system out NOx levels vary through the management cycle. Directly following the regeneration sequence, system out NOx levels reach their lowest levels of 5 ppm. This represents an instantaneous trapping efficiency of 96%. As the sorption period continues, and storage sites on the catalyst become occupied, NOx slip begins to occur. By the end of the 120-second sorption, the catalyst is only trapping 58%, with system out NOx levels reaching 50 ppm. This is followed by the 20-second regeneration period. Of the 20-second regeneration period, fuel was injected for the first 10 seconds. The remaining 10 seconds was a delay in switching the valves. This valve delay throttles the exhaust flow across catalyst long enough for the reductant to completely pass through the catalysts. The geometry of the exhaust aftertreatment system is a dual leg system with one leg serving as a bypass during catalyst regeneration. This single chamber system allows the entire engine out NOx to circumvent the LNT during the 20-second regeneration. In a single chamber system, this fraction of exhaust, which goes untreated inevitably, leads to a lower overall NOx reduction efficiency. However, in an actual application this single chamber system could be expanded into a two-chamber system by adding a catalyst to the bypass leg.

For the purpose of this study the catalysts are evaluated by their trapping efficiencies. The trapping efficiency is defined as the percentage of NOx stored by the catalyst during the sorption period. The catalyst's trapping efficiency varies with changes in engine conditions and catalyst management parameters.

Figure 59 shows the air-fuel ratio measured directly upstream of the oxidation catalyst and the fuel flow to both the engine and injectors. With an air-fuel ratio of 17.1 representing stoichiometric conditions, it can be seen here that lean conditions exist through the sorption period. Following the injection and closing of the valve, an oxygen depleted/reductant rich exhaust condition is created in which the stored NOx can be released and reduced. Another crucial parameter for system evaluation is the amount of fuel required for regeneration. As the

energy from this fuel supplies no power to the end user, it is considered a fuel penalty and is defined as the percentage of fuel injected to that which is supplied to the engine. During the injection, an instantaneous fuel penalty of 20% is measured. However, over a full cycle, this is only a 1.7% fuel penalty.

Figure 60 shows temperatures at the cores of the oxidation, reformer and lean NOx trap catalysts as well as the exhaust temperature at the turbo outlet. The temperature oscillations of the catalyst bricks are due to the exothermic oxidation of the methane. The wide temperature difference between the turbo outlet and the catalyst bricks is due to heat loss along the exhaust pipe.

*Optimizing Regeneration Parameters*

The trapping efficiency as well as the associated fuel penalty are primary parameters for evaluating the aftertreatment system. These evaluation parameters are highly dependent on engine conditions (i.e. exhaust temperatures and NOx flow rates) as well as the conditions used for catalyst management (i.e. injection rates and sorption period). The system was evaluated at a matrix of injection rates and sorption periods for 10%, 25% and 50% engine loads. The results from this test matrix revealed the optimal conditions for catalyst management at a given engine condition. The injection rate was used to control the exhaust stoichiometry during regeneration. Oxygen depleted exhaust with lambda values of 0.5, 0.6, 0.7 and 0.8 were targeted for the test matrix. A ten second injection duration was used for all testing. After the injection sequence, switching of the valves was delayed until the stoichiometry downstream of the catalyst reached lean conditions (lambda > 1.0). This ensured enough time for the reductant to pass through the catalysts. The performance was allowed to stabilize with sorption periods of 30, 60, 120 and 240 seconds for each targeted lambda value.

Figures 61 through 63 below show the results of the test matrix for engine conditions at 50% load. The four sorption periods are shown across the x-axis and each curve represents a different injection rate. A sixty second sorption period yields greater than 90% trapping efficiencies for all lambda values. Beyond this period the trapping efficiencies begin to drastically fall off. A shorter sorption period of 30 seconds yields modest gains in trapping efficiencies, yet results in markedly higher fuel penalties. In optimizing the regeneration strategy it is often necessary to compromise one performance parameter for gains in another. Because the ARES program targets NOx ratings of 0.1 g/hp-hr, this was the deciding factor in determining the optimal parameters for regeneration. Figure 63 shows that injecting for 0.6 lambda with a sorption period of 60 seconds achieves a 0.088 g/hp-hr NOx rating. This was just within the ARES target, thus it was chosen as the optimal regeneration scheme. This optimal scheme for steady state conditions at 50% engine load results in a 2.84% fuel penalty. Figure 63 also shows the NOx profiles through 5 cycles for this optimal regeneration scheme.

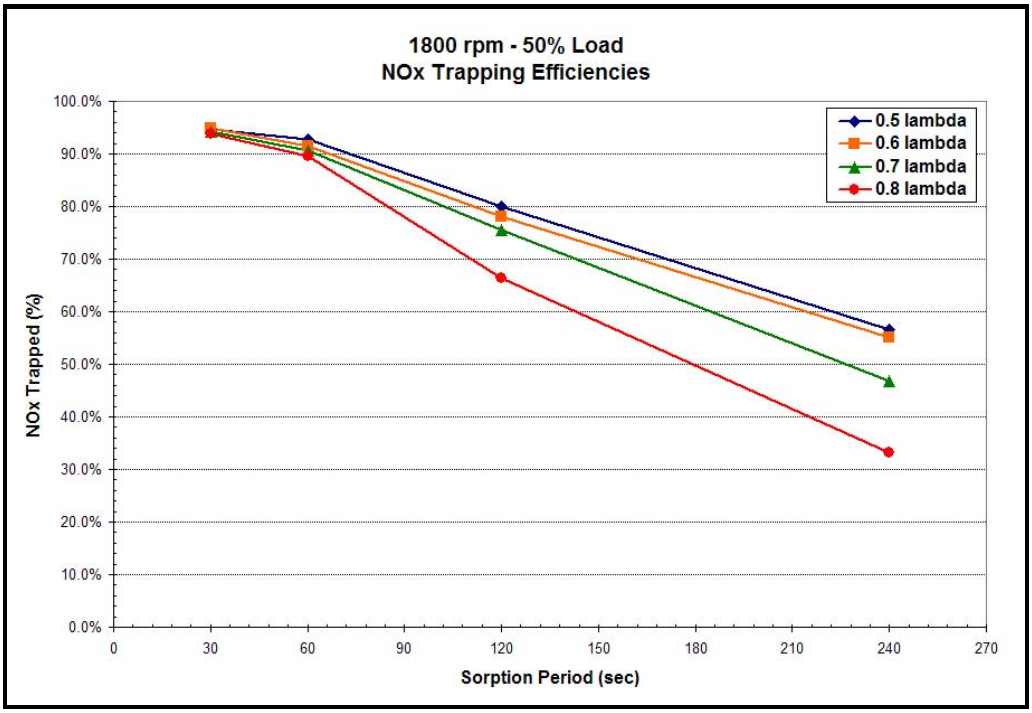


**Figure 61 50% Load NOx Trapping Efficiencies**

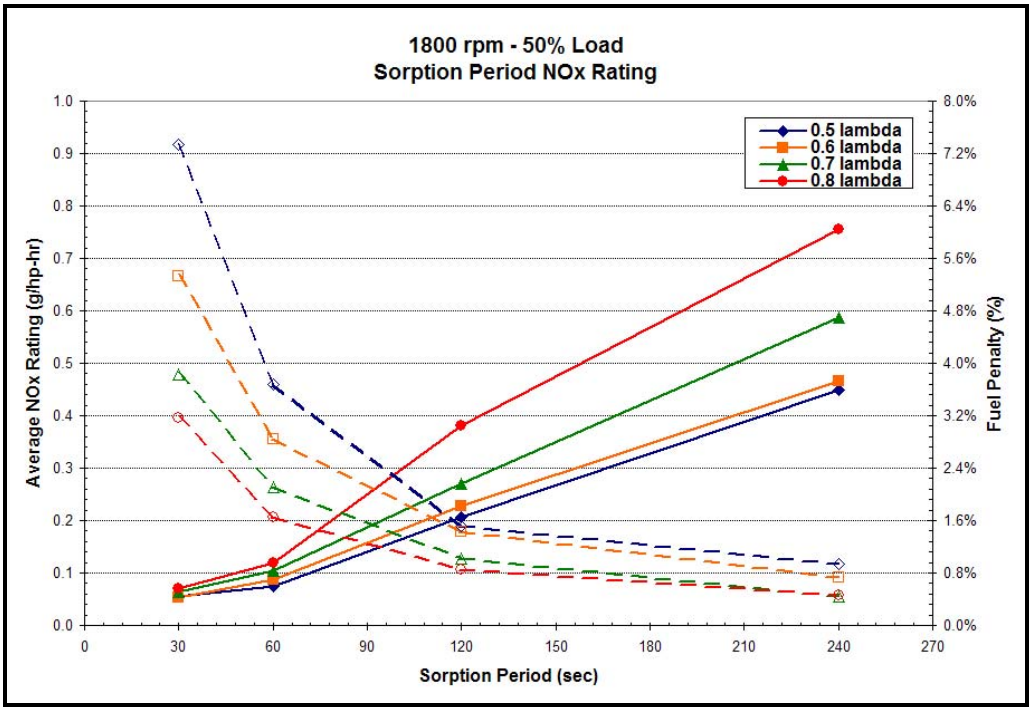


**Figure 62 50% Load NOx Ratings and Fuel Penalties**

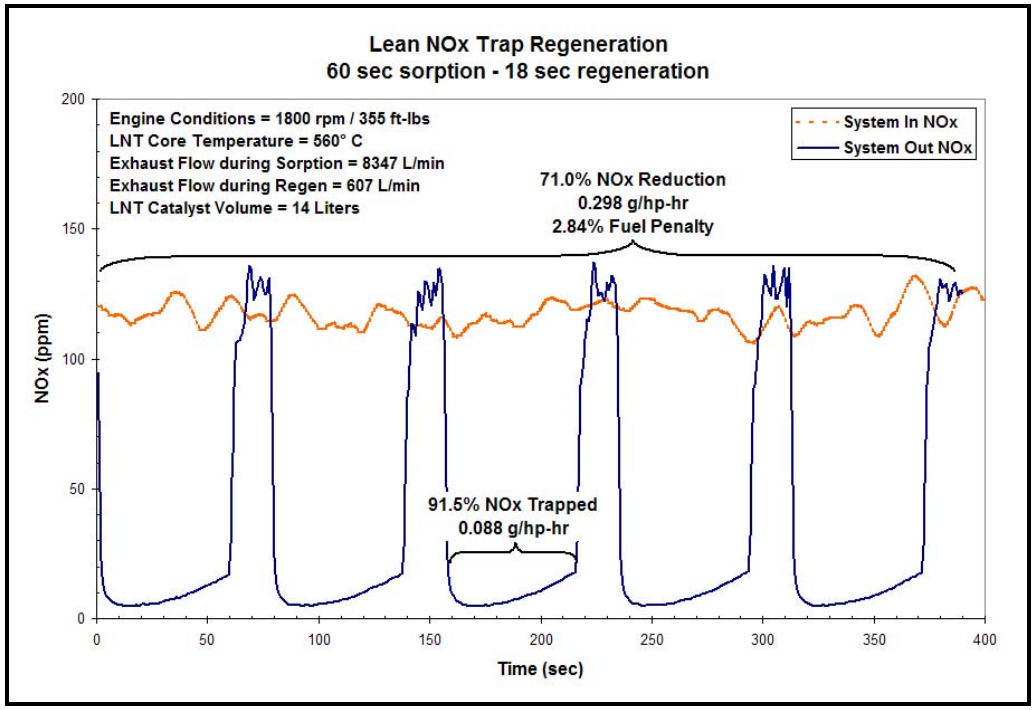


**Figure 63 50% Load NOx Profiles for Optimal Regen**

Figures 64 through 66 below show the results of the test matrix for engine conditions at 25% load. A 120 second sorption period with injections for 0.5 lambda yields trapping efficiencies higher than 97% and NOx ratings as low as 0.05 g/hp-hr. These optimal regeneration conditions for steady state conditions at 25% engine load lead to a 1.62% fuel penalty. NOx profiles through 5 regeneration cycles for these optimal conditions is shown in Figure 66. It is important to note that the optimal adsorption period for 25% load (120 seconds) is twice what it was for 50% load (60 seconds). This is in part due to the lower catalyst temperatures at 25% load. The storage capacity of the lean NOx trap is a function of its temperature. Thus, as the exhaust temperatures increase with increasing load, the catalyst's storage capacity will decrease as will the effective adsorption period. This concept is explored in more detail later in this chapter.

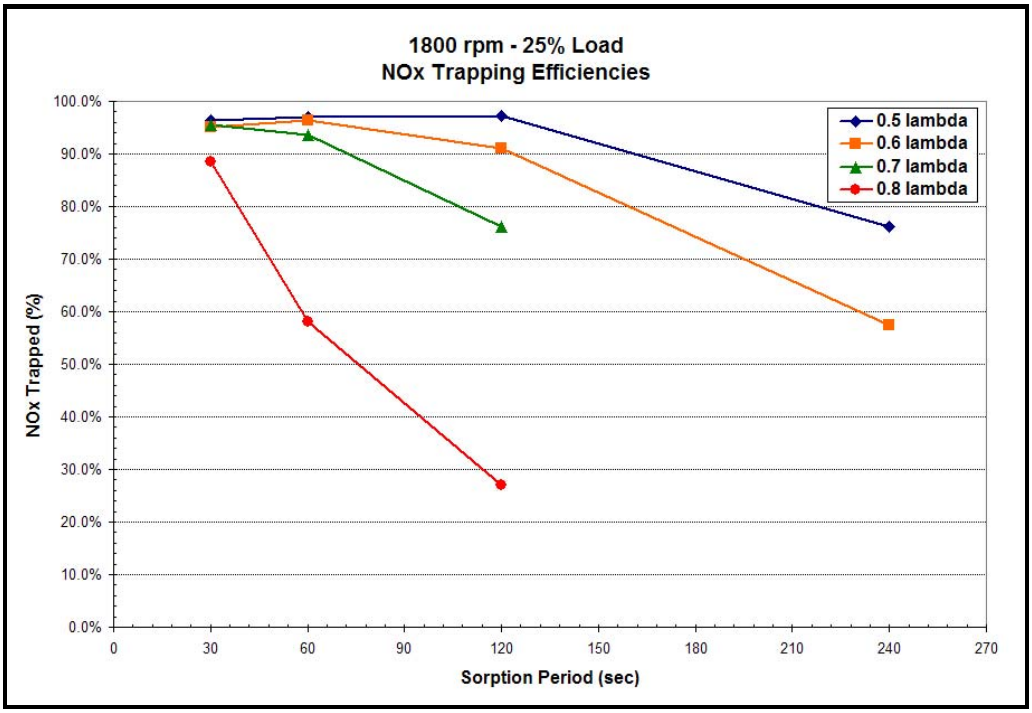


**Figure 64 25% Load NOx Trapping Efficiencies**

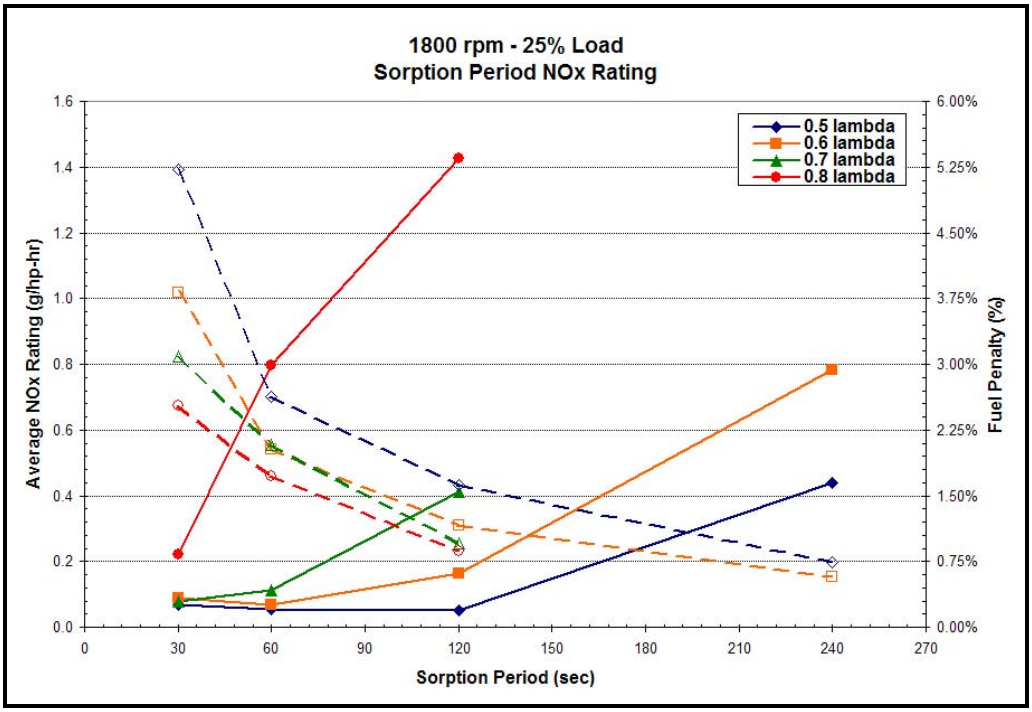


**Figure 65 25% Load NOx Ratings and Fuel Penalties**

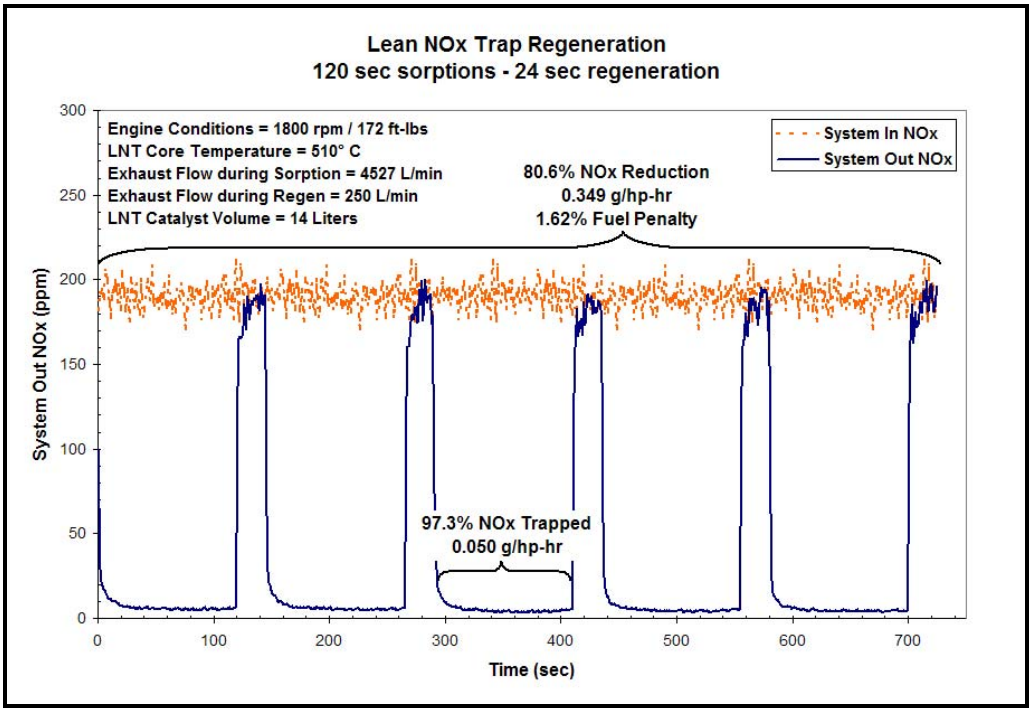


**Figure 66 25% Load NOx Profiles for Optimal Regen**

Figures 67 through 69 below show the results of the test matrix for engine conditions at 10% load. A 30 second sorption period with 0.5 lambda yields a 91% trapping efficiency. With an engine out NOx rating of 5.00 g/hp-hr, this trapping efficiency achieves an average rating of 0.47 g/hp-hr and instantaneous ratings of 0.36 g/hp-hr. These results fall well short of the ARES goal. These conditions resulted in a 3.66% fuel penalty. Besides not achieving high enough trapping efficiencies at 0.5 lambda, the catalyst would not regenerate beyond 120 second sorption periods. Trapping efficiencies dropped off to zero, thus the data is not presented in the following figures. Similar results occurred beyond 60 second sorptions for 0.6 lambda and beyond 30 second sorptions for 0.7 and 0.8 lambda. There are two explanations for this inability to regenerate the catalyst at 10% engine load. The first, is that low catalyst temperatures hinder the reforming of methane into the $H_2$ and CO necessary for regeneration.

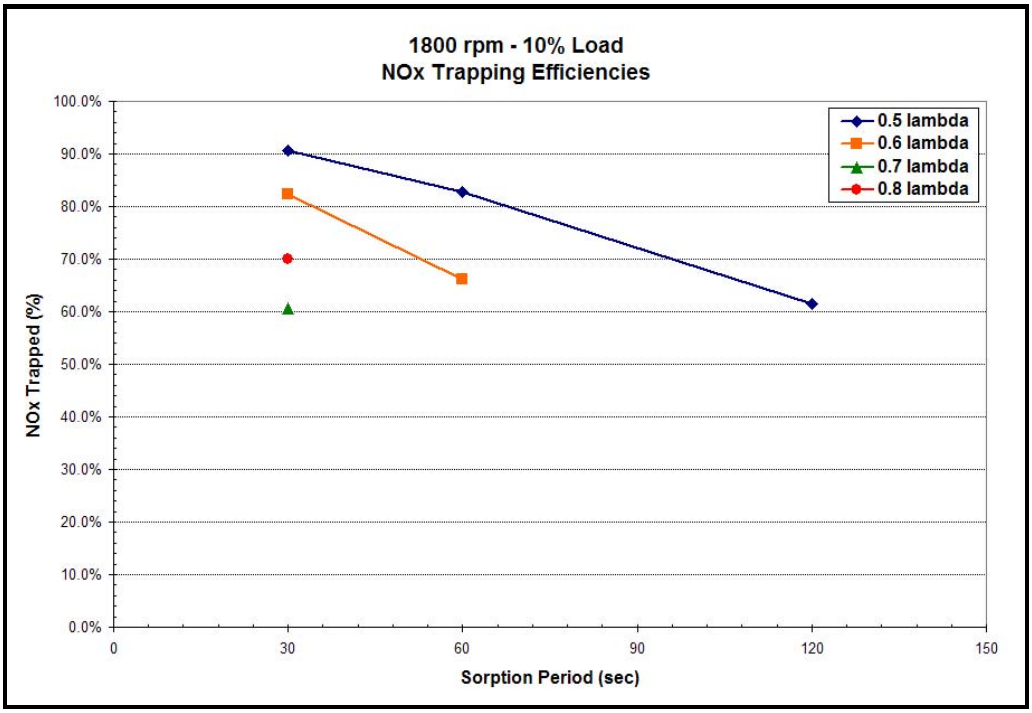


**Figure 67 10% Load NOx Trapping Efficiencies**

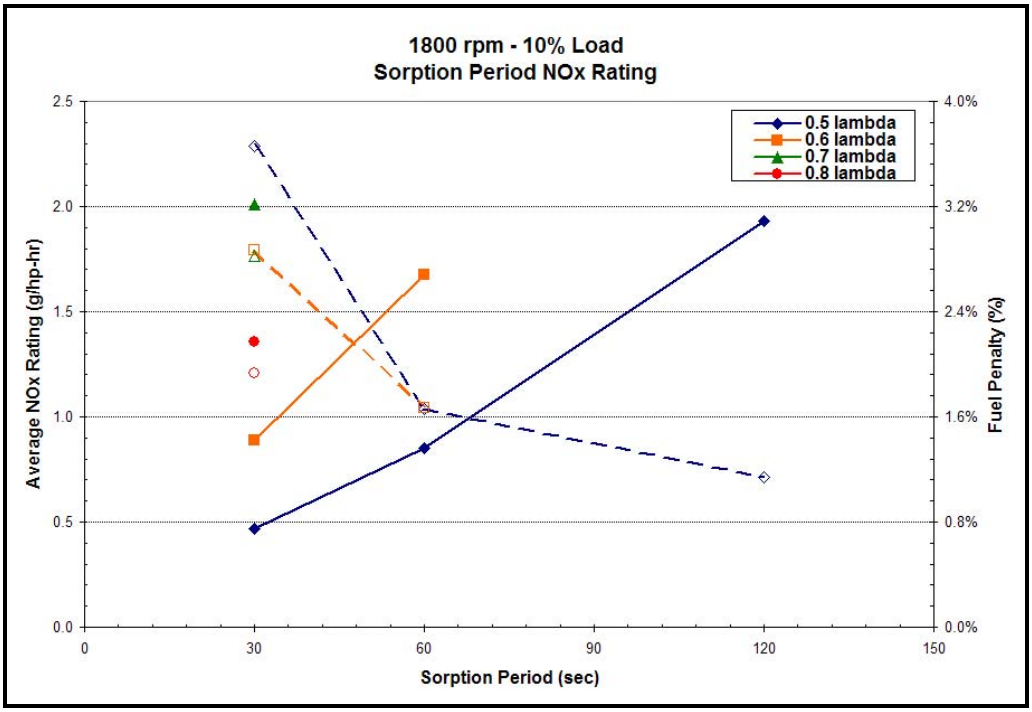


**Figure 68 10% Load NOx Ratings and Fuel Penalties**

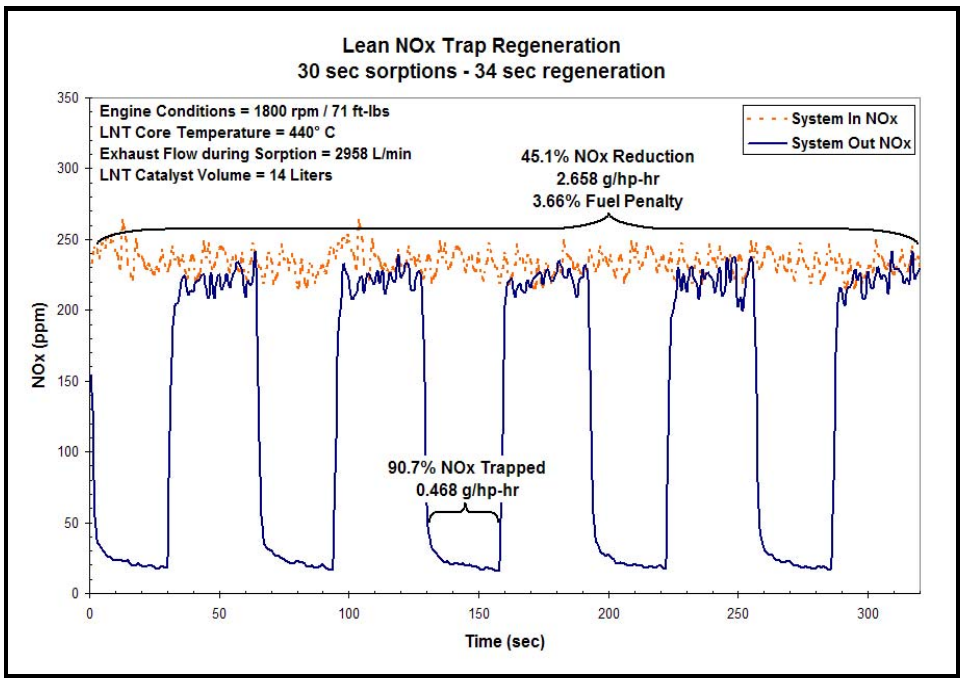


**Figure 69 10% Load NOx Profiles for Optimal Regen**

At 10% load catalyst temperatures are 440° C. At these low temperatures, the oxidation catalyst has not reached its light off temperature as indicated in Figure 57. Thus, not enough of the injected methane is being catalytically combusted to create the conditions necessary for regeneration. The second explanation for poor performance is that the mass flow of exhaust, which must slip past the closed valve for regeneration, becomes too low. Although the targeted lambda values are met, the mass of fuel injected is simply not enough to fully regenerate a saturated catalyst. This second explanation is explored with further testing and the results are presented in the following section.

*Adjusting Flow Rates for Regeneration*

The exhaust flow that slips past the valve during regeneration becomes very low at 10% load. This results in a low injection of reductant to attain the desired stoichiometry. The poor catalyst performance at 10% load could result from an insufficient mass of fuel injection to regenerate the catalyst. A potential solution to this problem would be to prevent the valve from fully closing, thus allowing higher mass flow rates of exhaust during regeneration. This would result in higher injection rates of fuel necessary to attain the desired stoichiometry. Segments of the test matrix were repeated for this scenario, in which the valve was left wide open during regenerations. Fuel injection rates were set to achieve 0.7 lambda for 60, 120 and 240 second sorption periods. Figures 70 through 72 show results from these tests.

As can be seen in Figure 70, the trapping efficiency reached 97.4% for 0.7 lambda and 120 second sorptions. As the original test matrix revealed the catalystwould not even regenerate under these conditions with the valve fully closed during regeneration. The 97.4% trapping efficiency achieved a 0.129 g/hp-hr NOx rating and instantaneous ratings as low as 0.10 g/hp-hr. These conditions resulted in a 2.62% fuel penalty. The catalysts trapping efficiency is maintained at 95.6% with 240 second sorptions. These conditions yielded fuel penalties as low as 1.05%.

These results prove that the position of the flow control valve during regeneration can play a role in further optimizing the system. This is particularly true for lower loads, and is recommended as a next step in LNT evaluation studies.

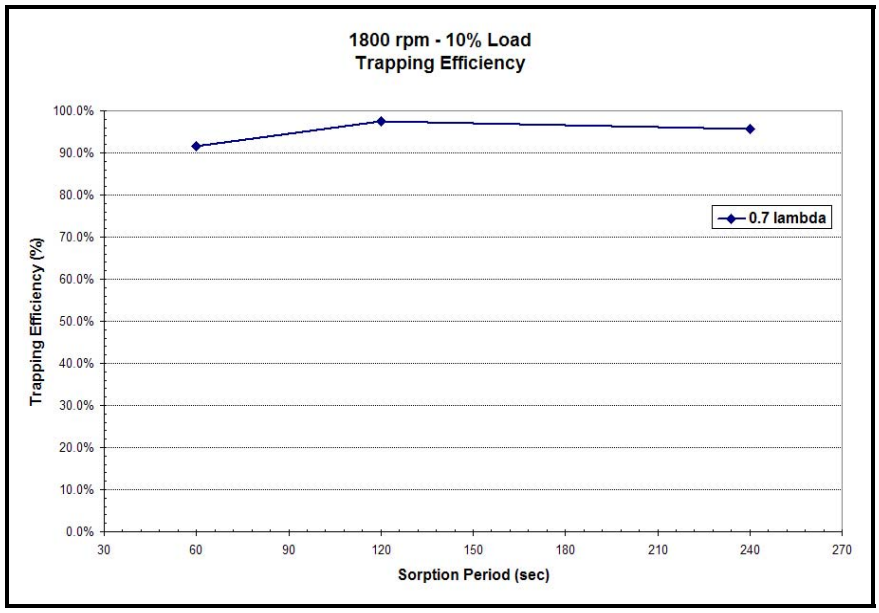


**Figure 70 10% Load NOx Trapping Efficiencies with Full Slip Flow**

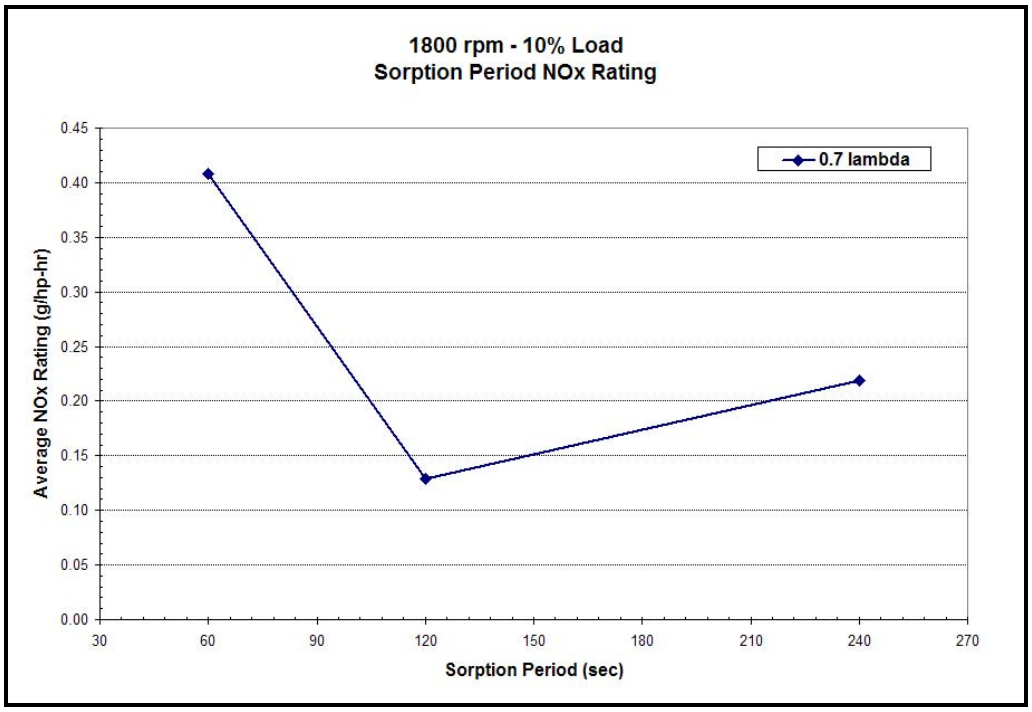


**Figure 71 10% Load NOx Ratings with Full Slip Flow**

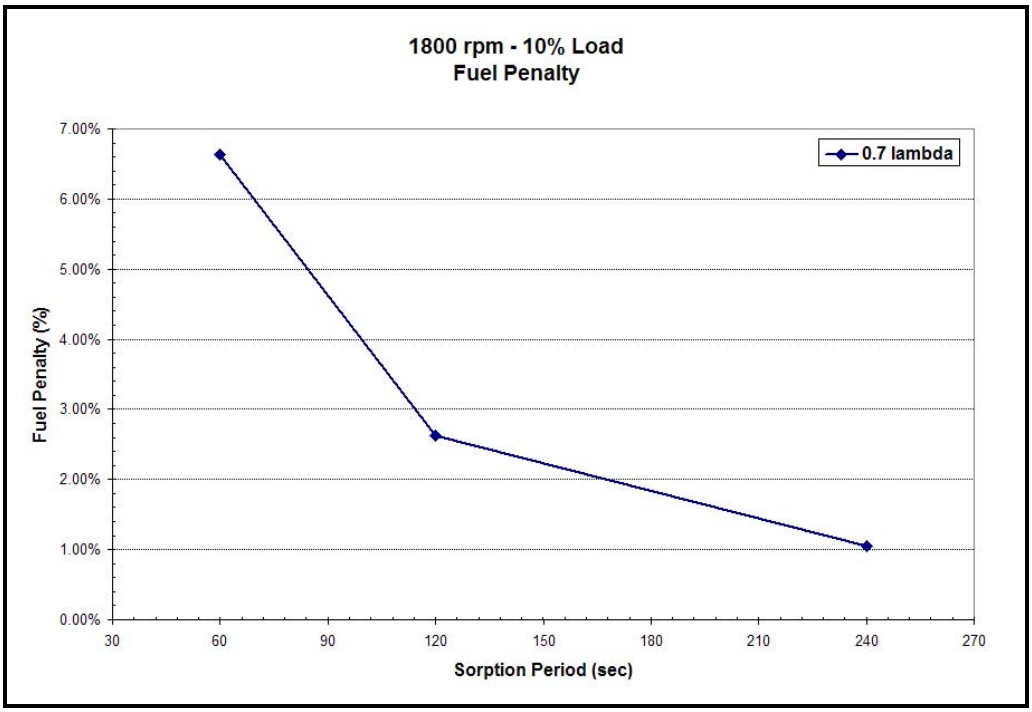


**Figure 72 10% Load Fuel Penalties with Full Slip Flow**

*NOx Storage Capacities*

The previous section outlined experiments designed to find the optimal injection rates and sorption periods for catalyst management, and presented an evaluation of the system based on trapping efficiencies and fuel penalties. Another critical characteristic in evaluating a LNT catalyst is its capacity to store NOx. NOx storage capacity is defined as the mass of NOx (as $NO_2$) stored on the catalyst during the sorption period, until trapping efficiencies fall below 90%. Typically, the capacity is normalized per catalyst volume, giving it units of grams per liter. As stated previously, the storage capacity of a Lean NOx Trap is a function of catalyst temperatures. Thus, thermal management becomes a key factor in optimizing the exhaust aftertreatment system. It is desirable to maximize capacities because this can decrease the catalyst volume required for a particular application, thus reducing capital costs. Higher capacities also result in longer periods between catalyst regeneration thus reducing fuel penalties. This section investigates NOx storage capacities as a function of catalyst temperatures.

For this experiment, the storage capacity of the LNT was tested at three different catalyst temperatures. The aftertreatment system was operated with the optimal regeneration parameters found from the test matrix for 10%, 25% and 50% engine loads until catalyst temperatures stabilized to their respective temperatures; 440° C, 510° C and 560° C. The regeneration sequence was then stopped and the catalyst was allowed to adsorb until trapping efficiencies fell

below 90%. Analysis of the results yielded Figure 73, which shows the dependence of the NOx storage capacity on catalyst temperatures. The predicted storage capacity from bench flow reactor and baseline engine data is also shown. Because they were extrapolated from experiments with more controlled conditions, results for predicted storage capacities are higher than actual storage capacities. Nevertheless, both show the same general trend of decreasing capacities with increasing temperatures. Comparing the temperature dependence of the LNT for storage capacity (Figure 73), with the temperature dependence of the oxidation catalyst for methane oxidation (Figure 57), reveals a narrow temperature window for optimizing performance.

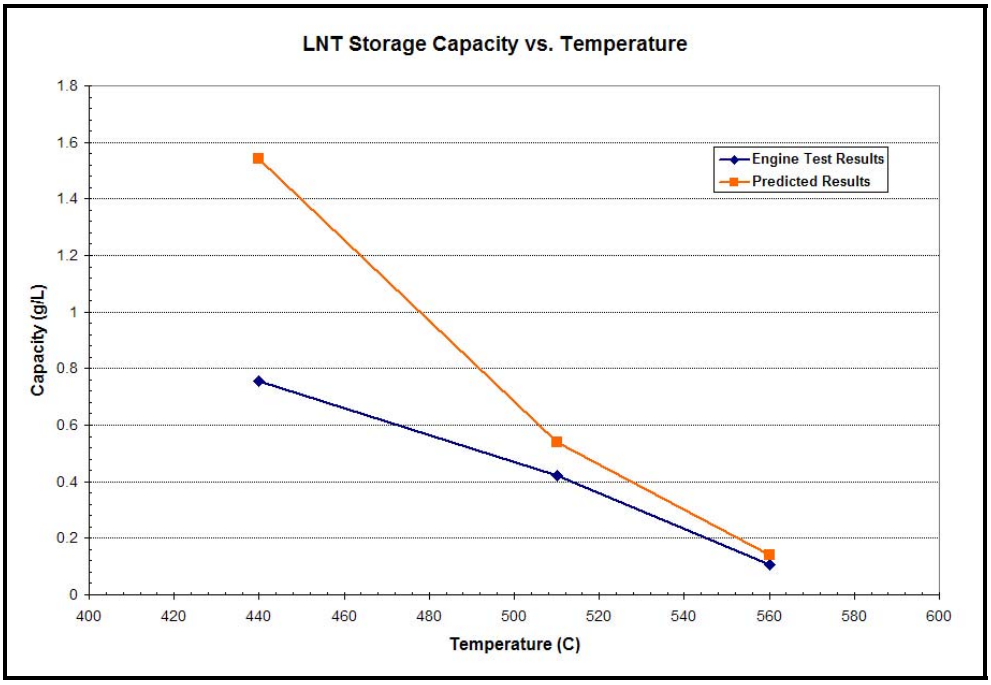


**Figure 73 LNT Storage Capacity vs. Temperature**

*Fixed Temperature Adsorpation*

Because the LNT and the oxidation catalyst require different temperature ranges for optimal performance, one potential solution would be to physically separate the two catalyst bricks. Placing the oxidation catalyst closer to the outlet of the turbocharger would allow it to be maintained at higher temperatures for methane oxidation. Placing a waste heat recovery system in front of the LNT would allow it to be maintained at a lower temperature for higher NOx storage capacities. Ideally, the LNT would be maintained at a constant temperature regardless of engine load. The following experiment was used to simulate such a scenario. Here, the aftertreatment system is operated with the optimal regeneration parameters for 25% engine load. Once the catalyst temperatures stabilize to 510° C, the engine load is changed to 50%, the regeneration sequence is stopped, and the catalyst immediately begins to adsorb. By doing this, the NOx flux from the engine has been changed to that of the higher load, but the catalyst temperatures have not been given time to change. Thus, the catalyst is adsorbing NOx at the higher engine load but with a constant 510° C. The same procedure was repeated for each engine load. The average NOx rating for the 5 engine modes was calculated until the trapping efficiency fell below 90%. Figure 74 shows these average NOx ratings, as well as minimum NOx ratings

and NOx flux rates for each engine mode. These results show that when the LNT adsorbs at a constant 510° C, NOx reduction is possible at higher engine loads. Even with the high NOx flow rates an average NOx rating of 0.17 g/hp-hr and instantaneous ratings of 0.06 g/hp-hr are achievable at 75% load. At 100% load average ratings of 0.63 g/hp-hr and instantaneous ratings of 0.17 g/hp-hr are possible. These results demonstrate the potential improvements to be gained by a better thermal management system for the catalyst.

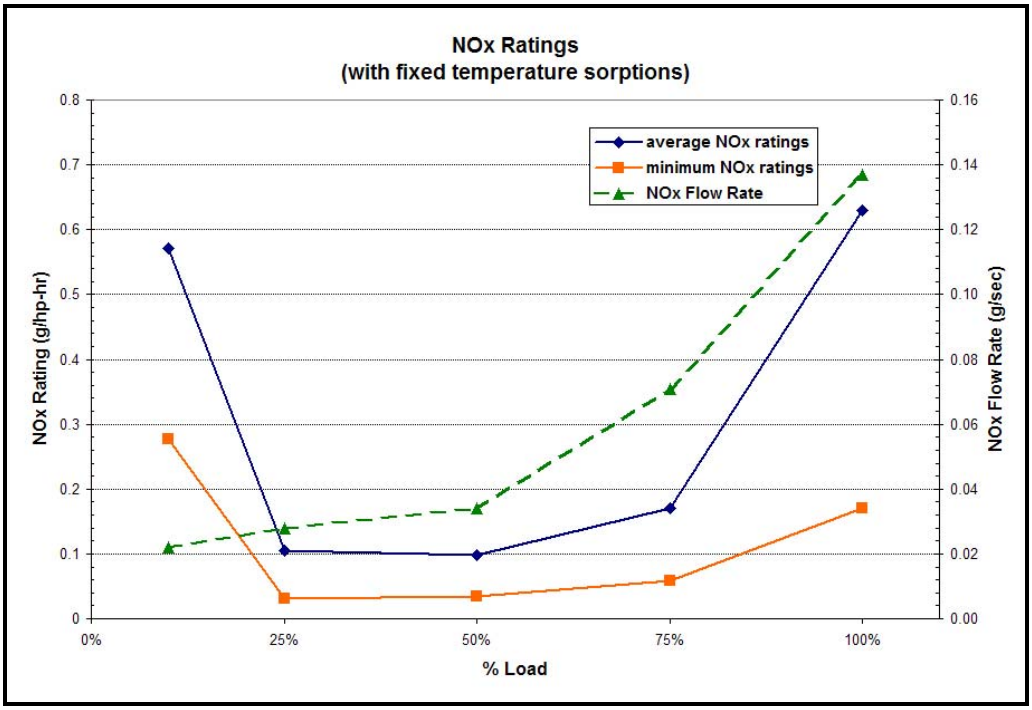


**Figure 74 NOx Ratings with Fixed Temperature Adsorption**

*Methane Utilization*

Experiments proved that the oxidation catalyst could successfully combust methane at high enough temperatures. However, in addition to burning out excess oxygen through methane combustion, the rich combustion products CO and $H_2$ must be formed. The following experiments explored the production and utilization of CO for the range of injection rates used in the test matrix. These experiments were conducted at 25% and 50% engine loads, where catalyst bricks are above their light off temperature. CO levels were measured at three positions along the catalyst chamber during the regeneration sequence; Oxi Cat In, Oxi Cat Out and LNT Out as indicated in Figure 56. Figures 75 and 76 show the grams of CO at each of these positions when injecting for lambda values of 0.5, 0.6, 0.7, 0.8 and 0.9. The results show an increase in CO levels measured at the Oxi Cat Out position as exhaust entering the catalyst becomes richer. For 50% load CO production stabilizes beyond 0.7 lambda. CO levels measured at the LNT Out position are consistently lower than those measured at the Oxi Cat In position. This indicates that the Lean NOx Traps are utilizing some of the CO for regeneration. For 50% engine load, the quantity of CO produced at 0.9 lambda, is small enough that it is entirely consumed by the regeneration mechanism. Similarly, for 25% engine load, all of the CO produced at 0.8 and 0.9 lambda is consumed. Unlike CO levels sampled at the Oxi Cat Out position, CO levels sampled at LNT Out do not taper off beyond 0.7 lambda. This indicates that the reformer catalyst is also

producing CO. Because of the catalyst can assembly, it was not possible to access a sample point between the reformer catalyst and the LNT. A more in-depth investigation of methane utilization would require sampling CO levels after the reformer, and is recommended as a next step in methane utilization studies.

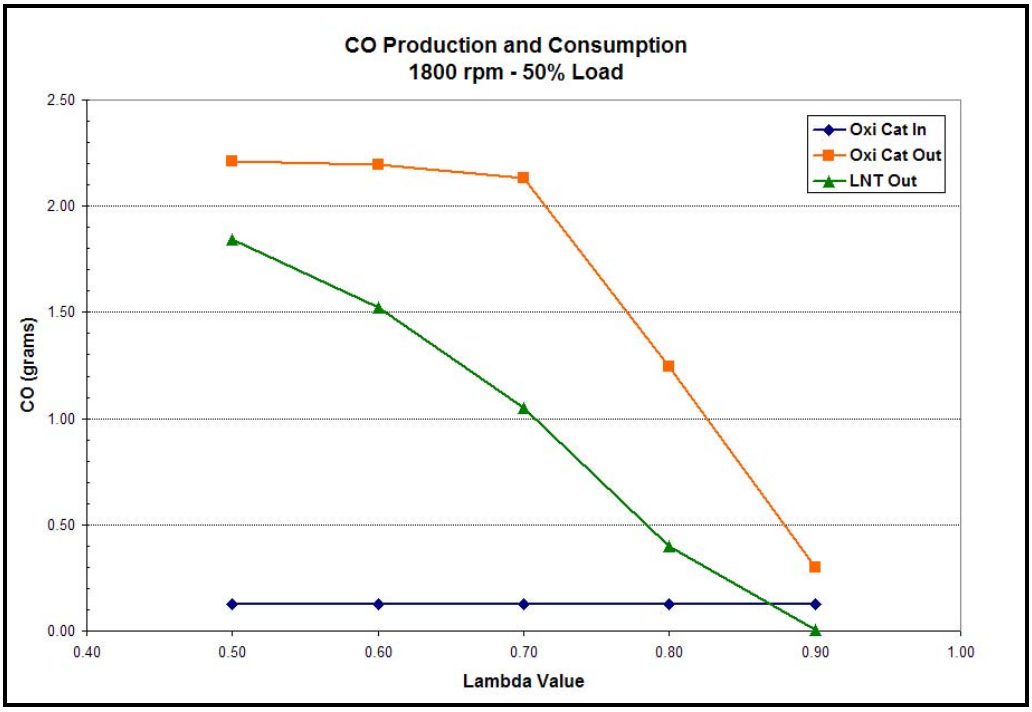


**Figure 75 50% Load CO Production and Consumption**

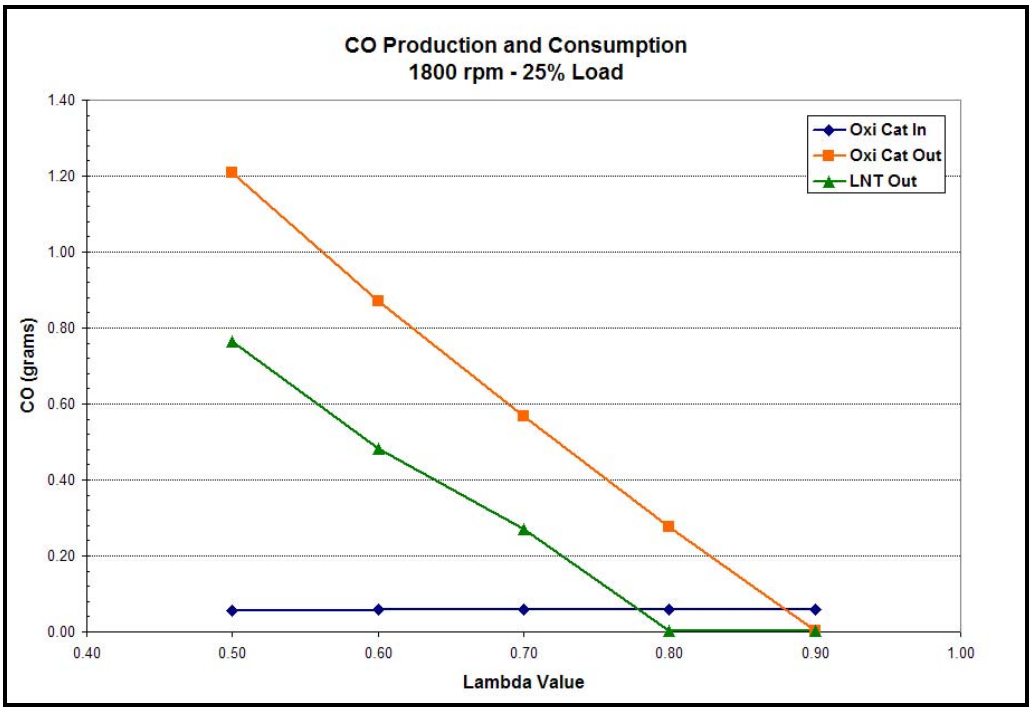


**Figure 76 25% Load CO Production and Consumption**

## Future Work

In the final year of the project, the activity will focus on the fabrication and testing of the oxidation catalyst, the system optimization of the LNT system and finally the system integration of the two systems. An outline is listed below:

1. Fabrication of the four-way reversing valve
2. Engine testing and optimization of the reverse flow catalyst system
3. LNT control development and regeneration optimization
4. Complete reverse flow catalyst and LNT system integration and optimization

**Nomenclature**

$a(x)$ = *Catalytic surface area per unit volume*, $cm^2/cm^3$

$A_V$ = *Frontal area of the monolith*, $cm^2$

$C_{g,i}$ = *Concentration of species i in the bulk gas stream*, *mole fraction*

$C_{s,i}$ = *Concentration of species i in the solid phase*, *mole fraction*

$D_i$ = *Diffusivity of the species i in the relative mixture*, $cm^2/s$

$C_{pg}$ = *Specific heat of gas*, $J/g.K$

$C_{ps}$ = *Specific heat of solid*, $J/g.K$

$h$ = *Heat transfer coefficient*, $J/cm^2.s.K$

$K_{mi}$ = *Mass transfer coefficient of the specied i*, $cm/s$

$R_h$ = *Hydraulic radius of channel*, $cm$

$R_g$ = *Universal gas const.*

$(R_a)_H$ = *Specific reaction rate in gas phase for species i*, $mol/cm^2Pd.s$

$(R_a)_{surface}$ = *Specific surface reaction rate for species i*, $mol/cm^2Pd.s$

$S$ = *Geometric surface area per unit volume*, $cm^2/cm^3$

$T_s$ = *Solid Temperature*, $K$

$T_{gas}$ = *Gas Temperature*, $K$

$v$ = *Linear Superficial velocity of exhaust gas*, $cm/s$

$W_g$ = *Mass flow rate*, $g/s$

$Y_{surface}$ = *Mole fraction on the surface*

$Y_{gas}$ = *Mole fraction of species in gas phase*

*Symbols*

$\phi$ = *Void fraction of the monolith*

$\lambda_s$ = *Thermal conductivity of the solid*, $J/cm.s.K$

$\rho_g$ = *Gas Density*, $g/cm^3$

$\rho_s$ = *Solid Density*, $g/cm^3$

## Bibliography


1. M.Zheng, E.Mirosh, W.Klopp, D.Ulan, M.Pardell, P.Newman, G.Bunimovich, Y.Matros, and A. Nishimura, "Development of a Compact Reverse-Flow Catalytic Converter for Diesel Dual Fuel LEV", SAE paper 1999-01-3558.
2. M.Zheng, E.Mirosh, D.Ulan, W .Klopp, M.Pardell, P .Newman, and A. Nishimura, "A Novel Reverse-Flow Catalytic Converter Operated on an ISUZU-6HH1 Diesel Dual Fuel Engine", 1999 ASME-IEC Fall Technical Conference, October 17-20,1999.
3. B. Liu, R. E. Hayes, M. D. Checkel, M. Zheng and E. Mirosh, "Reverse Flow Catalytic Converter for a Natural Gas/Diesel Dual Fuel Engine", Journal of Chemical Engineering Science, 56 (2001) 2641-2658, Oxford, New York, Pergamon Press.
4. V. Strots, G. Bunimovich, Y. Matros, M. Zheng, and E. Mirosh, 1998, "Novel Catalytic Converter for Natural Gas Powered Diesel Engines", SAE 980194.
5. R. McCormick, A. Newlin, D. Mowery, M. Graboski, and T. Ohno, 1996, "Rapid Deactivation of Lean-Burn Natural Gas Engine Exhaust Oxidation Catalysts", SAE paper 961976.
6. J. Lampert, M. Kazi, and R. Farrauto, "Palladium Catalyst Performance for Methane Emissions Abatement from Lean Burn Natural Gas Vehicles", Applied Catalyst B: Environmental 14, pp. 211-223, 1997.
7. Robert J. Farrauto and Kenneth E. Voss, "Monolithic Diesel Oxidation Catalysts", Applied Catalyst B: Environmental 1 0, pp. 29-51, 1996.
8. Cullis, C.F. and B.M. Willat. “Oxidation of methane over supported precious metal catalysts”, J.Cat., 83 267-285, 1983.
9. Duggal, Vinod K., Roy Meyer, David Meyers, Syed M. Shahed. “Development of a Heavy Duty On-Highway Natural Gas-Fueled Engine”. SAE Paper No. 922362, Warrendale, Pennsylvania: Society of Automotive Engineers, Inc., 2000.
10. Fussel, Lori M., Jeffrey W. Hodgson, and David K. Irick. “Automotive Engines and Vehicles” Encyclopedia of Environmental Analysis and Remediation, New York: John Wiley and Sons, Inc., 1998.
11. Hayes, R.E., Kolaczkowski, S.T., Introduction to Catalytic Combustion. Amsterdam, The Netherlands: Gordon and Breach Science Publishers, 1997.
12. Helden, R., Verbeek, R., Aken, M., Genderen, M., Patchett, J., Straten, T., Kruithof, J., and Saluneaux, C., 2002, “Engine Dynamometer and Vehicle Performance of a Urea SCR-System for Heavy-Duty Truck Engines”, SAE paper 2002-01-0286.
13. Heywood, John B. Internal Combustion Engine Fundamentals. New York, NY: McGraw-Hill, Inc., 1988.
14. Lisenby, Paul M., “An Experimental Investigation of Natural Gas Catalysts Using a Bench-Flow Reactor”, M. Sc. Thesis, Department of Mechanical Engineering, The University of Tennessee – Knoxville, 1995.
15. Mital, R., S. C. Huang, B. J. Stroia, Robert C. Yu, and C. Z. Wan 2002, “ A Study of Lean NOx Technology for Diesel Emission Control”, SAE paper 2002-01-0956.
16. Quiros, Edwin N., Yasuhiro Daisho, Turo Yaeo, Takahisa Koseki, Takeshi Saito, Ryoji Kihara. “Combustion and Exhaust Emissions in a Direct-Injection Diesel Engine Dual

Fueled with Natural Gas", SAE Paper No. 950465, Warrendale, Pennsylvania: Society of Automotive Engineers, Inc., 2000.

17. Stone, Richard. Introduction to Internal Combustion Engines. Warrendale, Pennsylvania: Society of Automotive Engineers, Inc., 1999.
18. Subramanian, S., Kudla, R.J., Chattha, M.S., "Treatment of Natural Gas Vehicle Exhaust", SAE Paper No. 930223, Warrendale, Pennsylvania: Society of Automotive Engineers, Inc., 1993.
19. Turns, Stephen R. An Introduction to Combustion, Concepts and Applications. New York, NY: McGraw-Hill, Inc., 2000.
20. Zhang, G., Pflung, A., Raine, R.R., "Comparison of Emissions from Natural Gas and Gasoline Fuelled Engines – Total Hydrocarbon and Methane Emissions and Exhaust Gas Recirculation Effects", SAE Paper No. 970743, Warrendale, Pennsylvania: Society of Automotive Engineers, Inc., 1997.
21. Zheng, M., Mirosh, E., Liu, B., Checkel, M.D., Hayes, R.E., "Experimental and Modeling Study of Variable Cycle Time for a Reversing Flow Catalytic Converter for Natural Gas/Diesel Dual Fuel Engines", SAE Paper No. 2000-01-0213, Warrendale, Pennsylvania: Society of Automotive Engineers, Inc., 2000.
22. Zheng, Ming, Edward A. Mirosh, Vadim O. Strots, Grigorii A. Bunimovich, Yurii Sh. Matros. "Novel Catalytic Converter for Natural Gas Powered Diesel Engines". SAE Paper No. 980194. Warrendale, Pennsylvania: Society of Automotive Engineers, Inc., 2000.
23. M. van Sint Annaland, R. C. Nijssen, "A novel reverse flow reactor coupling endothermic and exothermic reactions: an experimental study," Chemical Engineering Science pp. 4967-4985, 2002
24. Krzysztof Gosiewski, Ulrich Bartmann, Marek Moszczynski, Leslaw Mleczko, "Effect of the intraparticle mass transport limitations on temperature profiles and catalytic performance of the reverse-flow reactor for the partial oxidation of methane to synthesis gas," Chemical Engineering Science pp. 4589-4602, 1999
25. F. Cunill, L. van de Beld, K. R. Westerterp, "Catalytic Combustion of Very Lean Mixtures in a Reverse-Flow Reactor Using an Internal Electric Heater," Ind. Eng. Chem. Res. pp. 4198-4206, 1997
26. Jason M. Keith, David T. Leighton, Jr., Hsueh-Chia Chang, "A New Design of Reverse-Flow Reactors with Enhanced Thermal Dispersion," Ind. Eng. Chem. pp. 667-682, 1999
27. M. van Sint Annaland, J. A. M. Kuipers, W. P. M. van Swaaij, "Safety analysis of switching between reductive and oxidative conditions in a reaction coupling reverse flow reactor," Chemical Engineering Science, pp. 1517-1524, 2001
28. B. Liu, R. E. Hayes, M. D. Checkel, M. Zheng, E. Mirosh, "Reversing flow catalytic converter for a natural gas/diesel dual fuel engine," Chemical Engineering Science pp. 2641-2658, 2001
29. H. Zufle, T. Turek, "Catalytic combustion in a reactor with periodic flow reversal. Part 1. Experimental results," Chemical Engineering and Processing pp. 327-340, 1997
30. H. Zufle, T. Turek, "Catalytic combustion in a reactor with periodic flow reversal. Part 2. Steady-state reactor model," Chemical Engineering and Processing pp. 341-352, 1997

31. Moshe Ben-Tullilah, Einat Alajem, Rina Gal, Moshe Sheintuch, “Flow-rate effects in flow-reversal reactors: experiments, simulations and approximations,” Chemical Engineering Science, 2002

32. Yu. Sh. Matros, G. A. Bunimovich, V. O. Strots, E. A. Mirosh, “Reversed flow converter for emission control after automotive engines,” Chemical Engineering Science pp. 2889-2898

33. R. Quinta Rerreira, C. Almeida Costa, S. Masetti, “Reverse-flow reactor for a selective oxidation process,” Chemical Engineering Science pp. 4615-4627

34. F. Moallemi, G. Batley, V. Dupont, T. J. Foster, M. Pourkashanian, A. Williams, “Chemical modeling and measurements of the catalytic combustion of CH4/air mixtures on platinum and palladium catalysts,” Catalysis Today pp. 235-244, 1999

35. Byung-Chul Choi, Geon-Seog Son, Eugene Kim, Kwi-Young Lee, “Effective Parameters on the Catalytic Reaction of NGV Catalytic Converter,” SAE 960239, 1996

36. Athanasios G. Konstandopoulos, Margaritis Kostoglou, “Periodically Reversed Flow Regeneratino of Diesel Particulate Traps,” SAE 1999-01-0469, 1999

37. Montiero, D. Zemlyanov, F.H. Ribiero., “Complete Methane Oxidation on Palladium Model Catalyst”. G. Zhu, J. Han, R.S. 2003.

38. Viatcheslav I. Naoumov, Viktor G. Kriukov, Airat L. Abdullin., “Chemical Kinetics Software System for the propulsion and power engineering”, 41st Aerospace Science Meeting and exhibit. 2003.

39. Warren R. Smith, Ludmilla N. Bobrova., “Mathematical modeling of a reverse flow reactor with catalytic surface dynamics”. Chemical Engineering Science. 57, pp. 393 – 407, 2002.

40. Moshe Ben Tullilah, Einat Alajem, Rina Gal, Moshe Sheintuch, “Flow – Rate effects in flow reversal reactors: Experiments, simulation and approximations”, Chemical Engineering Science. 2002.

41. Dragos Ciuparu, Maxim R. Lyubovsky, Eric Altman, Lisa D. Pfefferle and Abhaya Datye, “Catalytic Combustion of Methane over Palladium Based Catalysts”, Catalytic Reviews. 44 (4), pp. 593 – 649, 2002.

42. Eduardo Lopez, Noemi S. Schbib, Carlos E. Gigola and Veronica Bucala, “Influence of the Methane Combustion Kinetic Model on the Operating Conditions of an Auto thermal Catalytic Reactor”, Ind. Eng. Chem. Res, 40, pp. 5199 – 5205, 2001.

43. Roberts E. Hayes, Stan T. Kolaczkowski, Paul K.C. Li, “The palladium catalyst oxidation of methane: reaction kinetics and the effect of diffusion barriers”, Chemical Engineering Science. 56 (16), pp. 4815 – 4835, 2001.

44. R.S. Monteiro, D. Zemlyanov, J.M. Storey and F.H. Ribeiro, “Turnover Rate and reaction orders for the complete oxidation of methane on a palladium foil in excess oxygen”, Journal of Catalysis. 199, pp. 291 – 301, 2001.

45. F. Moallemi, G. Batley, V. Dupont, T.J. Foster, M. Pourkashanian, A. Williams. Chemical modeling and measurements of the catalytic combustion of $CH_4$ / air mixtures on platinum and palladium catalysts. Catalysis Today. 47, pp. 235 – 244, 1999.

46. O. Deutschmann, R. Schmidt, F. Behrendt and J. Warnatz, “Numerical Modeling of Catalytic Ignition”. 26th Symposium on combustion. pp. 1747 – 1754, 1996.

47. Pio Forzatti, Gianpiero Groppi, “Catalytic combustion for the production of energy”, Catalysis Today. 54, pp. 165 – 180, 1999.

48. Quinta Ferrreira, C. Almeida Costa. S. Masseti, “Reverse flow reactor with selective oxidation process”, Chemical Engineering Science. 54, pp. 4615 – 4627, 1999.

49. Ruoyu Hong, Xin Li, Hongzhong Li, Weikang Yuan, “Modeling and simulation of $SO_2$ oxidation in a fixed bed reactor with periodic flow reversal”, Catalysis Today. 38, pp. 47 – 58, 1997.

50. Robert Jahn, Dalimi Snita Milan Kubicek, Milos Marek, “3 – D modeling of monolith reactors”, Catalysis Today. 38, pp. 39 – 46, 1997.

51. Robert Hayes, Stan T. Kolaczkowski, W. John Thomas and James Titiloye, “Transient Experiments and Modeling of the catalytic combustion in a monolith reactor”, Ind. Eng. Chem. Res., 35(2), pp. 406 – 414, 1996.

52. Naktsuji, T., Yasukawa, R., Tabata, K., Sugaya, T., Ueda, K., and Niwa, M.,“*Highly Durable NOx Reduction System and Catalysts for NOx Storage Reduction System,*” SAE Technical Paper Series 980932, 1998.

53. Bragan, M. S., Clark, A. D., and Brisley, R. J.,“*Recent Progress in Nox Trap Technology*,” SAE Technical Paper Series 980933, 1998.

54. Mahzoul, H., and Brilhac, P. G., *“Experimental and Mechanistic Study of NOx Absorption over NOx Trap Catalysts*,” Applied Catalysis B: Environmental 20 pp.47-55, 1999.

55. Larsson, M., Andersson, L., Fast, O., Litorell, M., and Mukuie, R., 1999, *“NOx Trap Control by Physically Based Model,”* Society of Auto motive Engineers 1999-01-3503, 1999.

56. Fridell, E., Persson, H., Westerberg, B., Olsson, L., and Skoglundh, M., *“The Mechanism for NOx Storage,”* Catalysis Letters 66 (2000) pp.71-74, 2000.

57. Lietti, L., Forzatti, P., Nova, I., and Tronconi, E.,*“NOx Storage Reduction over Pt- Ba/γ-$Al_2O_3$ Catalyst,”* Catalysis Letters 204 pp.175-191, 2001.

58. Laurent, F., Pope, C.J., Mahzoul, H., Delfosse, L., and Gilot, P.,*“Modelling of NOx Adsorption over NOx Adsorbers,”* Chemical Engineering Science 58 (2003) 1793-1803, 2002.

59. Wagner, G. J., Ph.D.,*“Advanced Reciprocating Engine Systems Bench Flow Reactor Testing of NOx Absorber Catalyst for Lean- Burn Natural Gas Engine: Efficiency of Regeneration Process Utilizing Methane Oxidation and Reforming Catalysts,”* Research Report for Oak Ridge National Lab.,2003.